

# UC Santa Barbara

## UC Santa Barbara Electronic Theses and Dissertations

### Title

Investigating the secular geochemical and geodynamic evolution of accretionary orogens with zircon petrochronology: A case study from West Antarctica

### Permalink

<https://escholarship.org/uc/item/8bs289cp>

### Author

Nelson, Demian Alan

### Publication Date

2018

### Supplemental Material

<https://escholarship.org/uc/item/8bs289cp#supplemental>

Peer reviewed|Thesis/dissertation

UNIVERSITY OF CALIFORNIA

Santa Barbara

Investigating the secular geochemical and geodynamic evolution of accretionary orogens  
with zircon petrochronology: A case study from West Antarctica

A dissertation submitted in partial satisfaction of the  
requirements for the degree Doctor of Philosophy  
in Geological Sciences

by

Demian Alan Nelson

Committee in charge:

Professor John Cottle, Chair

Professor Matthew Jackson

Professor Roberta Rudnick

September 2018

The dissertation of Demian Alan Nelson is approved.

---

Roberta Rudnick

---

Matthew Jackson

---

John Cottle, Committee Chair

July 2018

Investigating the secular geochemical and geodynamic evolution of accretionary orogens  
with zircon petrochronology: A case study from West Antarctica

Copyright © 2018

by

Demian Alan Nelson

## ACKNOWLEDGEMENTS

This dissertation is almost entirely the result of a fortunate series of events, mentors, and circumstances with only a dash of hard work. The first fortunate circumstance was having a loving and supportive mother who, through exceptional grit, raised me to be the best person I could be. Next I would like to acknowledge a dear friend and mentor, Mike Sears, who has been a constant source of motivation, inspiration, and invaluable advice without which I may have never recognized the empowerment of education. I certainly never would have pursued a PhD without the encouragement, inspiration, and mentorship of Professor James Day who exposed me to research and opened many doors. With his support I was awarded a coveted National Science Foundation Graduate Research Fellowship and, therefore, I must acknowledge the critical role NSF has had in ensuring successful completion of my PhD. I hesitate in writing ‘successful’ in fear that it may attract criticism from the most instrumental member of this list of acknowledgements, my PhD advisor Professor John Cottle. John has elevated the expectations I hold for myself and provided me the tools to meet those expectations. He has supported me in every aspect of my research and provided ample opportunity to explore my own curiosity. It has been a pleasure working together and I suspect I will never be able to learn all I can from him. I must also acknowledge how important the UCSB Earth Science Department has been. The department has collected an incredible group of world-renowned scientists and talented graduate students who I have had the pleasure of interacting with and learning from for five years. In particular, I would like to thank the following mentors, students, and friends: Roberta Rudnick, Matthew Jackson, Bradley Hacker, Frank Spera, Gareth Seward, Andrew Kylander-Clark, Robert Holder, Sophie Briggs, Joshua Garber, Graham Hagen-Peter, Forrest Horton, Tyson McKinney, Jacob Poletti, Carina Edelman, and Elizabeth Erickson.

## VITA OF DEMIAN ALAN NELSON

July 2018

### EDUCATION

**2018** University of California, Santa Barbara, Advisor: Dr. John Cottle  
Ph.D. Geological Science, *4.0 GPA*, and Certificate in College and University Teaching

Dissertation title: “Investigating the secular geochemical and geodynamic evolution of accretionary orogens with zircon petrochronology: A case study from West Antarctica.”

**2013** University of California, San Diego, Advisor: Dr. James Day  
B.Sc. Earth Sciences Honors with High Distinction, *Summa Cum Laude, 3.90 GPA*

Thesis title: Platinum group element (PGE) mineralization in chromitite layers within mafic-ultramafic layered intrusions.”

**2010** Cuesta Community College, San Luis Obispo,  
A.A. Arts and Humanities with High Honors, *3.95 GPA*

### PROFESSIONAL EXPERIENCE

2013-2018 Graduate Student Researcher / Teaching Assistant / Teaching Associate,  
Department of Earth Science, University of California, Santa Barbara

2018 NSF GRIP Intern, United States Geological Survey, Volcano Science Center, Menlo Park, CA

2012-2013 Undergraduate Research Assistant, Scripps Isotope Geochemistry Laboratory,  
University of California, San Diego

### RESEARCH INTERESTS/EXPERIENCE

Fields: petrochronology, tectonics, volcanology, accretionary orogens

Secular evolution of accretionary orogens: petrochronologic studies of Phanerozoic arc-related rocks in southern Gondwana and Cenozoic slab-window rocks of coastal California.

Interaction between water and volcanic glass: detailed investigations of layered glassy volcanic rocks in Antarctica and Japan.

Technical applications: LA-MC-ICP-MS, LA-Q-ICP-MS, TIMS, SEM, EPMA, SIMS, FTIR, XRF, XRD

### TEACHING EXPERIENCE

Certificate of College and University Teaching (June 2018)  
Summer Teaching Institute for Associates (Summer 2017)

*Associate/Instructor, UCSB, 2017*

Earth 10 Antarctica – The Last Place on Earth: themed introduction to physical geology and oceanography.

*Assistant, UCSB, 2013 – present*

Earth 6 Mountains, Boots, and Backpacks (field-based)

Earth 10 Antarctica – The Last Place on Earth

Earth 20 Geological Catastrophes

Earth 118 Summer Field Geology (field-based)

Earth 196 Senior Honors Thesis – students: Keith Chancey and Chris Strong.

Earth 199 Independent Studies

## AWARDS

2017 NSF Graduate Research Internship Program Award (\$13,000)

2016 GSA 35<sup>th</sup> IGC travel grant (\$3000)

2016 Goldschmidt Conference NASA travel grant (\$600)

2016 Global Field Travel Fund, UCSB departmental travel grant (\$1800)

2015 Fugro Field Award, Fugro Company (\$1500)

2015 GSA Mineralogy, Geochemistry, Petrology, and Volcanology Award (\$2000)

2015 Exxon Mobil/Geological Society of America Student Research Grant (\$7500)

2014 Antarctic Science Bursary Award (\$8000)

2014 Earth Research Institute Fellowship (\$2000)

2014 Graduate Opportunity Award, UCSB departmental research grant (\$4000)

2014 Global Field Travel Fund, UCSB departmental travel grant (\$1800)

2013 NSF Graduate Research Fellowship (\$32k/year x3)

2013 UCSB Doctoral Scholar Fellowship (\$24k/year x2)

2013 Outstanding Undergraduate of the Year, Scripps Institution of Oceanography

2012 Student Research Grant, Society of Economic Geologists - SEG (\$2500)

2012 Student Field Trip Grant Cu-Porphyry Systems of Peru, SEG (\$2000)

2012 McNair Pre-Doctoral Scholar, UCSD

2012 Darcy and Robert Bingham Scholarship, UCSD (\$2000)

2010-2013 Provost Honors, UCSD

2010 Warren Hansen Scholar Athlete of the Year, Cuesta Community College

## FIELDWORK

(Ongoing) Coast Ranges, California, sample collection of Coast Range Volcanics

2016 Central Transantarctic Mountains, Antarctica, NSF Award: #1443296

2016 Orange River, South Africa, field reconnaissance

2016 Rebun Island, Japan, sample collection of the Momo-Iwa Cryptodome

2015 Dry Valleys, Antarctica, NSF Award: #1443296  
2014 Central Andes, Chile, field assistant mapping volcanic deposits  
2014 Advanced Field Methods, UCSB, Iron Mountain, CA, Instructor: Phil Gans  
2014 Iceland summer field course, University of Iceland  
2014 6-week summer field course: New Mexico and North Lake Tahoe  
2012 Isle of Rum, Scotland, sample collection of the Eastern Layered Intrusion  
2012 Stillwater, Montana, sample collection of the Stillwater Igneous Complex  
2012 SEG Student Dedicated Field Course, Cu-Porphyry systems of Southern Peru

#### JOURNAL PUBLICATIONS

Nelson, D. A., & Cottle, J. M. (in review). Tracking voluminous Permian volcanism of the Choiyoi Province into central Antarctica. *Lithosphere*.

Nelson, D. A., & Cottle, J. M. (2018). The secular evolution of accretionary orogens: linking the Gondwana arc record of West Antarctica, Australia, and South America. *Gondwana Research*. doi.org/10.1016/j.gr.2018.06.002

Nelson, D. A., & Cottle, J. M. (2017). Long-term geochemical and geodynamic segmentation of the paleo-Pacific margin of Gondwana: Insight from the Antarctic and adjacent sectors. *Tectonics*, 36. doi.org/10.1002/2017TC004611

#### CONFERENCE ABSTRACTS

Nicole, F., Kimbrough, D., Behl, R., and Nelson, D. A. (2017). Laser ablation ICP-MS zircon U-Pb dating of Monterey Formation tuff in the Los Angeles and Santa Barbara basins. *Geological Society of America Abstracts with Programs (Vol. 49, No. 6)*.

Browne, N., Cottle, J., and Nelson, D. A. (2017). Petrogenesis of late-stage, high-K magmas within a continental arc: an example from the Ross Orogen, Antarctica. *Geological Society of America Abstracts with Programs (Vol. 49, No. 6)*.

Nelson, D. A., and Cottle, J. M. (2016). Formation of layering in a hypabyssal intrusion by shear-induced fracture, exsolution, and rapid devitrification. *Goldschmidt Abstracts (2262)*.

Nelson, D.A., and Cottle, J.M. (2016). Origin of the Hanson Formation, Antarctica—unlocking the pre-breakup history of the paleo-Pacific margin of Gondwana. *35<sup>th</sup> IGC*, Cape Town, South Africa.

Nelson, D.A., and Cottle, J.M. (2015). Petrogenesis of the Butcher Ridge Igneous Complex, a unique layered glassy silicic intrusion within the Ferrar Large Igneous Complex, Antarctica. *XII International Symposium on Antarctic Earth Science*, Goa, India.

Nelson, D. A., Cottle, J. M., Barboni, M., & Schoene, B. (2014). Petrologic significance of silicic magmatism in the Ferrar Large Igneous Province: geochemistry and geochronology of

the Butcher Ridge Igneous Complex, Antarctica. In *AGU Fall Meeting Abstracts* (Vol. 1, p. 4831).

#### INVITED TALKS

February 2018. Evolution of the paleo-Pacific margin of Gondwana in the Antarctic sector. Lithosphere Dynamics Lecture Series, University of Southern California

October 2017. The Metamorphic and Magmatic History of the Ross Orogen in Southern Victoria Land, Antarctica. 3rd Interdisciplinary Antarctic Earth Sciences meeting, Washington

December 2016. The Metamorphic and Magmatic History of the Ross Orogen in Southern Victoria Land, Antarctica. McMurdo Station Science Lecture Series

## ABSTRACT

Investigating the secular geochemical and geodynamic evolution of accretionary orogens  
with zircon petrochronology: A case study from West Antarctica

by

Demian Alan Nelson

Subduction-related processes in accretionary orogens modulate Earth's geochemistry. Uncovering the secular geodynamic evolution of accretionary orogens, therefore, is the key to Earth's geochemical history. A record of the secular geodynamic evolution of accretionary orogens is preserved in the tempo, geochemistry, and distribution of subduction-related magmatism. Zircon is ubiquitous in subduction-related magmas and provides a valuable time integrated geochemical proxy for the secular geodynamic evolution of accretionary orogens via U-Pb geochronology, Hf isotopes, and trace-elements (i.e., zircon petrochronology). The paleo-Pacific margin of Gondwana, including South America, eastern Australia, and West Antarctica, provides an ideal opportunity to investigate the secular geodynamic evolution of accretionary orogens with zircon petrochronology because it contains the most long-lived and best-preserved record of accretionary orogenesis on Earth.

This dissertation represents the first comprehensive zircon petrochronologic study of Phanerozoic subduction and accretionary orogenesis in West Antarctica and combines the results with existing data from adjacent regions in eastern Australia and South America to refine our understanding of the secular evolution of accretionary orogens. **Chapter 1**

investigates volcanoclastic sedimentary rocks in the central Transantarctic Mountains and documents episodic isotopically depleted magmatism along the Antarctic margin of Gondwana. Comparisons of these data from the central Transantarctic Mountains demonstrate a shared tectonic history between Antarctica, Zealandia, and Australia that contrasts with that of South America.

**Chapter 2** applies zircon petrochronology to the plutonic rocks in eastern Marie Byrd Land and Thurston Island. These new data combined with existing data from the Antarctic Peninsula, western Marie Byrd Land, and central Transantarctic Mountains provides an ~450 million year geochemical and geodynamic history for the Antarctic margin of Gondwana. This record is then compared with compilations from South America and Australia to determine similarities and differences in geochemical and geodynamic evolution along the Gondwana margin. **Chapter 3** traces the source of Permian volcanic deposits in central Antarctica to a voluminous volcanic province in South America, the Choiyoi Province, which may have contributed to Permian climate change and environmental degradation.

## Table of Contents

<b>I. Long-term geochemical and geodynamic segmentation of the paleo-Pacific margin of Gondwana: insight from the Antarctic and adjacent sectors</b> .....	<b>1</b>
<b>Abstract</b> .....	<b>1</b>
<b>Geologic Background</b> .....	<b>4</b>
Hanson and Fremouw Formations.....	5
Potential volcanic sources.....	7
<b>Sampling and Methods</b> .....	<b>8</b>
<b>Results</b> .....	<b>10</b>
Geochronology.....	10
Trace elements.....	11
Hafnium isotopes.....	12
<b>Discussion</b> .....	<b>13</b>
Zircon geochronologic record in the cTAM.....	13
Zircon trace element petrochronology.....	16
Zircon Hafnium isotopes and geodynamic evolution.....	18
Pan-paleo-Pacific margin Hf isotopes.....	21
<b>Conclusions</b> .....	<b>26</b>
<b>Acknowledgements</b> .....	<b>27</b>
<b>Figures</b> .....	<b>28</b>
<b>II. Zircon U-Pb and Hf isotopes link the Gondwana arc record of West Antarctica, Australia, and South America and highlight the secular development of accretionary orogens</b> .....	<b>38</b>

<b>Abstract</b> .....	<b>38</b>
<b>Introduction</b> .....	<b>39</b>
<b>Geologic Background</b> .....	<b>42</b>
Western Marie Byrd Land (Ross Province) .....	43
Eastern Marie Byrd Land (Amundsen Province) .....	45
Thurston Island.....	46
<b>Analytical Techniques</b> .....	<b>47</b>
<b>Results</b> .....	<b>48</b>
<b>Discussion</b> .....	<b>52</b>
Zircon record of West Antarctica (Cambrian – Cretaceous).....	52
Zircon Hf isotopes and geodynamic evolution of the Gondwana margin.....	57
Implications for Phanerozoic accretionary orogens.....	69
<b>Conclusions</b> .....	<b>73</b>
<b>Acknowledgements</b> .....	<b>74</b>
<b>Figures</b> .....	<b>76</b>
<b>III. Tracking voluminous Permian volcanism of the Choiyoi Province into central Antarctica</b> .....	<b>86</b>
<b>Abstract</b> .....	<b>86</b>
<b>Introduction</b> .....	<b>87</b>
<b>Geological Background</b> .....	<b>89</b>
Polarstar Formation, Ellsworth Mountains .....	93
Mt. Glossopteris Formation, Ohio Range .....	94
Pecora Formation, Pensacola Mountains .....	95
<b>Analytical Methods</b> .....	<b>96</b>

<b>Results .....</b>	<b>97</b>
<b>Discussion .....</b>	<b>99</b>
Regional Temporal Correlations of Permian Volcanism.....	99
Hf Isotopic Constraints On Provenance.....	101
Along Arc Geochemical Variation.....	104
Zircon Trace Element Constraints On Source.....	106
Environmental Impacts of the Choiyoi Flare-up .....	108
<b>Conclusions .....</b>	<b>111</b>
<b>Acknowledgements .....</b>	<b>112</b>
<b>Figures.....</b>	<b>113</b>
<b>Appendix: Supplementary Information .....</b>	<b>124</b>
<b>Zircon U-Pb geochronology .....</b>	<b>124</b>
<b>Zircon Hf isotopes.....</b>	<b>125</b>
<b>References Cited .....</b>	<b>127</b>

# **I. Long-term geochemical and geodynamic segmentation of the paleo-Pacific margin of Gondwana: insight from the Antarctic and adjacent sectors**

*Note: available at <https://doi.org/10.1002/2017TC004611>*

## **Abstract**

Combined zircon geochemistry and geochronology of Mesozoic volcanoclastic sediments of the central Transantarctic Mountains, Antarctica, yield a comprehensive record of both the timing and geochemical evolution of the magmatic arc along the Antarctic sector of the paleo-Pacific margin of Gondwana. Zircon age populations at 266–183 Ma, 367–328 Ma, and 550–490 Ma correspond to episodic arc activity from the Ediacaran to the Jurassic. Zircon trace element geochemistry indicates a temporal shift from granitoid-dominated source(s) during Ediacaran to Early Ordovician times to mafic sources in the Devonian through Early Jurassic. Zircon initial  $\epsilon_{\text{Hf}}$  shifts to more radiogenic Hf isotope compositions following the Ross Orogeny, and is inferred to reflect juvenile crustal growth within an extensional arc system during progressive slab rollback. These new ages and Hf isotopic record are similar to that from the Australian sector, indicating these regions constituted an ~3000 km laterally continuous extensional arc from at least the Carboniferous to the Permian. Conversely, the South American sector records enriched zircon Hf isotopic compositions and compressional/advancing arc tectonics during the same time period. Our

new data constrain the location of this profound along-arc geochemical and geodynamic ‘switch’ to the vicinity of the Thurston Island block of West Antarctica.

## **Introduction**

The paleo-Pacific margin of Gondwana (Fig. 1A) was a relatively continuous active convergent margin from at least the Ediacaran until initial supercontinent breakup in the Early Jurassic (Cawood, 2005; Collins et al., 2011). The volcanic, plutonic, metamorphic, and sedimentary products of this protracted convergence are found within various allochthonous, autochthonous, and para-autochthonous terranes throughout Peru, Chile, Antarctica, New Zealand, and Australia (Fig. 1A). Recent work has significantly improved our knowledge of this major arc system, primarily through detrital and igneous zircon geochronology and geochemistry of rocks from South America and Australia (e.g., Kemp et al., 2009; Cawood et al., 2011; Pepper et al., 2016). However, the segment of the post-Ordovician arc system within the Antarctic sector (Fig 1B), i.e., the various crustal blocks of Zealandia and particularly West Antarctica, remains poorly understood due to a lack of data, largely a result of poor exposure and/or inaccessibility (i.e., ice covered or submarine continental crust). Unraveling the history of this segment of the arc is further complicated by a lack of robust paleomagnetic constraints on the relative locations and relationships between crustal blocks of West Antarctica and Zealandia from their presumed initial formation in the Neoproterozoic to Cambrian through to their breakup in the Cretaceous. In addition, extensive rifting, rotation, and translation of these crustal blocks since the Cretaceous means that this segment of the arc is highly dissected and makes reconstructing the pre-breakup

configuration of the paleo–Pacific margin of Gondwana a difficult task (Dalziel and Elliot, 1982; Grunow et al., 1987; Storey et al., 1988) and has resulted in a gap in the record of the broad history of the paleo–Pacific margin of Gondwana.

A comprehensive archive of post–Ordovician arc volcanism along the Antarctic sector is recorded in Mesozoic volcanoclastic sediments deposited in a foreland basin setting that is now exposed in the Transantarctic Mountains (TAM; Barrett et al. 1986, Fig. 2). In contrast to West Antarctica and Zealandia, which have undergone large–scale translation and rotation, sediments in the TAM were deposited onto a section of the East Antarctic craton that remained tectonically undissected during supercontinent breakup. The Mesozoic strata studied here, the Fremouw and Hanson Formations, therefore provide an opportunity to characterize the evolution of the segment of the arc outboard of the TAM without the need for extensive paleogeographic reconstructions and associated uncertainties. The source(s) outboard of the TAM for volcanic detritus in these formations is presumed to be located in Zealandia, West Antarctica, and/or Patagonia (Fanning et al., 2011; Elsner et al., 2013; Elliot, et al., 2016; Elliot et al., 2017). This contribution presents the first study that combines zircon U–Pb geochronology, trace elements, and Hf isotopes for volcanoclastic sediments in the TAM in order to determine major periods of arc volcanism, the relative roles of crustal growth and recycling, and reconstruct the large–scale tectonic history of the Antarctic sector arc of the Gondwana margin. These data are further interrogated along–side data from other portions of the margin to infer the geodynamic and mantle evolution of the Antarctic sector relative to the South American and Australian sectors.

## **Geologic Background**

Volcaniclastic sedimentary rocks of the Hanson and Fremouw Formations are amongst the youngest rocks (the Victoria Group) of the Devonian to Lower Jurassic strata of the Beacon Supergroup found throughout the TAM (Fig. 2). The Beacon Supergroup was deposited in the Transantarctic Basin that extends roughly the length of the TAM and formed between the stable East Antarctic Craton and the active magmatic arc of the paleo-Pacific Gondwana margin (Collinson et al., 1994). The oldest sediments of the Beacon Supergroup, the Taylor Group, are separated unconformably from the crystalline basement (Granite Harbour Intrusives, GHI, Gunn and Warren, 1962) of the Neoproterozoic to Ordovician Ross Orogen by the Kukri Erosion Surface (LeMasurier and Landis, 1996). Pre-Ross-age igneous rocks in the TAM are limited to Proterozoic to Mesoarchean orthogneisses exposed in the Miller Range, cTAM (Goodge and Fanning, 2016).

The GHI of the Ross Orogen were emplaced between c. 590–485 Ma (Cox et al., 2000; Goodge et al., 2012; Hagen-Peter et al., 2015; Paulsen et al., 2013) and represent initiation of arc magmatism along the Antarctic sector of the paleo-Pacific margin of Gondwana in the Ediacaran (Walker et al., 2013). The Delamarian Orogen in Australia contains correlative rocks to the Ross Orogen, both of which are components of the larger Terra-Australis Orogen (Cawood, 2005; Foden et al., 2006). Isolated examples of Ross-Delamerian-aged rocks also occur in West Antarctica and Zealandia (Gibson and Ireland, 1996; Pankhurst et al., 1998b; Mukasa and Dalziel, 2000; Allibone et al., 2009).

Following the termination of the Ross Orogeny in the Ordovician, the magmatic arc migrated outboard into West Antarctica, the Antarctic Peninsula, and Zealandia (summarized

in Elliot, 2013). During this time the Transantarctic basin developed behind the arc and evolved from a back–arc basin in the Early Permian to a foreland basin during the Gondwanide Orogeny in the Late Permian–Triassic times (Collinson et al., 1994). Major influxes of volcanic detritus into the Transantarctic basin occurred in the late Early Permian with accumulation continuing through the Early Jurassic (Elliot, et al., 2016; Elliot et al., 2017). Volcanic and magmatic rocks similar in age to the volcanic detritus in the Transantarctic basin occur in Zealandia, West Antarctica, the Antarctic Peninsula and Patagonia (summarized in Elliot 2013). For this reason, workers have variously attributed the source of the TAM volcanic detritus to contemporary arc volcanism in one or more of these regions (Elliot and Fanning, 2008; Elsner et al., 2013; Elliot, et al., 2016; Elliot, Fanning, et al., 2016; Elliot et al., 2017; Fanning et al., 2011). However, correlations between the volcanoclastic sedimentary rocks of the Hanson and Fremouw Formations and their potential source region(s) rely chiefly on geochronology rather than a combination of geochronology and complimentary isotopic and elemental tracer data for unaltered/unmodified volcanoclastic sediments or minerals (i.e., zircon). Consequently, previous detrital zircon studies in the TAM have not been able to better constrain the igneous source regions, nor derive an unambiguous record of the geochemical evolution of the arc through time.

### ***Hanson and Fremouw Formations***

Well–exposed sections of Triassic to Jurassic Beacon Supergroup strata in the central TAM (cTAM) contain fluvial sediments of the Triassic Fremouw Formation (Fig. 2;

Collinson et al., 1994; Elliot and Fanning, 2008). Variable amounts of volcanic detritus throughout the Fremouw Formation and the underlying Buckley Formation are inferred to record contemporaneous volcanism sourced from the outboard magmatic arc (Barrett et al., 1986; Elliot and Fanning, 2008). Recent zircon geochronology for the Fremouw Formation provide early Triassic maximum deposition ages of  $245.9 \pm 2.9$  Ma and  $242.3 \pm 2.3$  Ma, improving the record of contemporaneous volcanism (Elliot et al., 2017).

Overlying the Fremouw Formation is the Late Triassic Falla Formation and the Early Jurassic volcanoclastic-rich Hanson Formation. The Hanson Formation consists of tuffs, tuffaceous sandstones, arkosic grits and sandstones, and lapillistones that comprise a 235 m thick section at the type locality at Mount Falla (Fig. 2; Elliot, 1996; Elliot, et al., 2016). The only other section of correlative Early Jurassic reworked silicic tuffs with exposed upper and lower contacts, the Shafer Peak Formation, occurs in the Deep Freeze Range in northern Victoria Land (NVL, Fig. 1B, Schoener et al., 2007; Elsner et al., 2013). Tuffs of the Hanson Formation are dacitic to rhyolitic in composition ( $\sim 67$  to 78 wt %  $\text{SiO}_2$ ) with the majority containing evidence for fluvial reworking, with relatively few primary tuffs that, where present, are interpreted to represent unmodified airfall deposits resulting from distal (super)plinian eruptions (Elliot, 2000; Elliot et al., 2007; Elliot, et al., 2016). Whole-rock geochemistry and Ar–Ar geochronology are compromised by admixed detrital material and zeolite alteration (Elliot et al., 2007). However, whole rock major- and trace-elements, and Sr and Nd isotopic data for the least modified tuffs suggest derivation from a volcanic arc (Elliot, et al., 2016).

The Hanson and Shafer Peak Formations are designated Early Jurassic in age because they are younger than the Upper Triassic *Dicrodium*-bearing sandstones of the underlying

Falla (cTAM) and Section Peak (NVL) Formations and are overlain by the ~182.8 Ma Kirkpatrick lavas and pyroclastics of the Prebble and Exposure Hill Formations (Fig. 2; Burgess et al. 2015). An early Jurassic age for tuffs of the Hanson Formation is supported by U–Pb zircon ages of  $182.7 \pm 1.8$  Ma,  $186.2 \pm 1.7$  Ma, and  $194.0 \pm 1.6$  Ma (Elliot et al., 2007; Elliot et al., 2016). These age constraints indicate that Hanson tuff deposition continued up to, and was perhaps contemporaneous with, emplacement of mafic sills and lavas of the Early Jurassic Ferrar Large Igneous Province (LIP) that forms a 3500 km linear belt along the TAM (Elliot and Fleming, 2004; Burgess et al., 2015). However, the tectono–magmatic relationship between Early Jurassic volcanism as preserved in the Hanson Formation and the Ferrar LIP magmatism remains unknown (Elliot et al., 2007). U–Pb detrital zircon dates from Shafer Peak and Section Peak formations provide maximum deposition ages spanning from ~190 Ma through the Upper Triassic (Elsner et al., 2013). All of these formations also contain significant proportions of principally Ediacaran to Ordovician and late Mesoproterozoic to early Neoproterozoic detrital zircon, i.e., a typical “Gondwana Signature,” inferred to originate from erosion of proximal crystalline basement and/or lower Paleozoic strata, recycling from underlying strata, or from similar aged rocks outboard in West Antarctica and Zealandia (Elliot et al., 2015, 2016b, 2017).

### ***Potential volcanic sources***

Numerous examples of Paleozoic–Mesozoic magmatic and volcanic potential source rocks have been discovered throughout the paleo–Pacific margin of Gondwana (Fig. 1B;

Elliot, 2013). However, notwithstanding complications from contamination and/or alteration of isotopic ratios by detrital components and zeolite alteration, Elliot et al. (2007; 2016) suggested that dissimilar whole-rock Sr and Nd isotopic compositions of available Mesozoic West Antarctic magmatic rocks indicates they are not a direct source for the Early Jurassic Hanson Formations. Despite a lack of isotopic data, Permian and Triassic arc-related rocks within West Antarctica and Patagonia have also been suggested to represent potential source regions for Permian–Triassic volcanoclastic units in the cTAM (Fanning et al., 2011; Elliot et al., 2017).

Potential sources also exist in Zealandia, where both *in-situ* magmatic rocks and detrital zircons record arc activity throughout the Mesozoic and earlier (Fig. 1B; Elliot, 2013; Kimbrough et al., 1994; Adams et al., 2002; Adams et al., 2013; Mortimer et al., 2015). Nevertheless, unexposed/undiscovered magmatic rocks in West Antarctica (e.g., Marie Byrd Land), remain the prevailing volcanic source region hypothesis for volcanic detritus material in the cTAM Beacon Supergroup (Elliot, et al., 2016; Elliot et al., 2017; Elsner et al., 2013).

## **Sampling and Methods**

This study presents zircon geochronology and geochemistry from 25 rock samples of the Hanson Formation and 5 rock samples of the Fremouw Formation selected from the Polar Rock Repository ([doi:10.7289/V5RF5S18](https://doi.org/10.7289/V5RF5S18)) representing various stratigraphic heights and sections in the cTAM. Zircons were separated using standard mineral separation techniques (i.e., disk milling, water table, magnetic separation, and heavy liquids). Representative

zircons from each sample were mounted in epoxy and polished to expose equatorial sections. Prior to isotopic analysis, zircons were imaged via Cathodoluminescence (CL) on an FEI Quanta400f scanning electron microscope (SEM) and used to guide selection of locations for LASS (U–Pb and trace elements) and Lu–Hf measurements.

Zircon U–Pb isotopes and trace element concentrations were obtained simultaneously with using the ‘split stream’ approach (Kylander–Clark et al., 2013) at UCSB under standard operating conditions (McKinney et al., 2015). Instrumentation consists of a 193 nm ArF excimer laser ablation (LA) system coupled to Nu Plasma high–resolution multi collector–inductively coupled plasma mass spectrometer (MC–ICP–MS) for U/Pb and an Agilent 7700S Quadrupole ICPMS for trace elements. Between 60 and 100 grains were measured for U–Pb and trace element analysis from each sample. Subsequent Lu–Hf analyses were performed by LA–MC–ICPMS exclusively on zircon younger than Ordovician ( $n = 15$  per sample) to better characterize the geochemistry of post–Ross–aged zircon. All data reduction was performed using Iolite v2.5 (Paton et al., 2010, 2011) and  $^{207}\text{Pb}$  corrected  $^{206}\text{Pb}/^{238}\text{U}$  ages were calculated for zircon younger than c. 800 Ma using the method of Andersen (2002) and ISOPLOT/EX (Ludwig, 2003). Detailed analytical methods, data reduction protocols and results of reference zircon analyses and unknown data are in the Supplementary Information, and Datasets S1 and S2 provided in the Appendix (Patchett and Tatsumoto, 1980, 1981, Wiedenbeck et al., 1995, 2004; Chu et al., 2002; Jackson et al., 2004; Thirlwall and Anczkiewicz, 2004; Woodhead and Hergt, 2005; Blichert-Toft, 2008; Sláma et al., 2008; Liu et al., 2010).

## Results

### *Geochronology*

22 of the 25 samples of the Hanson Formation and all samples of the Fremouw Formation contain zircon age populations near the inferred stratigraphic age of the sample and allow for determination of maximum deposition ages (summarized in Table 1). In addition, populations of older detrital zircon are also present (representative examples are plotted in Fig. 3). To compute maximum depositional ages, Kernel Density estimates (KDE, Vermeesch, 2012) were constructed for each sample using only zircon near the stratigraphic age of the formation (i.e., zircon  $< 205$  Ma for the Hanson Formation and  $< 260$  Ma for the Fremouw Formation) and a subset of the youngest of those dates were used to calculate a weighted mean age (Fig. 3). Overall, maximum deposition ages young upward, consistent with the stratigraphic relationships, and range from  $199.5 \pm 0.7$  to  $184.9 \pm 1.3$  Ma for the Hanson Formation and  $247.9 \pm 1.7$  to  $241.2 \pm 1.3$  Ma for the Fremouw Formation. These ages support an Early Jurassic depositional age for the Hanson Formation and an Early to Middle Triassic age for the Fremouw Formation (Collinson and Elliot, 1984; Elliot, Larsen, et al., 2016; Elliot et al., 2017).

The remaining zircon in each sample ( $> 205$  Ma in the Hanson Formation and  $> 260$  Ma in the Fremouw) make up a considerable proportion of the total data, ranging from  $\sim 17$  to  $68$  % of measured zircon in each sample (Fig. 3). To enable direct comparison amongst all data, zircon in the Hanson Formation and Fremouw Formation are compiled and illustrated on a single KDE (Fig. 4). The most abundant zircon sub-populations in both formations are

those near the formation's stratigraphic age. The Hanson Formation, however, also contains a continuous range of zircon ages from the Early Jurassic to the Late Permian as well as a minor Devonian–Carboniferous population. Similarly, the Fremouw Formation contains an overlapping Permo–Triassic sub–population but a more abundant Devonian–Carboniferous sub–population than samples of the Hanson Formation. Combined, the Hanson and Fremouw formations contain zircon ages ranging from 266 to 183 Ma and 367 to 328 Ma (Fig. 4) In addition, approximately one quarter of all analyzed zircon from both formations are Ordovician or older, and collectively represent a typical “Gondwana Signature,” characterized by a peak between 550 to 490 Ma (corresponding to the Ross–Delamarian Orogeny), a peak between 1210 to 1000 Ma (corresponding to the Grenville Orogeny), and a minor component older than 1.3 Ga (not shown).

### *Trace elements*

Zircon trace element data are provided in Dataset S1 and discriminatory trace elements and ratios, i.e., Hf ppm and Th/U, are plotted in Fig 5. The ‘short’ classification and regression tree (CART) were applied to the zircon trace element data to define source rock type (Belousova et al. 2002). Figure 5 suggests a change in source rock type through time, from predominantly granitoid during the Ross Orogeny to dolerite in the Devonian–Jurassic arc, with 96 % of zircon with >10150 Hf ppm classified as granitoid, 97 % with 8000–10150 Hf ppm classified as dolerite, and zircon with <8000 Hf ppm classified as either basalt (89%) or carbonatite (11%) (Fig. 5A). Overall, the average ( $\pm 1$  SD) zircon Hf concentration

decreases through time from  $10850 \pm 1400$  ppm during the Ross–Orogeny,  $9770 \pm 1560$  ppm for the Devonian—Carboniferous,  $9630 \pm 1430$  ppm for the Permian—Triassic, and  $9200 \pm 1420$  ppm for the Early Jurassic. Similarly, the average ( $\pm 1$  SD) zircon Th/U increases steadily through time from  $0.51 \pm 0.29$  during the Ross Orogeny to  $1.06 \pm 0.52$  in the Early Jurassic, and a small population of exclusively Ross-age zircon yields zircon with Th/U  $< 0.1$  potentially indicative of a metamorphic origin (Rubatto, 2002). Similarly, Figure 5B shows a decrease in granitoid source rock type from 62 % during the Ross Orogeny to 21 % in the Early Jurassic. This decrease is correlated with a concomitant increase in mafic source rock type (i.e., basalt + dolerite) from 31 % during the Ross Orogeny to 77 % in the Early Jurassic.

### *Hafnium isotopes*

Zircon Hf isotope data are provided in Dataset S2. To better characterize the geochemical evolution of post–Ross-age arc magmatism, Lu–Hf isotopic measurements were exclusively made on 266 – 183 Ma and 367 – 328 Ma zircon sub–populations (Fig. 6). These data are combined with recent data for the Ross Orogen (Hagen–Peter et al., 2015) to illustrate the zircon Hf isotopic evolution of the arc as recorded in the Transantarctic Mountains. 95% of zircon with ages between 205 – 183 Ma ( $n = 273$ ) record initial  $\epsilon_{\text{Hf}}$  values of  $-1.8$  to  $+6.6$ . Similarly, approximately 97% of zircon dated between 270 – 240 Ma ( $n = 97$ ) yield initial  $\epsilon_{\text{Hf}}$  values of  $-0.4$  to  $+13.9$ , overlapping the ‘new crust’ evolution line

(Dhuime et al., 2011) and the depleted mantle evolution line (Vervoort and Blichert-Toft, 1999). Finally, all 367 – 328 Ma zircon (n = 37) range from –1.8 to +10.3 initial  $\epsilon_{\text{HF}}$ .

## **Discussion**

### ***Zircon geochronologic record in the cTAM***

The 266 – 183 Ma and 367 – 328 Ma sub-populations preserved in the Hanson and Fremouw formations provide a comprehensive archive of post-Ross-age detrital zircon in the Beacon Supergroup consistent with, and significantly expanding on, the published data (Elliot and Fanning, 2008; Elliot et al., 2016b, 2017). Our data are characterized by large proportions of zircon ages close to the stratigraphic age of the sample (due to contemporaneous volcanism) and, therefore, reflect deposition adjacent to a magmatic arc along a convergent plate margin (Cawood et al., 2012). Consequently, our observations agree with those of Elliot et al. (2016) and Elliot et al. (2017) who argue that these age ranges correspond to continuous periods of intensified volcanism in the arc directly outboard of the Transantarctic Basin. Previous workers have also thoroughly reviewed the provenance of the characteristic “Gondwana Signature” observed in these rocks (Elliot et al., 2015, 2016b, 2017).

Tuffs of the Hanson Formation are the best-preserved sequence of volcanoclastic sediments in the TAM and contain fine- to very-fine-grained silicic ash with distal Plinian eruption sources and medium-grained tuffs and accretionary lapilli that indicate more

proximal sources (Elliot, et al., 2016). According to plate reconstructions, the arc would have been a maximum of 600–800 km from the cTAM in the Early Jurassic (Lawver et al., 2014; Elliot, et al., 2016). Although the inferred ash transport distances are considerable they are not without precedent. Recent workers have shown that Cretaceous super-eruptions along the paleo-Pacific margin of Gondwana transported zircon some 2300 km from their volcanic source (Barham et al., 2016). It is therefore reasonable to conclude that the detrital zircon record from the cTAM may be an integrated record of active volcanism from a significant portion of the outboard arc.

Existing detrital and crystalline basement zircon dates from West Antarctica, southern South America (i.e., Patagonia), Zealandia, and Australia indicate that all regions record overlapping periods of arc-related igneous activity in the Paleozoic and Mesozoic. A thorough review of the Devonian through Early Jurassic arc recorded in these regions is provided by Elliot (2013) and is therefore only briefly summarized here. In particular, granites and detrital zircon associated with the Lachlan and New England orogenies of Australia record a Devonian–Carboniferous and a Permian–Triassic arc (Cawood, 2005; Veevers et al., 2006; Cawood and Buchan, 2007; Kemp et al., 2009; Cawood et al., 2011; Phillips et al., 2011; Shaw et al., 2011; C. J. Adams et al., 2013; Jeon et al., 2014; Li et al., 2015; Shaanan et al., 2015). The Median Batholith and volcanoclastic sediments of Zealandia contain a similar record of arc activity for these time periods (Kimbrough et al., 1994; Cawood et al., 1999; Mortimer et al., 1999, 2014, 2015; Adams et al., 2007; Allibone et al., 2009; Tulloch et al., 2009; C J Adams et al., 2013a, 2013b). Detrital and igneous dates for the southern section of the South American arc compiled by Pepper et al. (2016) provide a comprehensive record of near continuous activity with several pulses of increased magma

production throughout the Paleozoic and Mesozoic. The record is more scattered in the ice-covered regions of West Antarctica (i.e., Marie Byrd Land, Thurston Island, the Ellsworth–Whitmore block, and the Antarctic Peninsula), but limited geochronologic data available suggest the bedrock contains Devonian through Early Jurassic magmatic and volcanic rocks (Pankhurst et al., 1993; Mukasa and Dalziel, 2000; Millar et al., 2002; Yakymchuk et al., 2015; Craddock et al., 2017a, 2017b; Riley et al., 2017).

Comparing the detrital zircon data from Pepper et al. (2016) to detrital zircon data from Australia and Zealandia (combined) illustrates broad differences in the timing of arc magmatic activity between these regions and the cTAM (Fig. 7). The most important similarity between these regional datasets is that they both display a nearly continuous record of zircon dates from the Devonian through the Early Jurassic. However, an apparent difference emerges between the timing of pronounced peaks representing increased magmatic activity. Data from southern South America indicate increased magmatic activity from 400 – 350 Ma (or older), 325 – 245 Ma, and a sharp peak in the Early Jurassic that overlap with magmatic lulls (or gaps) in the data from Australia and Zealandia. Increased magmatic activity in Australia and Zealandia occurs from 360 – 295 Ma and 275 – 215 Ma, partially overlapping lulls in the South American data and the zircon peaks from the cTAM. Along-arc variation in episodic behavior similar to that observed here from South America to Zealandia–Australia has also been observed in other arcs and may indicate a major change in tectonism or subduction dynamics (Paterson and Ducea, 2015) between these two regions. The similarity between the cTAM zircon ages and the detrital zircon record from Australia and Zealandia suggests that they may have a shared history of tectonism and subduction, and that a continuous arc system may have extended from Australia, through Zealandia, and

outboard of the cTAM from the Devonian to at least the Triassic. Based on the difference in zircons etc. this arc system is likely to have been decoupled, at least temporally, from the southern South American sector arc.

Studies of the crystalline basement and detrital zircon record of the Antarctic Peninsula indicate that it is more closely related with the arc history of southern South America, i.e., Patagonia, rather than Zealandia or Australia (Bradshaw et al. 2012; Castillo et al. 2015; Fanning et al. 2011). For this reason, and for comparative purposes, the Antarctic Peninsula data are grouped with the South American data.

### ***Zircon trace element petrochronology***

As mentioned earlier, the rocks studied here contain older detrital zircon comprising a typical “Gondwana Signature” (Fig. 4). The presence of these zircon, as well as the range of zircon dates discussed above, in all of the samples included in this study, indicates that whole rock elemental and isotope geochemistry reflects the concentration–weighted cumulative contribution of material from numerous isotopically and temporally distinct reservoirs and therefore does not accurately record the time–resolved isotopic evolution of the magmatic source. For this reason we focus exclusively on zircon isotope and elemental geochemistry to track the geochemical evolution of the arc through time.

The zircon trace element data reported here are the first of their kind for Early Jurassic and Permian strata of the Transantarctic Mountains and provide insight into the geochemical evolution of the arc. The utility of detrital zircon trace element geochemistry is

in relating the concentrations and ratios of key trace elements to either a particular source rock type (Belousova et al., 2002b), a tectono–magmatic setting (Grimes et al., 2015), and/or to the concentration and/or ratio of various trace elements in the source rock (Chapman et al., 2016). These techniques have been met with some skepticism, partially due to the difficulty in determining reliable zircon/bulk rock trace element partition coefficients (Hoskin and Ireland, 2000; Chapman et al., 2016). Nevertheless, application of the techniques from Grimes et al. (2015) and Chapman et al. (2016) indicate that zircon from the cTAM fall on the magmatic arc array and have light rare earth element enrichment, typical of magmatic arcs, supporting our assertion that the source region(s) for the CTAM zircon is located in the arc outboard of the paleo–Pacific margin.

Application of the short ‘CART’ classification tree of Belousova et al. (2002b), yields apparent variations in rock type through time, with a mostly granitoid source rock during the Ross Orogeny and a predominantly mafic source rock (basalt and dolerite) for the Devonian–Jurassic arc (Fig. 5). Zircon Hf concentration is a distinguishing characteristic of the ‘short’ CART tree, and the data show a decrease in Hf concentration from the Ross Orogeny through the Devonian–Jurassic zircon ages indicating a switch to more juvenile mafic magmatism following the termination of the Ross Orogeny. The classification of dolerite or basalt for many of the Early Jurassic zircon from the Hanson Formation is apparently at odds with petrographic studies and whole rock geochemical data for Hanson tuffs that suggests a primarily rhyolitic source from explosive plinian eruptions interpreted to record silicic arc volcanism (Elliot et al., 2016). In contrast, the designation of Ediacaran–Ordovician zircon as mostly granitoid appears to be an accurate classification as the corresponding Ross Orogen is dominated by granitic batholiths (e.g., Cox et al., 2000). The apparent mismatch between

zircon geochemistry and bulk rock geochemistry of Permian–Early Jurassic volcanoclastic sediments may be a result of the relatively long transport distances. It has been demonstrated that during atmospheric transport, crystal fractionation can occur, modifying the apparent bulk composition of the resulting sediments (Fruchter et al., 1980; Hinkley et al., 1980; Taylor and Lichte, 1980). This suggests that the volcanic components in the Hanson and Fremouw formations may in fact reflect mafic volcanism rather than silicic. In any event, a decrease in zircon Hf concentration correlated with an increase in Th/U indicates a more mafic, primitive, less evolved, arc system (McKay et al., 2016a) prevailed in Devonian through Early Jurassic time compared to the Ross Orogeny (Fig. 5). This switch from felsic–to mafic–dominated magmatism may indicate the development of an extensional or retreating arc system following the termination of the advancing tectonics during the Ross Orogeny (Collins, 2002a).

### ***Zircon Hafnium isotopes and geodynamic evolution***

The positive initial  $\epsilon_{\text{Hf}}$  values for Devonian and younger zircons contrast with negative values for zircon from granites of the Ross Orogen (Fig. 6; Hagen-Peter et al., 2015). The relative change in zircon initial  $\epsilon_{\text{Hf}}$  through time in magmatic arcs has been linked to the tectonic evolution of the arc (Kemp et al., 2009). In particular, Kemp et al. (2009) argued that a relative increase in initial  $\epsilon_{\text{Hf}}$  is indicative of a retreating arc system associated with an outboard migration of subduction zone magmatism during slab rollback and associated crustal extension and thinning. The increase in initial  $\epsilon_{\text{Hf}}$  in the inferred retreating

arc system results from either a reduced amount of crustal assimilation during crustal extension and thinning and/or melting of upwelling depleted asthenospheric mantle. Conversely, an advancing arc system is associated with a decrease in the initial  $\epsilon_{\text{Hf}}$  composition during periods of compression when the slab is advancing and the arc is contracting (i.e., crustal thickening). Hf compositions decrease in advancing arc systems due to increasing crustal assimilation during crustal thickening and/or mantle enrichment by an elevated contribution of subducted material to the mantle wedge. This model of “tectonic switching” (Collins, 2002a) provides a conceptual framework within which to interpret the data from the cTAM. It should be noted, however, that alternatives to the Collins (2002a) model used here have been proposed for the paleo-Pacific margin of Gondwana (Crawford, 2003; Aitchison and Buckman, 2012; Gibson et al., 2015). These models generally support “quantum tectonics” which refers to switching of subduction polarity, subduction flip, along the Gondwana margin resulting in periods of island arc formation, accretion, and switch to continental arc formation (Aitchison and Buckman, 2012). This is in contrast to the “accordion tectonics” hypothesis endorsed in this study that supports a nearly continuous continental arc, i.e., accretionary orogen, undergoing periods of extension during slab retreat, and compression during slab advance (Collins, 2002a; Cawood et al., 2009). For our purposes, we interpret our data within the model of accretionary orogenesis because it has been widely applied to zircon Hf isotope datasets along the paleo-Pacific margin of Gondwana (e.g., Kemp et al., 2009; Rey et al., 2016; Pepper et al., 2016; Phillips et al., 2011; Li et al., 2015), and there remains no consensus on the appropriate tectonic model for the evolution of the margin (Aitchison and Buckman, 2013; Fergusson, 2013).

Recent studies suggest the Ross Orogeny mantle source was significantly modified due to the addition of subducted ancient crustal material, producing a mantle source with enriched, unradiogenic initial  $\epsilon_{\text{Hf}}$  compositions (Hagen–Peter et al., 2015; Couzinié et al., 2016). Consequently, the positive initial  $\epsilon_{\text{Hf}}$  values for zircon younger than the Ordovician cannot be explained without the addition of a juvenile, primitive depleted mantle component to the arc magma source region(s) following the Ross Orogeny. For this reason the increase in initial  $\epsilon_{\text{Hf}}$  from the Ordovician to the Devonian is interpreted as a change in the tectonic conditions from an advancing arc system undergoing crustal thickening and crustal recycling in the Ross Orogeny to a retreating arc system undergoing extension and reduced crustal recycling in the Devonian–Carboniferous (Cawood and Buchan, 2007). The period between the Ordovician and Devonian that contains few zircon ages possibly represents a magmatic lull in the Antarctic sector arc, but the lack of data precludes us from determining the precise time of tectonic switching from an advancing to a retreating system. Even though Devonian–Carboniferous magmas represent increased juvenile mantle melting compared to the Ross Orogeny, the zircon initial  $\epsilon_{\text{Hf}}$  is still far below the depleted mantle evolution line and also varies considerably from  $-2$  to  $+10$ . The variation in Hf composition is interpreted to represent either a minor contribution of subducted crustal material in an already heterogeneous mantle source and/or variable crustal assimilation during magma ascent. In either case, only a few of the lowest initial  $\epsilon_{\text{Hf}}$  zircon from the Devonian–Carboniferous can be explained by complete recycling of Ross–aged or older crust (assuming a  $\text{Lu}/\text{Hf} = 0.012$ , Rudnick and Gao, 2003). A similar case can be made for Permian–Triassic zircon, in which the  $\epsilon_{\text{Hf}}$  ranges from  $0$  to  $+14$  with an overall increase in the initial  $\epsilon_{\text{Hf}}$  composition through time. This suggests generation of juvenile crust related to continued extension and outboard

migration of the magmatic arc during slab retreat in the Late Permian to Early Triassic. The large variation in initial  $\epsilon_{\text{Hf}}$  is again interpreted as reflecting either a heterogeneous mantle source and/or assimilation of crust during ascent. Much of the Permian–Triassic initial  $\epsilon_{\text{Hf}}$  data, however, can be explained by recycling of juvenile Devonian–Carboniferous crust (assuming a  $\text{Lu}/\text{Hf} = 0.012$ ), so the degree of crustal growth in the Permian–Triassic is inferred to be limited. It is probable that Permian–Triassic magmas ascended through juvenile crust produced in the Devonian–Carboniferous as well as older crust (i.e., Ross, Grenville, etc.) and assimilated multiple crustal reservoirs. This makes it difficult to assess the amount of crustal growth that may have occurred during this time period.

In the Early Jurassic, initial  $\epsilon_{\text{Hf}}$  zircon composition shifts to more intermediate values of  $-1.8$  to  $+6.6$ , indicating increased crustal recycling relative to the Triassic. It is unclear whether these lower initial  $\epsilon_{\text{Hf}}$  compositions are generated by subduction modification of the mantle source and/or by crustal assimilation; however, a relative decrease in initial  $\epsilon_{\text{Hf}}$  implies a contraction of the magmatic arc during a switch to an advancing tectonic regime. The full range of initial  $\epsilon_{\text{Hf}}$  for the Early Jurassic can be explained by recycling of Devonian–Carboniferous and Permo–Triassic crust (assuming a  $\text{Lu}/\text{Hf} = 0.012$ , Fig. 6).

### ***Pan–paleo–Pacific margin Hf isotopes***

Our new zircon Hf isotope data enable the first opportunity to make broad comparisons between the cTAM and other portions of the paleo–Pacific margin of Gondwana. Compilations of both zircon and whole–rock Hf isotope data from igneous rocks

and detrital zircon (Fig. 8A) separated into two regions, Australia and Zealandia (Red), and South America (blue), and fields of major groupings of data from the cTAM (grey). These comparisons allow tracking of correlations inferred for arc systems and subduction dynamics through time to determine periods in which the Antarctic sector arc may have been coupled tectonically and geochemically with the Australian arc system, the South American arc system, or neither (decoupled). Devonian–Carboniferous zircon Hf data from the cTAM is generally positive and overlaps with data from Australia, Zealandia, and South America. Only data from Australia and Zealandia, however, overlap with the most positive values from the cTAM during this time. Permo–Triassic zircons from the cTAM on the other hand are highly positive and overlap almost entirely with data from Zealandia and Australia and only partially with low initial  $\epsilon_{\text{Hf}}$  values from South America.

The overlap of Permo–Triassic initial  $\epsilon_{\text{Hf}}$  between Australia–Zealandia and the cTAM zircon is a salient observation because it indicates a major period of crustal growth, extension, and slab retreat that was continuous along the arc from Australia through Zealandia, to outboard of the cTAM (Fig. 8 and 9). This is consistent with a stepping out in the position of the plate boundary along Australia and Antarctica during the late Paleozoic to Mesozoic Gondwanide Orogen (Cawood, 2005). The Early Jurassic zircon Hf record from Australia and Zealandia is limited, with only six individual zircon measurements available. Nevertheless, the data from the cTAM overlap with data from both Australia and Zealandia, and South America. South American zircon Hf values have a considerable range with a significant number of negative initial  $\epsilon_{\text{Hf}}$  values that indicate a difference between the South American Early Jurassic arc and the arc outboard of the cTAM. Overall, the generally positive initial  $\epsilon_{\text{Hf}}$  compositions from the Ordovician through the Early Jurassic correlate

strongly with the positive initial  $\epsilon_{\text{Hf}}$  compositions of the Zealandia and Australian sectors of the margin but contrast strongly with the negative values recorded in the South American sector.

To support this postulated shared history between Antarctic and Australian sectors, mean initial  $\epsilon_{\text{Hf}}$  values are calculated in 20 m.y. bins for Zealandia and Australia (red), and South America (blue) (Fig 8B). Calculating mean values enable a more statistically rigorous determination of periods of increasing or decreasing Hf isotope compositions through time and allow identification of periods in which the Australian and South American arc system are geochemically and tectonically decoupled. The Paleozoic history of the Australian arc system, as inferred from this compilation, includes extension, crustal growth, and slab retreat during the Devonian, a period of slab advance and increased recycling in the Carboniferous, and a shift back to crustal growth during slab retreat and extensional tectonics that persists until at least the Middle Triassic. These inferred tectonic switches based on our compilation of Hf isotope data are consistent with, and reinforce, the findings of (Kemp et al., 2009). The Late Triassic and Early Jurassic data from Australia and Zealandia are limited but may indicate a switch to slab advance. Overall, the mean Hf isotopic evolution of the Australian sector arc system represents an extensional (retreating) arc system or orogen (Collins, 2002b; Cawood et al., 2009; Kemp et al., 2009) with major periods of crustal growth during extension and outboard migration of the arc associated with slab rollback.

In contrast to the Australia and Zealandia segment, the Hf compilation from the South American sector illustrates a significantly different inferred geodynamic evolution. In particular, the Paleozoic history is dominated by relatively constant, negative initial  $\epsilon_{\text{Hf}}$  compositions, indicating increased recycling of ancient crust during slab advance, consistent

with previous work (Pepper et al. 2016; Bahlburg et al. 2009). The Late Triassic history of South America reported by Hervé et al. (2014) includes a shift to positive  $\epsilon_{\text{Hf}}$  values and extension following the Gondwanide Orogeny. During Early Jurassic time initial  $\epsilon_{\text{Hf}}$  values return to negative values, suggesting a switch back to advancing tectonics and crustal recycling.

Overall, the initial  $\epsilon_{\text{Hf}}$  composition of the South American arc remains fairly negative throughout the Paleozoic and Early Mesozoic, suggesting that the subduction zone remained proximal to the continental margin and recycling ancient crust in an advancing arc system (Cawood et al., 2009). Previous authors have noted this along arc geochemical and geodynamic variation between South America and Australia (Collins et al., 2011), but the nature of the arc between these two regions (i.e. Antarctica) has, until now, remained largely unknown. Castillo et al. (2015) observed a general increase in Permian detrital zircon initial  $\epsilon_{\text{Hf}}$  from Patagonia to the Antarctic Peninsula and attributed it to decreased sediment erosion and subduction due to Mesozoic glaciation. Similarly, in our compilation we observe an increase in initial  $\epsilon_{\text{Hf}}$  during periods of glaciation in eastern Australia from the mid-Carboniferous (c. 327 Ma) to the early Late Permian (c. 260 Ma) (Fig. 8B; Fielding et al., 2008) that may also correspond to reduced sediment erosion and subsequent subduction rather than a switch to a retreating arc system, as is suggested here. This process, however, cannot explain the high initial  $\epsilon_{\text{Hf}}$  during the Late Permian—Early Triassic (c. 250 Ma) in non-glaciated eastern Australia that match well with our data from the cTAM. We would expect a significant decrease in the initial  $\epsilon_{\text{Hf}}$  during nonglacial periods (e.g., c. 250 Ma) if arc chemistry were controlled by fluctuations in continental erosion related to glaciation rather than geodynamics of the arc system. Instead, it is argued that major periods of juvenile

crustal growth during slab retreat and outboard migration of the Antarctic sector arc and reflect the continuity of the Australian–sector retreating arc into the regions outboard of the TAM, namely Marie Byrd Land and crustal blocks of Zealandia (Fig. 9). This connection is further supported by similarities in zircon ages from the cTAM and detrital zircon from Australia and Zealandia, as discussed above (Fig. 7), and a switch to mafic volcanism indicative of retreating arc systems as identified in our zircon trace element data (Collins, 2002b).

Permian plate reconstructions combined with these new observations indicate that the locus of a major along–arc geochemical and geodynamic shift between Australia and South America occurred in the vicinity of the Thurston Island block and the surrounding area in West Antarctica (Fig. 9). These regions have limited combined precise geochronologic and isotopic data, e.g., zircon U–Pb and Hf isotopes, for Late Paleozoic and Mesozoic rocks. In Marie Byrd Land, the Ford granodiorite suite (375–345) has initial  $\epsilon_{\text{Hf}}$  values ranging from +2 to –5 (Yakymchuk et al., 2015). On Thurston Island, a granodioritic gneiss (349 Ma) has an initial  $\epsilon_{\text{Hf}}$  ranging from +10 to +2, and a Middle Triassic diorite (239 Ma) has an initial  $\epsilon_{\text{Hf}}$  ranging from +0.3 to –7.6 (Riley et al., 2017). Despite the limited dataset, diorite from Thurston Island has similar initial  $\epsilon_{\text{Hf}}$  values to those from the Antarctic Peninsula (Flowerdew et al., 2006) and may reflect a continuity of the South American sector Permo–Triassic advancing arc system. Currently, there are no Permian–Jurassic zircon Hf data available from Marie Byrd Land. However, a granite at Kinsey Ridge in Marie Byrd Land has a Rb–Sr isochron age of  $239 \pm 4$  Ma and an initial  $\epsilon_{\text{Nd}}$  value of +4.7 that corresponds to an initial  $\epsilon_{\text{Hf}}$  value of +9.2, (using the Nd – Hf conversion equation from Vervoort & Blichert–Toft (1999). This hints at a possible source for Middle Triassic zircon in the cTAM

and that a record of Permo–Triassic crustal growth may be present in the Admundsen province of Marie Byrd Land. Ultimately, limited available data support a possible Marie Byrd Land source for the zircon in the cTAM and validate reconstructions that place proto–Marie Byrd Land directly outboard of the TAM in the Paleozoic.

## **Conclusions**

Zircon from volcanoclastic sediments in the cTAM record the timing and geochemical evolution of the Paleozoic–Mesozoic magmatic arc along the paleo–Pacific margin of Gondwana. Post–Ross–age zircon ages correspond to periods of arc volcanism at 266 – 183 Ma and 367 – 328 Ma. Zircon trace element geochemistry is consistent with a more mafic source rock type (i.e, basalt and dolerite) than previously reported and a continental magmatic arc setting. The generally positive initial  $\epsilon_{\text{Hf}}$  zircon values represent juvenile crustal growth during a major period of long–lived slab rollback and upper plate extension that began shortly after, or synchronous with, the termination of the Ross Orogeny. The Hf isotope data record a geodynamic history for the Antarctic sector of the arc that is similar to the Australian sector arc and indicates continuity of an extensional arc system from Australia to Antarctica after ~500 Ma. This extensional arc system underwent an along–arc tectonic switch to advancing compressional tectonism in the South American sector arc throughout at least the Permian.

## **Acknowledgements**

This material is based upon work supported by the National Science Foundation Graduate Research Fellowship under Grant No. 1650114 and support from NSF—ANT—1443296, NSF—ANT—1043152. We are grateful to Anne Grunow and the Polar Rock Repository for providing samples and assisting with sample selection. We also acknowledge the original sample collectors: P.J. Barrett and D.H. Elliot. Special thanks to S. Briggs and R. Holder for fruitful discussions and constructive criticism during preparation of this manuscript. Constructive reviews by P. Cawood, G. Gibson and the associate editor, J. Aitcheson, significantly improved this manuscript. Additional analytical details and data tables can be obtained in the Supplementary Information and Datasets.

## Figures

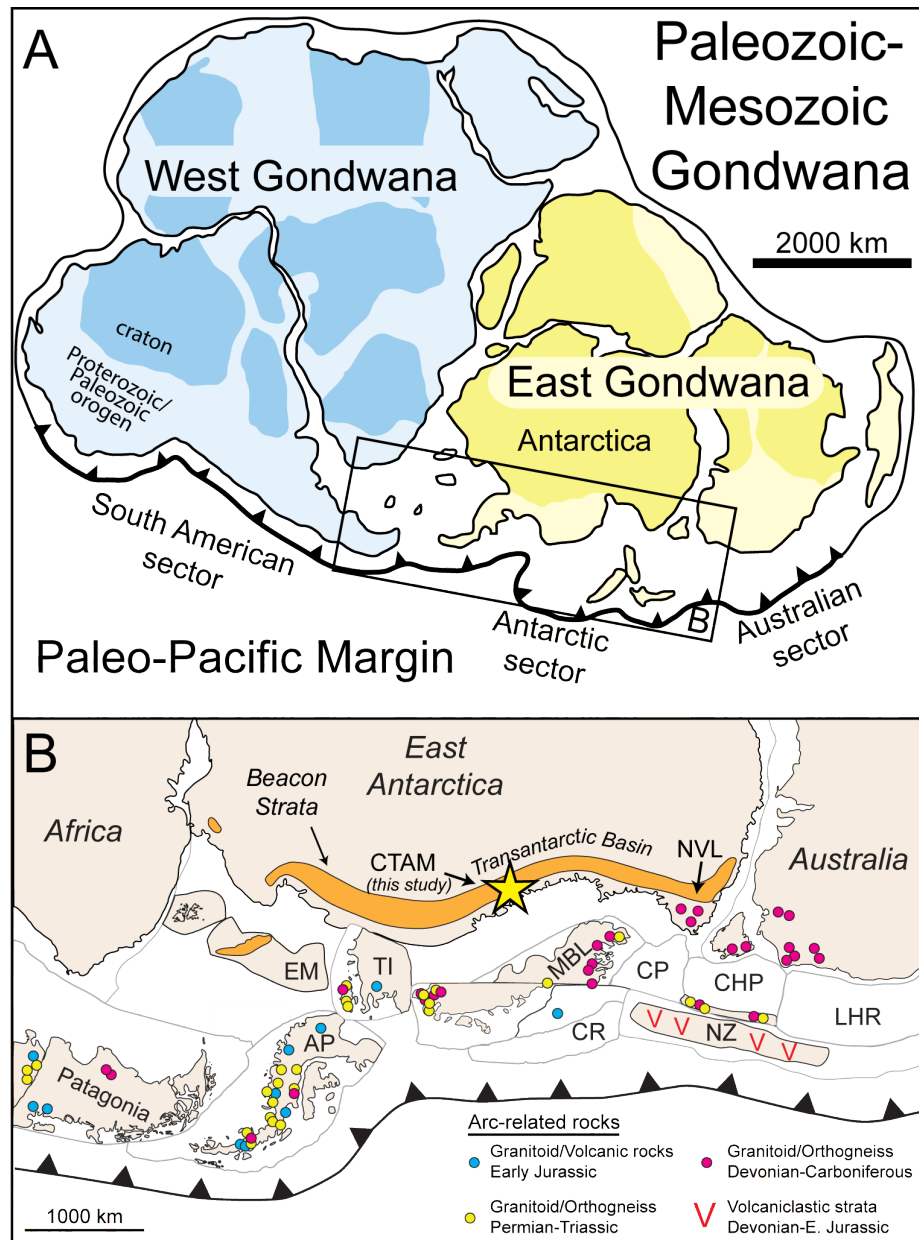


Figure 1. (A) Paleogeographic reconstruction of supercontinent Gondwana during the Paleozoic–Mesozoic, and the major sectors of the active paleo–Pacific margin of Gondwana. (modified from Meert and Lieberman, 2008) (B) Reconstruction of the Antarctic sector of the Gondwana plate margin during the late Paleozoic–early Mesozoic, showing the location of the study area in the cTAM relative to the distribution of Devonian through early Jurassic arc-related rocks located within the various outboard crustal blocks (Elliot, 2013). West Antarctica: EM, Ellsworth Whitmore; TI, Thurston Island; AP, Antarctic Peninsula; MBL, Marie Byrd Land. Zealandia: CR, Chatham Rise; CP, Cambell Plateau; NZ, East New Zealand; LHR, Lord Howe Rise; CHP, Challenger Plateau and West New Zealand.

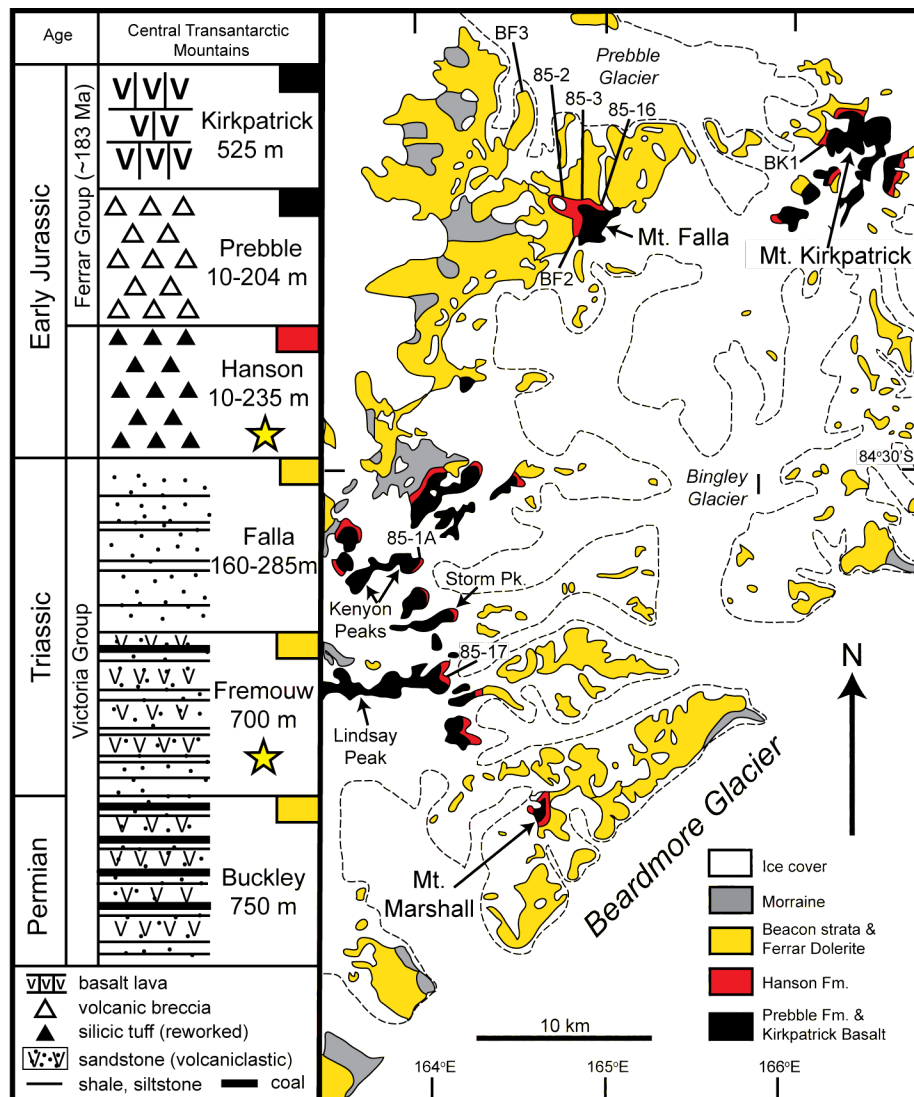


Figure 2. Simplified geologic map of the cTAM and a generalized stratigraphic column. Letters and/or numbers refer to the original collector's sampling locations and measured stratigraphic columns (modified from Elliot, et al., 2016). Shenk Peak, Mount Rosenwald, and Mount Black are out of the map area.

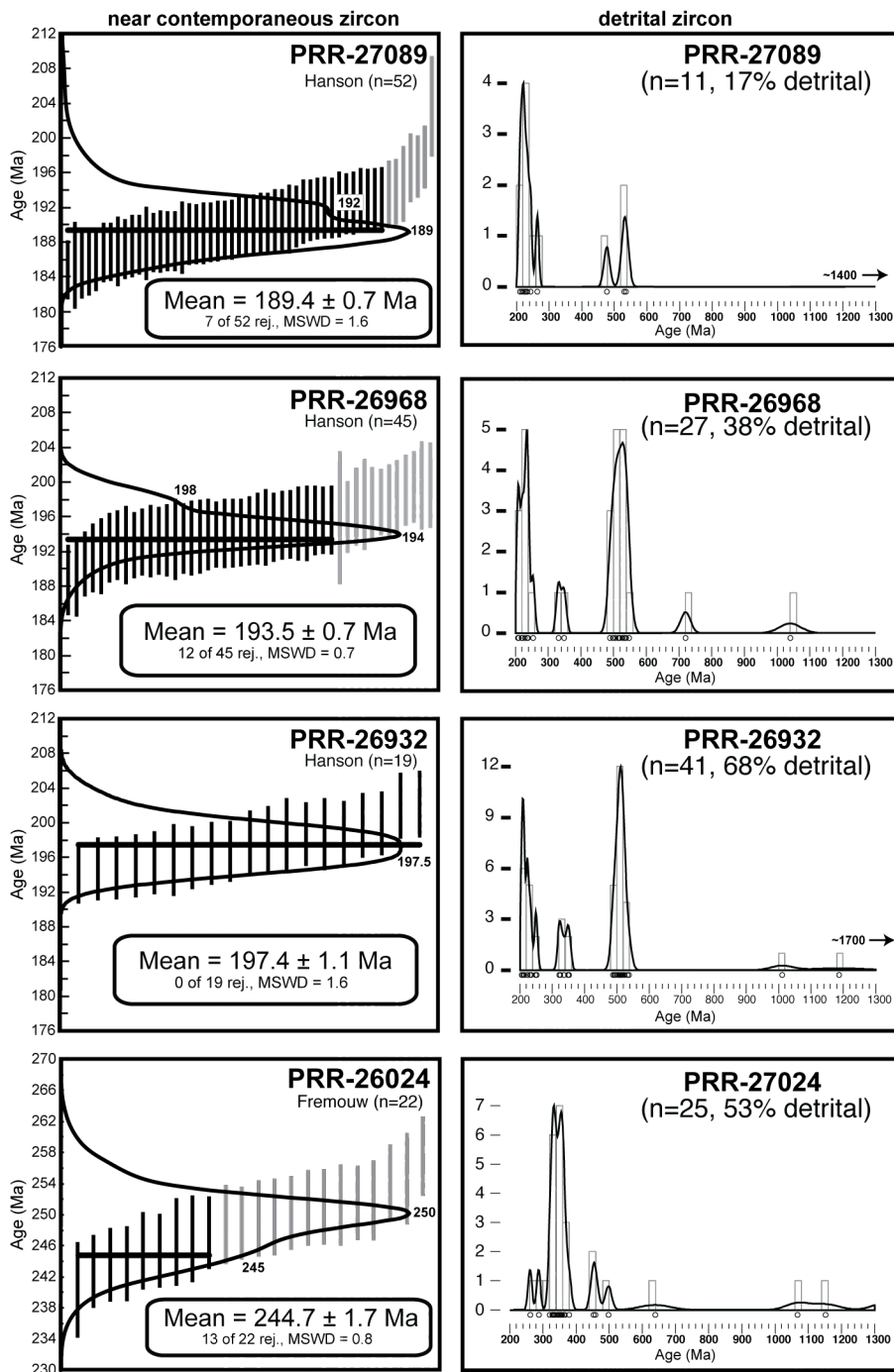


Figure 3. Zircon LASS U–Pb geochronology data for representative samples of the Hanson and Fremouw Formations. Left column: calculated weighted mean  $^{207}\text{Pb}$  corrected- $^{206}\text{Pb}/^{238}\text{U}$  maximum deposition ages for near contemporaneous zircon (see text for explanation). Right column: kernel density estimate (KDE) plot for detrital zircon of the same sample from the left column. See Dataset S1 for full U–Pb dataset.

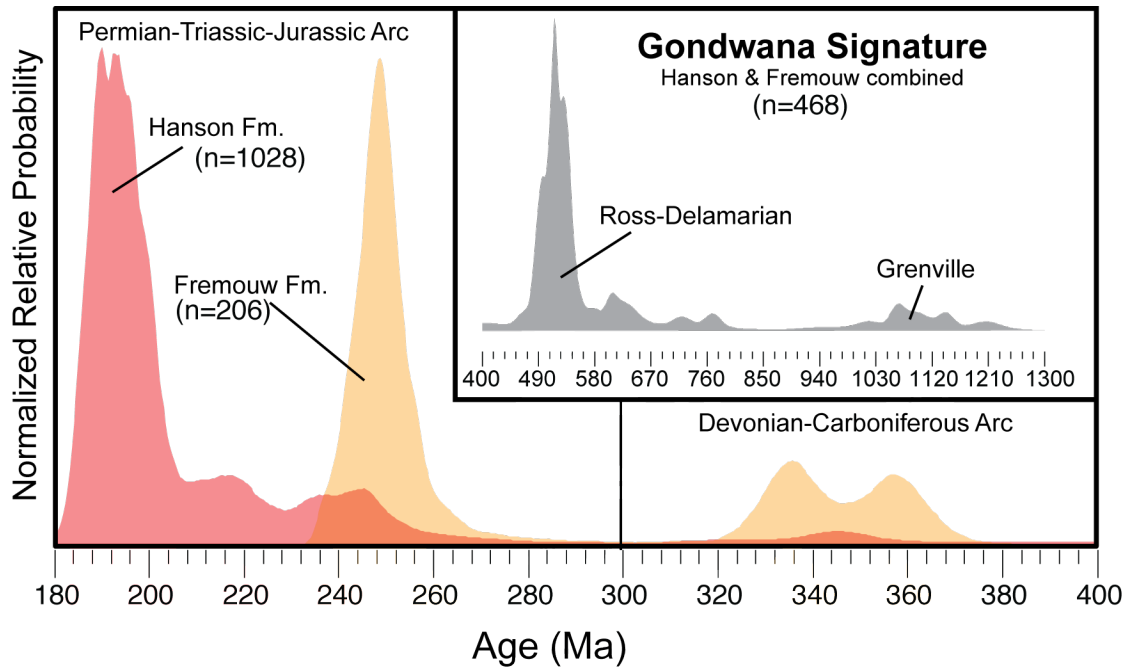


Fig. 4. Kernel density estimate summarizing all zircon U–Pb geochronology data from this study. Devonian and younger zircon ages are grouped according to formation, and all older ages are combined. Zircon ages >1300 Ma have been omitted. See Dataset S1 for full U-Pb dataset.

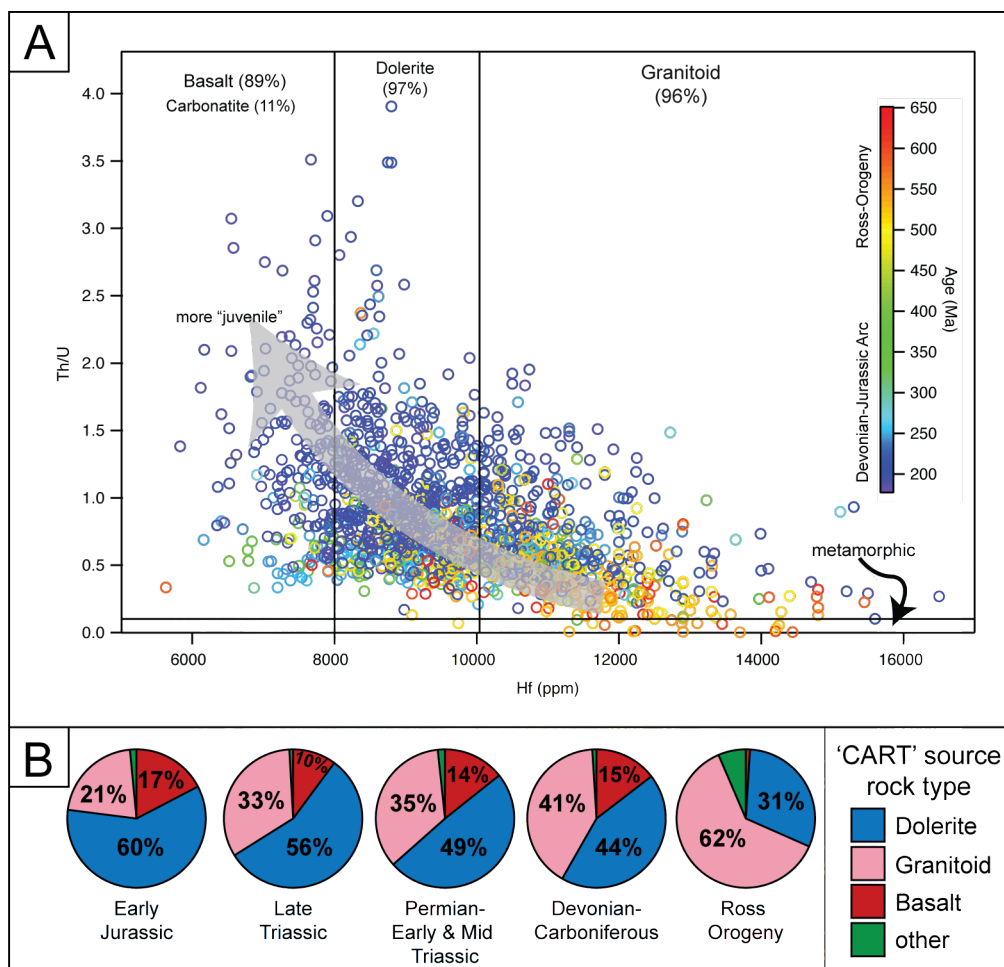


Figure 5. (A) Plot of zircon Hf ppm versus zircon Th/U colored according to the associated  $^{207}\text{Pb}$  corrected– $^{206}\text{Pb}/^{238}\text{U}$  date. Three broad fields of Hf concentration, <8000 ppm, 8000–10150 ppm, and >10150 ppm, are provided based on the short 'CART' system of Belousova et al. (2002b). The percentage of zircon within these fields that correspond to a specific rock type is provided for each field. The field for metamorphic zircon (i.e., Th/U < 0.1) is taken from Rubatto (2002). (B) Summary pie charts of inferred source rock type through time. Source rock type "other" refers to carbonatite, Syenite, nepheline Syenite, and Monzonite (Belousova et al., 2002b). This scheme has a 80 % probability of correctly classifying dolerite zircon, 64 % probability of classifying basaltic zircon as sourced from basalt or dolerite, and 78 to 97 % probability of correctly classifying granitoid zircon (Belousova et al., 2002b). See Dataset S1 for full zircon trace element dataset.

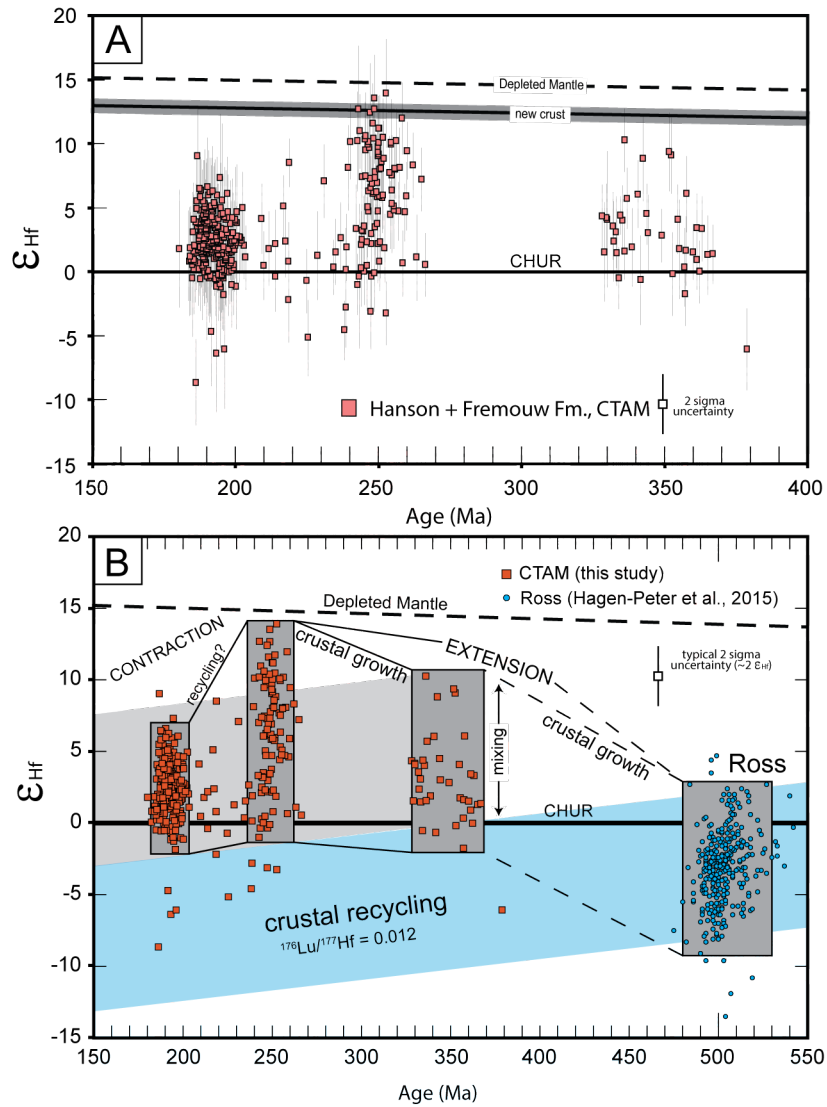


Fig. 6. (A) Zircon age versus initial  $\epsilon_{\text{Hf}}$  plot summarizing all Hf isotopic data from this study. (B) Hf isotopic data from this study combined with data for the Ross Orogen from (Hagen-Peter et al., 2015) and the inferred geodynamic evolution of the Antarctic sector arc system. Inclined grey and blue fields correspond to hypothetic fields of crustal recycling assuming a  $\text{Lu}/\text{Hf} = 0.012$  ((Rudnick and Gao, 2003)). Hf isotopic values for depleted mantle and new crust are from Vervoort and Blichert-Toft (1999) and Dhuime et al. (2011). CHUR—chondritic uniform reservoir. See Dataset S2 for full zircon Hf isotope dataset.

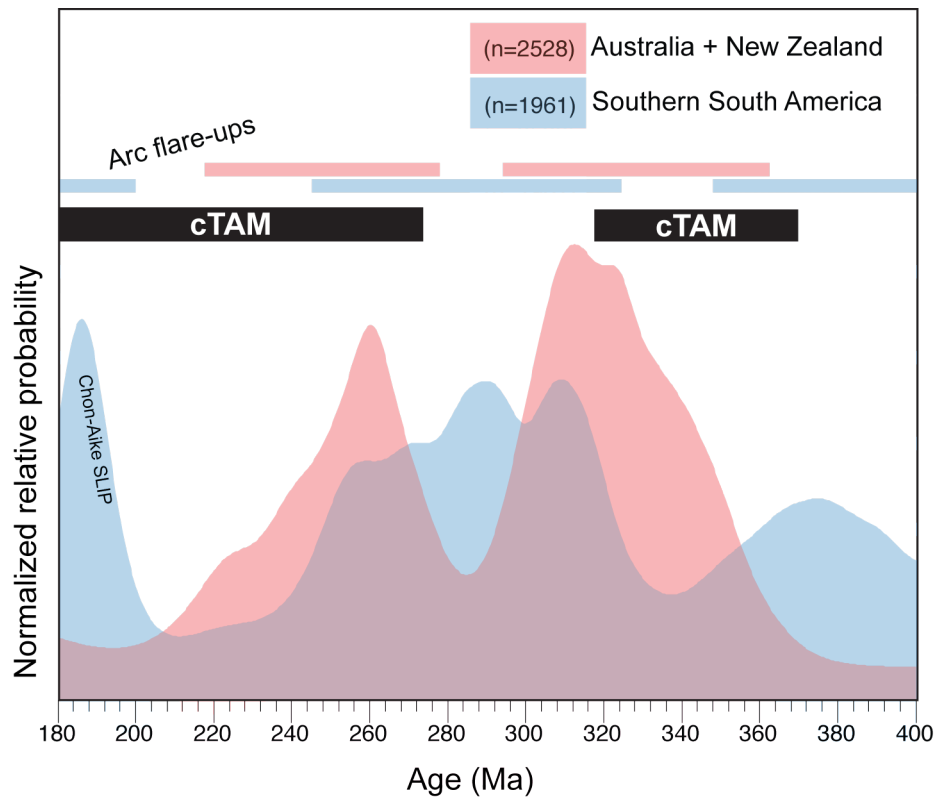


Fig. 7. Compilation of detrital zircon data from Australia–Zealandia (red) and southern South America (blue). Increased magmatic activity corresponds to broad peaks in zircon growth. The range of zircon dates from the cTAM (this study) are provided in black for comparison. Data for Australia–Zealandia are from: Adams et al. (2007, 2013); Scott et al. (2009, 2011); Li et al. (2015); Shaanan et al. (2015); Murgulov et al. (2007). Data for southern South America are from new and compiled data of Pepper et al. (2016).

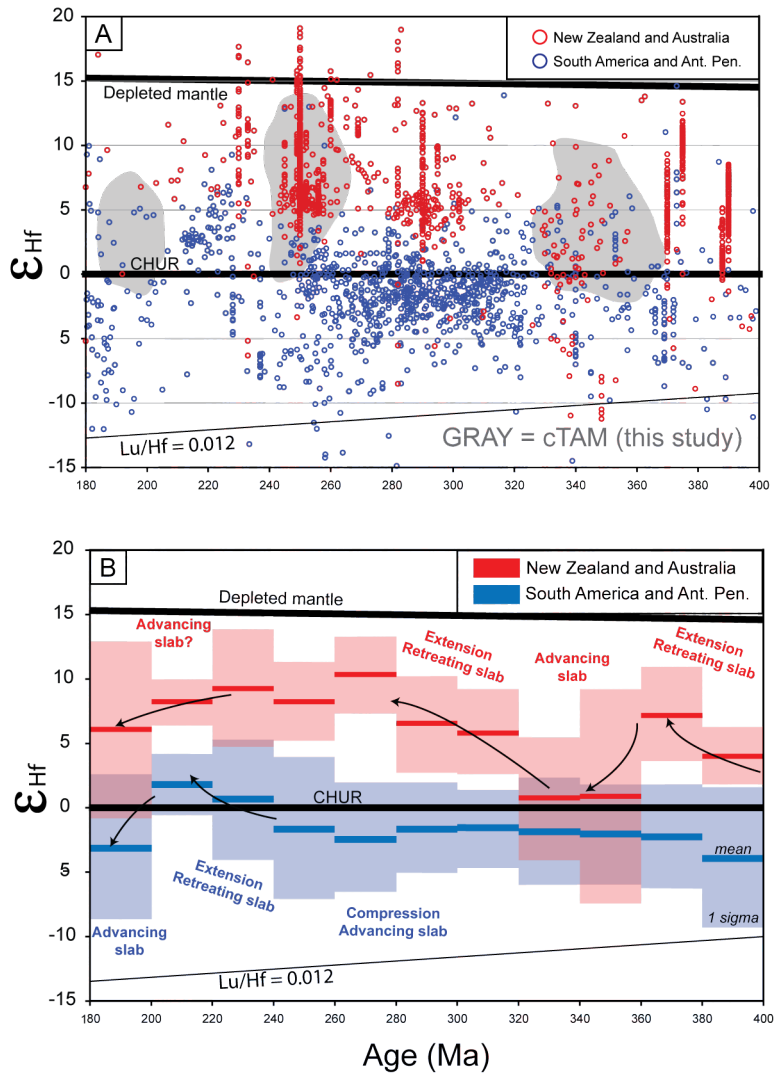


Fig. 8. Compilation of zircon Hf isotope data from Australia–Zealandia (red) and South America–Antarctic Peninsula (blue). Fields for Hf isotope data from the cTAM (this study) are provided in gray. Data for Australia–Zealandia are from: Veevers et al., 2006; Li et al., 2015; Shaw et al., 2011; Phillips et al., 2011; Kemp et al., 2005, 2007, 2009; Jeon et al., 2014; Regmi et al., 2016; Murgulov et al., 2007; Nebel et al., 2007; Hiess et al., 2015; Scott et al., 2009; Milan et al., 2016. Data from South America–Antarctica Peninsula are from: Bahlburg et al., 2009; Flowerdew et al., 2006; Bradshaw et al., 2012; Castillo et al., 2015; Fanning et al., 2011; Pepper et al., 2016; Rey et al., 2016; Pankhurst et al., 2016; Canile et al., 2016. (B) Mean and 1 sigma uncertainty for data from (A) grouped into 20 million year bins, and the inferred intervals of increasing or decreasing initial  $\epsilon_{\text{Hf}}$  combined with geodynamic interpretations. Hf isotopic values for depleted mantle and new crust are from Vervoort and Blichert–Toft (1999). CHUR—chondritic uniform reservoir.

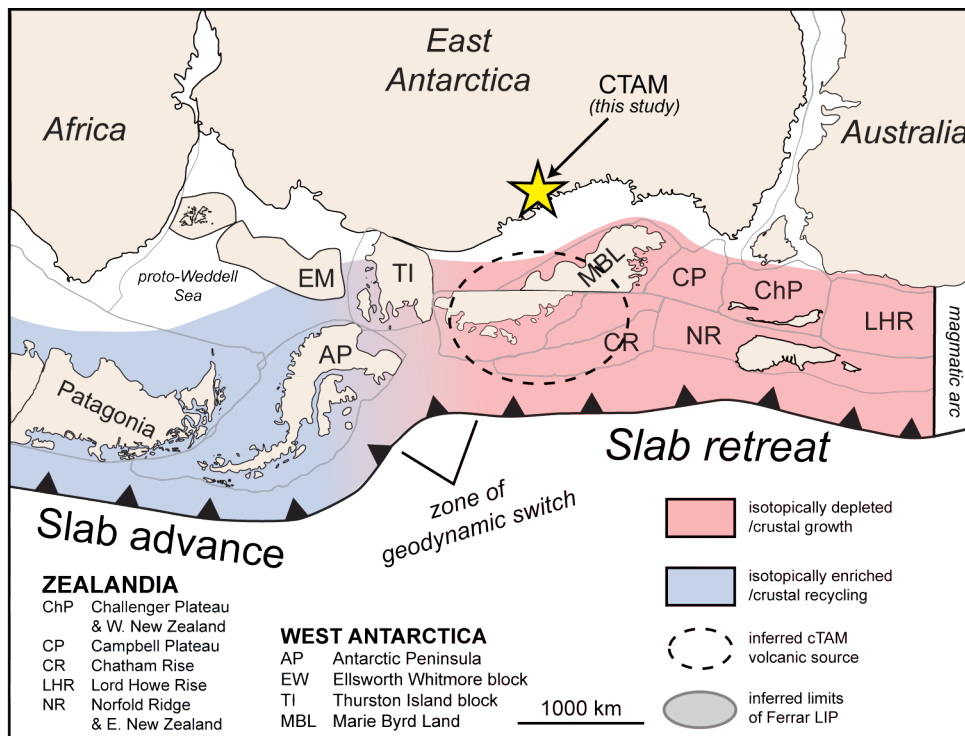


Figure 9. Reconstruction of the Gondwana plate margin, c. Permian (Elliot, 2013). Shown are the inferred limits of the continuous retreating arc system that is isotopically depleted (red) and the advancing arc system that is isotopically enriched (blue). The zone of the geochemical and geodynamic switch occurs in the vicinity of the Thurston Island block. The region outboard of the cTAM is interpreted to be the isotopically depleted arc source for volcanoclastic sediments of the cTAM.

Table 1. Summary of maximum deposition ages from zircon U-Pb geochronology

	PRR#	Location <sup>1</sup>	Max Deposition Age (Ma)	MSWD	n (< 205 Ma)	rejected	n (> 205 Ma)	% detrital
Hanson Fm.	PRR-26916	Kenyon Peaks	<b>189.3 ± 0.7</b>	1.3	71	13	15	15
	PRR-26917	Kenyon Peaks	<b>184.9 ± 1.3</b>	1.4	20	5	36	59
	PRR-26932	Mt. Falla	<b>197.4 ± 1.1</b>	1.6	19	0	41	68
	PRR-26934	Mt. Falla	<b>199.5 ± 0.7</b>	1.0	75	0	13	15
	PRR-26943	Mt. Falla	n.d.		23		24	51
	PRR-26949	Mt. Falla	<b>195.1 ± 0.6</b>	1.0	53	10	24	28
	PRR-26951	Mt. Falla	<b>188.0 ± 0.9</b>	0.7	24	7	46	60
	PRR-26960	Mt. Falla	<b>187.8 ± 0.7</b>	0.9	32	1	31	48
	PRR-26968	Mt. Falla	<b>193.5 ± 0.7</b>	0.7	45	12	27	32
	PRR-26979	Mt. Falla	<b>189.5 ± 2.4</b>	2.5	16	8	40	63
	PRR-26981	Mt. Falla	<b>189.3 ± 3.2</b>	1.8	7	0	83	92
	PRR-26982	Mt. Falla	n.d.		7		49	88
	PRR-27068	Mt. Petlock	<b>191.1 ± 0.8</b>	1.2	40	13	38	42
	PRR-27084	Mt. Falla	<b>193.1 ± 1.1</b>	1.1	29	9	23	38
	PRR-27089	Mt. Falla	<b>189.4 ± 0.7</b>	1.6	52	7	11	16
	PRR-27102	Storm Peak	<b>194.4 ± 1.0</b>	0.6	46	20	26	28
	PRR-27112	Storm Peak	<b>190.0 ± 0.8</b>	1.0	36	9	27	38
	PRR-27184	Mt. Falla	n.d.				71	100
	PRR-27252	Mt. Falla	<b>191.0 ± 2.1</b>	0.5	8	2	86	90
	PRR-05127	Mt Kirkpatrick	<b>190.8 ± 0.6</b>	0.8	45	5	6	11
PRR-05493	Mt Falla	<b>187.9 ± 0.9</b>	1.5	36	4	28	41	
PRR-34456	Mt. Falla	<b>193.4 ± 1.3</b>	2.2	31	11	17	29	
Fremouw Fm.	PRR-26024	Shenk Peak	<b>244.7 ± 1.7</b>	0.8	22	13	26	43
	PRR-25978	Mt Rosenwald	<b>242.8 ± 1.7</b>	1.2	17	10	6	18
	PRR-25968	Mt Rosenwald	<b>241.2 ± 1.5</b>	0.4	52	44	5	5
	PRR-26040	Mt. Black	<b>247.9 ± 1.7</b>	1.1	16	8	47	66
	PRR-05099	Mt Kirkpatrick	<b>242.7 ± 2.9</b>	1.9	16	9	29	54

<sup>1</sup>Locations as shown in Fig. 2. GPS coordinates provided in Dataset 1.

## **II. Zircon U-Pb and Hf isotopes link the Gondwana arc record of West Antarctica, Australia, and South America and highlight the secular development of accretionary orogens**

*Note: available at <https://doi.org/10.1016/j.gr.2018.06.002>*

### **Abstract**

Combined zircon geochronology and Hf isotopes of plutonic rocks from eastern Marie Byrd Land and Thurston Island, Antarctica, provide a detailed record of Phanerozoic arc magmatism along the paleo-Pacific margin of Gondwana. Magmatism along the Antarctic margin initiated in a dominantly contractional arc setting with an isotopically enriched lithospheric mantle source during the Ross Orogeny (c. 540–485 Ma). After termination of the Ross Orogeny through the Cretaceous, detrital zircon and zircon from igneous rocks record relative increases in zircon  $\epsilon\text{Hf}_i$  inferred to represent episodes of lithospheric-scale extension and relative decreases during inferred contractional episodes along the Antarctic margin. Comparison of this secular isotopic evolutionary trend with similar data from along the paleo-Pacific margin of Gondwana demonstrates a shared history among Marie Byrd Land, Australia, and Zealandia that contrasts with the shared record of Thurston Island, Antarctic Peninsula, and South America. These two contrasting histories highlight an early Permian along arc geochemical and inferred geodynamic switch from an isotopically enriched contractional arc system in South America, Antarctic Peninsula, and Thurston Island to an isotopically depleted extensional arc system in Marie Byrd Land, Zealandia, and Australia. Despite differences in timing, all segments of the paleo-Pacific

margin underwent a similar secular isotopic evolution with dramatic shifts from enriched to juvenile isotopic compositions during extensional collapse.

## **Introduction**

Accretionary orogenesis describes the deformation, metamorphism, and crustal growth (i.e., magmatism and accretion) that takes place during ongoing subduction at convergent plate boundaries (e.g., Cawood et al., 2009). Accretionary orogens can switch between two contrasting tectonic states; retreating orogens undergoing extension and advancing orogens undergoing contraction (e.g., Collins, 2002a). These tectonic states establish the primary characteristics of continental arcs including the rate and composition of magmatism as well as lithospheric thickness and rheology (Collins, 2002a, 2002b; Behn et al., 2007; Cawood et al., 2009; DeCelles et al., 2009; Kemp et al., 2009; Currie et al., 2015). Consequently, the tectonic state of continental arcs may control volcanogenic atmospheric CO<sub>2</sub> output, continental crustal growth and differentiation, and recycling of lithosphere back into the mantle (Collins et al., 2011; Hacker et al., 2011; Currie et al., 2015; McKenzie et al., 2016; Cao et al., 2017). The secular temporal, geochemical, and tectonic (i.e., geodynamic) evolution of accretionary orogens, therefore, remains an important component in resolving Earth's geochemical evolution.

The paleo-Pacific margin of Gondwana was a long-lived active continental margin for ~18,000 km along the west coast of South America, the Transantarctic Mountains, West Antarctica, Zealandia, and the east coast of Australia (Fig. 1; Cawood, 2005; Collins et al.,

2011). These regions contain Phanerozoic arc-related plutonic and volcanic rocks, and volcanoclastic sedimentary rocks that preserve the temporal and geochemical history of magmatism within this broad accretionary orogenic system. Previous workers have characterized the geochemical history of the South American and Australian sectors of the margin (e.g., Kemp et al., 2009; Cawood et al., 2011; Pepper et al., 2016). However, the Antarctic sector, consisting of Zealandia, West Antarctica, and the Transantarctic Mountains remains a missing link between South America and Australia in efforts to reconstruct the large-scale geodynamic history of the paleo-Pacific margin of Gondwana (e.g., Riel et al., 2018). The paucity in the record is, in part, due to poor exposure and inaccessibility of West Antarctica and Zealandia, i.e., ice covered or submerged crust. Furthermore, reconstructing the history of the Antarctic sector is particularly problematic because it has been heavily dissected into numerous ‘microplates’ that have rotated and translated long distances (up to 2500 km) from their pre-Gondwana-breakup configuration (Fig. 1B, Dalziel and Elliot, 1982; Grunow et al., 1987; Storey et al., 1988).

The crustal blocks of West Antarctica–Marie Byrd Land, Thurston Island, and the Antarctic Peninsula–contain Paleozoic–Mesozoic arc-related rocks (Fig. 1) that potentially record the magmatic and tectonic history of the Antarctic sector of the Gondwana arc (summarized in Elliot, 2013). However, U-Pb geochronology and Hf-O isotopes of igneous and detrital zircon, suggest that the Antarctic Peninsula shares a temporal, geochemical, and tectonic history with the Patagonia and the South American sectors of the arc system and may not be representative of the Antarctic sector (Fanning et al., 2011; Bradshaw et al., 2012; Castillo et al., 2016, 2017b; Nelson and Cottle, 2017).

Arc-derived Permian–Jurassic volcanoclastic sedimentary rocks deposited on the stable East Antarctic craton, which was not dissected during late Mesozoic supercontinent breakup, provide the most reliable, albeit limited, record of long-lived arc activity in the Antarctic sector (Elliot and Fanning, 2008; Elliot et al., 2016b, 2017; Nelson and Cottle, 2017). Based on paleogeographic reconstructions and paleocurrent data, the source of this volcanic detritus is considered to be the outboard volcanic arc located in Marie Byrd Land (e.g., Elliot et al., 2017). It follows then that Marie Byrd Land is an ideal location to investigate the geologic history of the Antarctic sector of the Gondwana margin. Pioneering geochronology and geochemistry studies provided preliminary ages and a tectonic framework for Marie Byrd Land (Pankhurst et al., 1998; Mukasa and Dalziel, 2000) with more recent workers refining the record exclusively for western Marie Byrd Land and its relation to the broader evolution of the Gondwana margin (Siddoway and Fanning, 2009; Korhonen et al., 2010; Saito et al., 2013; Yakymchuk et al., 2013, 2015; Brown et al., 2016). However, modern petrochronologic (i.e., combined geochronologic and geochemical techniques such as Hf isotopes in zircon, e.g., Kylander-Clark, 2017) have yet to be applied over a wide region of eastern Marie Byrd Land, despite early reports that this region potentially contains arc-related rocks spanning a longer time period than western Marie Byrd Land and may therefore provide a longer comprehensive record of arc magmatism. Additionally, zircon Hf isotope compilations for South America, Antarctica, Australia, and Zealandia indicate a significant along arc isotopic transition in arc magmatism from enriched to juvenile in the vicinity of Thurston Island in c. Permian (Nelson and Cottle, 2017). Limited zircon Hf isotope data from Thurston Island (Riley et al., 2017) and eastern Marie Byrd Land prohibit more precise constraints on the exact location of this along arc

geochemical and inferred geodynamic shift (Nelson and Cottle, 2017). Consequently, the precise timing and duration of arc magmatism and the relative roles of crustal growth and recycling through time remains poorly understood for eastern Marie Byrd Land and the Antarctic sector of the Gondwana margin overall.

In this study, we present zircon U-Pb geochronology and zircon geochemistry (trace elements and Hf isotopes) to investigate the age of magmatism and crustal evolution of eastern Marie Byrd Land, and the adjacent Thurston Island block, spanning ~200 million years from the Silurian to Triassic. These data are combined with existing data from elsewhere within the Antarctic sector (i.e., eastern Marie Byrd Land and central Transantarctic Mountains), as well as the South American sector, and the Australian sector of the Gondwana margin to determine the nature of along-arc variation in timing, the geochemistry of arc magmatism, and differences in inferred subduction geodynamics (i.e., contractional/advancing or extensional/retreating arc systems). Finally, our new zircon Hf isotope compilation highlights a possible shared secular evolution among Phanerozoic accretionary orogens along the entire Gondwana margin.

## **Geologic Background**

The pre-Jurassic granitoid basement of Marie Byrd Land is subdivided into the western Ross (with 1.5—1.3 Ga Nd model ages) and eastern Amundsen (with 1.3—1.0 Ga Nd model ages) provinces (Fig. 2; Pankhurst et al., 1998). The boundary between these two provinces is loosely located in the vicinity of the Land Glacier region of the Rupert Coast

(Fig. 2; Pankhurst et al., 1998). Paleomagnetic data for crustal blocks of the Ross and Amundsen Provinces indicate they were originally separate prior to their amalgamation in the mid-Cretaceous (c. 117 Ma; DiVenere et al., 1995; Luyendyk et al., 1996). Early studies of Marie Byrd Land correlated the Amundsen Province to the Median Tectonic Zone of New Zealand, and Thurston Island and Antarctic Peninsula crustal blocks, while the Ross Province was viewed as a continuation of the Gondwana margin in southeast Australia, western New Zealand, and North Victoria Land (Pankhurst et al., 1998).

### ***Western Marie Byrd Land (Ross Province)***

The Ross Province includes exposed rocks of the Ford Ranges and Edward VII Peninsula (Fig. 2). The oldest unit within the Ross Province is a Neoproterozoic–Cambrian folded metaturbidite sequence, the Swanson Formation, containing detrital zircons ranging from c. 3.03 Ga to c. 500 Ma with pronounced peaks at 1.0–1.1 Ga, typical of Grenville-age crust of the East Antarctic Craton (e.g., Goodge and Fanning, 2016) and 500–600 Ma ages, corresponding to the Ross-Delamerian orogen (Cox et al., 2000; Cawood, 2005; Foden et al., 2006; Goodge et al., 2012; Hagen-Peter et al., 2015, 2016; Paulsen et al., 2015). Permian–Triassic metasedimentary rocks in the Alexandra Mountains near the Ross Sea (Fig. 2) were derived from local sources as recorded by 400–320 Ma and ~250 Ma detrital zircon age populations (Pankhurst et al., 1998). The Swanson Formation is intruded by the Ford Granodiorite suite emplaced between 375 to 345 Ma (Yakymchuk et al., 2015), coincident with Gondwana margin arc magmatism in Northern Victoria Land (Admiralty Intrusives,

Borg et al., 1986), the Western Province of New Zealand (Karamea Suite, Tulloch et al., 2009), eastern Australia (Melbourne Terrane, Chappell et al., 1988), and southern South America (Pankhurst et al., 2003; Hervé et al., 2016). The Ford Granodiorite suite has zircon Hf and O isotope compositions consistent with mixing of juvenile mantle melts with a melt of the Swanson Formation during arc magmatism (Yakymchuk et al., 2015). High-grade metamorphic equivalents to the Swanson Formation and Ford Granodiorite suite are found in the nearby Fosdick Mountains migmatite-granite complex of western Marie Byrd Land (Fig. 2) and contain Devonian–Carboniferous (370–355 Ma) and Cretaceous granites (146–96 Ma) (Siddoway and Fanning, 2009; Korhonen et al., 2010, 2012; Yakymchuk et al., 2013). Metamorphism in the Fosdick complex is interpreted to have occurred at mid-crustal depths during rifting of Zealandia from the Gondwana margin in the mid to late Cretaceous (Siddoway et al., 2004; Korhonen et al., 2010, 2012). Devonian–Carboniferous (370–355 Ma) granites in the Fosdick complex formed via mixing between melts of the Ford Granodiorite suite and the Swanson Formation (Yakymchuk et al., 2013). Cretaceous (146–96 Ma) granites in the Fosdick complex, in contrast, require a juvenile component in addition to the Ford Granodiorite suite and Swanson Formation components (Yakymchuk et al., 2013).

Zircon Hf isotopic compositions of c. 370–355 granitoids from the Ross Province are more evolved than granites from correlative suites across the Gondwana margin in the Western Province of New Zealand and eastern Australia (Yakymchuk et al., 2015). These isotopic differences are attributed to an along-arc change from typical extensional arc tectonics in eastern Australia to an advancing arc system in West Antarctica (Yakymchuk et al., 2015). Zircon U-Pb and Hf isotopes from volcanoclastic sedimentary rocks in the

Transantarctic Mountains, however, suggest that extensional tectonics continued into West Antarctica (Nelson and Cottle, 2017). In this contribution, we investigate the extent of extensional tectonics in West Antarctica by studying *in situ* plutonic rocks rather than their derivatives. These new data from eastern Marie Byrd Land also represent the first zircon Hf isotope data from this region and uncover a more complete history of arc geochemistry and geodynamics for West Antarctica.

### ***Eastern Marie Byrd Land (Amundsen Province)***

The Amundsen Province extends from the westernmost area of the Rupert Coast through Pine Island Bay, including the Hobbs and Walgreen Coasts and inland regions (Fig. 2). Paleozoic correlatives to the Swanson Formation are absent in the Amundsen Province but paragneisses at Mount Petras and Patton Bluff (Fig. 2) contain Devonian–Carboniferous detrital zircon similar in age to the Alexandra Mountains and the Ford Granodiorite suite in the Ross Province (Pankhurst et al., 1998; Yakymchuk et al., 2015). The Amundsen Province contains a more comprehensive record of arc-related plutonism than the Ross Province, spanning the Cambrian through Triassic, previously constrained by Rb-Sr isochron and multigrain fraction isotope dilution-thermal ionization mass spectrometry (ID-TIMS) zircon U-Pb ages (Pankhurst et al., 1998; Mukasa and Dalziel, 2000). Cretaceous gneisses and granites (128 to 113 Ma) in the Demas Range migmatite complex of the Amundsen Province (Fig. 2) overlap in age with the majority of granites from the Fosdick migmatite complex of the Ross Province and may represent a correlative event. Cretaceous subduction-related calc-

alkaline magmatic rocks are scattered throughout the Amundsen Province (Mukasa and Dalziel, 2000). The youngest calc-alkaline granite along the Rupert and Hobbs coast outcrops at Mt. Prince (Fig. 2) and is dated at  $110 \pm 1$  Ma; further towards the east the youngest calc-alkaline intrusion in Pine Island Bay (Fig. 2) has an age of  $96 \pm 1$  Ma (Mukasa and Dalziel, 2000). Initial rift-related magmatism at  $\sim 100$  Ma (e.g., Mt. Prince) is consistent with the inception of Pacific-Antarctic seafloor spreading at c. 81 Ma (Mukasa and Dalziel, 2000).

### ***Thurston Island***

Rocks of the Thurston Island crustal block crop out on a series of islands and Jones Mountains (Fig. 2). The exposed basement includes Carboniferous to Late Cretaceous volcanic and magmatic calc-alkaline igneous rocks recording subduction-related magmatism along the paleo-Pacific margin of Gondwana (Leat et al., 1993; Pankhurst et al., 1993; Riley et al., 2017). Early studies by Leat et al. (1993) and Pankhurst et al. (1993) documented the geochemistry and geochronology of the Thurston Island block relying exclusively on K-Ar,  $^{40}\text{Ar}/^{39}\text{Ar}$ , and Rb-Sr techniques. Recent work by Riley et al. (2017) revised the geochemistry and geochronology record utilizing zircon U-Pb and Hf isotopes for a limited suite of samples, identifying isolated episodes of magmatism at  $349 \pm 2$  Ma,  $239 \pm 4$  Ma,  $\sim 182$  Ma,  $151 \pm 2$  Ma and  $108 \pm 1$  Ma. The  $\sim 349$  Ma granodiorite gneiss from Thurston Island represents juvenile magmatism, indicated by zircon  $\epsilon\text{Hf}_i$  values from +10 to +2. In contrast, Triassic through Cretaceous magmatic rocks with ages of  $\sim 239$  Ma,  $\sim 151$  Ma, and  $\sim 108$  Ma

from Thurston Island incorporated more ancient crustal material in their petrogenesis, represented by  $\epsilon\text{Hf}_i$  from 0 to -9 (Riley et al., 2017).

### **Analytical Techniques**

Twenty three samples from the eastern Amundsen Province of Marie Byrd Land and Thurston Island (Fig. 2) were selected from the Polar Rock Repository (Repository, 2018) and provided by S. Mukasa and F. Fahnestock (Mukasa and Dalziel, 2000) to determine the timing and geochemical history of subduction-related magmatism within the Antarctic sector of the Gondwana margin. Zircon were separated using standard mineral separation techniques (i.e., disk milling, water table, magnetic separation, and heavy liquids), mounted in epoxy, and polished to expose equatorial sections. Prior to isotopic analysis, zircons were imaged via cathodoluminescence (CL) on an FEI Quanta400f scanning electron microscope (SEM) and used to guide selection of locations for laser ablation split-stream analyses (U-Pb and trace elements) followed by Lu-Hf measurements.

Zircon U-Pb isotopes were obtained at the University of California, Santa Barbara, under standard operating conditions (McKinney et al., 2015). Instrumentation consists of a 193 nm ArF excimer laser ablation (LA) system coupled to Nu Plasma high-resolution multi collector-inductively coupled plasma mass spectrometer (MC-ICP-MS). Approximately 60 crystals were measured for U-Pb analysis from each sample. Subsequent Lu-Hf analyses were performed by LA-MC-ICPMS ( $n = \sim 20$  per sample, and Lu-Hf isotope analysis location was placed directly over previous U-Pb and trace-element ablation pits. Data reduction was

performed using Iolite v2.5 (Paton et al., 2010, 2011) and  $^{207}\text{Pb}$ -corrected  $^{206}\text{Pb}/^{238}\text{U}$  ages were calculated for zircon younger than 800 Ma using the method of Andersen (2002) and ISOPLOT/EX (Ludwig, 2003). We use  $^{207}\text{Pb}/^{206}\text{Pb}$  ages for zircon older than 800 Ma. Detailed analytical methods, data reduction protocols and results of reference zircon analyses and unknown data are in the Supplementary Information, and Datasets S1 and S2 provided in the Appendix (Patchett and Tatsumoto, 1980, 1981, Wiedenbeck et al., 1995, 2004; Chu et al., 2002; Jackson et al., 2004; Thirlwall and Anczkiewicz, 2004; Woodhead and Hergt, 2005; Blichert-Toft, 2008; Sláma et al., 2008).

## Results

Zircon U-Pb ages and Hf isotopic data for 17 samples from eastern Marie Byrd Land and 6 samples from Thurston Island (Hf data for 3 samples) are provided in supplementary file 1 and summarized in Table 1. Representative cathodoluminescence (CL) images of zircon with locations of U-Pb and Hf isotope measurements are provided in Fig. 3. Tera-Wassurburg Concordia diagrams and  $^{207}\text{Pb}$ -corrected weighted mean  $^{206}\text{Pb}/^{238}\text{U}$  crystallization ages for Paleozoic–Mesozoic samples from both eastern Marie Byrd Land and Thurston Island are plotted in Figs. 4 and 5. Calculated weighted mean crystallization ages with two sigma uncertainties and mean squared weight deviation (MSWD) for samples from this study are discussed below. Zircon Hf isotope data for eastern Marie Byrd Land and Thurston Island are plotted in Fig. 6 and 7 and calculated weighted mean  $\epsilon\text{Hf}_i$  values are provided alongside their two standard error uncertainties below. All  $\epsilon\text{Hf}_i$  values were

calculated using chondritic uniform reservoir (CHUR) parameters of Bouvier et al. (2008) and  $^{176}\text{Lu}$  decay constant from Söderlund et al. (2004). Samples with atypical zircon Th/U ratios (i.e.,  $< 0.1$ ) are discussed below, all other samples contain typical igneous zircon Th/U ratios (Rubatto, 2002).

Sample MB 432.1, a biotite-hornblende granodiorite from Slater Rocks (Fig. 2), is the oldest sample in this study with an age of  $420 \pm 2$  Ma, MSWD = 0.8. This new age is consistent with a Rb-Sr isochron age of  $419 \pm 20$  Ma (MSWD = 17) obtained by Pankhurst et al. (1998). The  $\varepsilon\text{Hf}_i$  for this sample is  $+4.7 \pm 0.5$ , more juvenile than the  $\varepsilon\text{Hf}_i$  of  $+1.2$  calculated using whole rock Nd isotope data (Pankhurst et al., 1998) and the Nd – Hf conversion equation from Vervoort et al. (1999). Samples MB 201.15 from Mt. McCoy (Fig. 2) and MB 206.2 from Brunner Hill (Fig. 2) yield indistinguishable ages of  $348 \pm 1$  Ma (MSWD = 1.7) and  $348 \pm 8$  Ma (MSWD = 0.2), respectively. These new ages are within uncertainty of a previous Rb-Sr isochron age of  $330 \pm 20$  Ma for Mt. McCoy and a zircon U-Pb age of  $339 \pm 6$  Ma for Bruner Hill (Pankhurst et al., 1998). However, they are significantly older than an ID-TIMS multigrain fraction U/Pb zircon lower-intercept age of  $320 \pm 3$  Ma for Mt. McCoy obtained by Mukasa and Dalziel (2000). New Hf isotopic data for Mt. McCoy form a fairly tight range of  $\varepsilon\text{Hf}_i$  values and a weighted mean of  $+5.3 \pm 0.4$  consistent with whole-rock Nd isotopic data (Pankhurst et al., 1998). Zircon from Bruner Hill do not appear to luminesce under CL and are therefore not included in Figure 3. The zircon U-Pb data for Bruner Hill are generally discordant (Fig. 4) with an average zircon Th/U of 0.06 (see supplementary Dataset 1). The discordant U-Pb data and Th/U  $< 0.1$  suggest that zircon in the Bruner Hill sample records a high-grade metamorphic/anatectic event rather

than magmatism (Rubatto, 2002). The Hf isotopic data for Bruner Hill are highly variable but generally more enriched than Mt. McCoy, with an  $\epsilon\text{Hf}_i = +0.2 \pm 2.0$ .

Five new Permian magmatic ages were obtained for plutonic rocks of the Walgreen Coast (Fig. 2). A granite from Jeffrey Head (MB 406.7) of the Bear Peninsula (Fig. 2) is the oldest Permian sample,  $295 \pm 2$  Ma (MSWD = 1.6), and has the most radiogenic hafnium isotope composition,  $\epsilon\text{Hf}_i = +10.2 \pm 0.7$ . This new age is slightly younger than the  $312 \pm 10$  Ma age reported by Pankhurst et al. (1998) but the  $\epsilon\text{Hf}_i$  value is within range of their whole rock Nd isotopic composition,  $\epsilon\text{Hf}_i = +8.5$  (using the Nd – Hf conversion equation from Vervoort et al. (1999)). A granodiorite from the Bear Peninsula (BP3) yields a younger,  $287 \pm 1$  Ma (MSWD = 0.9), age and a similar  $\epsilon\text{Hf}_i = +9.0 \pm 1.1$ . A granodiorite from Mt. Isherwood (MB 400.1D, Fig. 2) yields an age of  $283 \pm 1$  Ma (MSWD = 1.0) and an  $\epsilon\text{Hf}_i = +3.0 \pm 0.5$ . This new age contrasts with two multi-fraction ID-TIMS zircon U-Pb lower intercept ages of  $243 \pm 29$  Ma and  $414 \pm 98$  Ma (Mukasa and Dalziel, 2000) from the same zircon separates. Quartz diorites from Mt. Wilbanks (MB 402.2, Fig. 2) and Mt. Strange (MB 403.3, Fig. 2) yielded ages of  $287 \pm 1$  Ma (MSWD = 1.2) and  $284 \pm 2$  Ma (MSWD = 0.6) and  $\epsilon\text{Hf}_i = +5.8 \pm 0.5$  and  $+6.0 \pm 0.8$ , respectively. These ages are within uncertainty of the  $283.0 \pm 0.5$  Ma age for Mt. Wilbanks published by Mukasa and Dalziel (2000) on the same zircon separate and a Rb-Sr isochron age of  $276 \pm 2$  Ma obtained by Pankhurst et al. (1998) for granitoids of the Kohler Range.

The earliest record of Mesozoic magmatism in eastern Marie Byrd Land recorded by our samples is a granite age of  $248 \pm 1$  Ma (MSWD = 0.6), with a  $\epsilon\text{Hf}_i = +10.9 \pm 0.6$ , from Kinsey Ridge of the Rupert Coast (MB 212.3P, Fig. 2). Six new ages were also determined for plutonic and migmatitic rocks from a migmatite complex in the Demas Range, Rupert

Coast, and refine the dominantly discordant U-Pb dates published by Mukasa and Dalziel (2000). A megacrystic granite (MB 163.1M) and leucogranitic gneiss (MB 204.3M) from Mt. Goorhigian (Fig. 2) have Late Jurassic ages of  $145 \pm 1$  Ma with  $\epsilon\text{Hf}_i = +3.5 \pm 0.5$  and  $150 \pm 1$  Ma with  $\epsilon\text{Hf}_i = +4.7 \pm 0.5$ , respectively. A monzogranite from Early Bluff is the next oldest sample and the most juvenile from eastern Marie Byrd Land with an age of  $117 \pm 1$  Ma and an  $\epsilon\text{Hf}_i = +6.5 \pm 0.9$ . A Cretaceous granite from Mt. Goorhigian (MB 204.1M, Fig. 2,) yielded more complex U-Pb data with an inferred crystallization age of  $103 \pm 1$  Ma and an  $\epsilon\text{Hf}_i = +3.7 \pm 0.5$ , but also including older concordant dates of 140 - 102 Ma and  $\sim 247$  Ma. Complex data were also observed in granites from Mt. Prince (MB 205.10M, Fig. 2) and Patton Bluff (MB 208.3, Fig. 2). The Mt. Prince granite contains a range of Cretaceous zircon ages with peaks at 108 and 120 Ma and an average  $\epsilon\text{Hf}_i = +4.2 \pm 0.7$ . Similarly, the Patton Bluff granite contains a range of ages with peaks at 109 Ma, 114 Ma, and 120 Ma with an average  $\epsilon\text{Hf}_i = +4.7 \pm 0.6$ . Younger dates were determined for a monzogranite from Early Bluffs (MB 426.4) and a dike from Mt. Prince (MB 205.3V) of  $106 \pm 1$  Ma with an average  $\epsilon\text{Hf}_i = +0.8 \pm 0.5$  and  $100 \pm 0.4$  Ma with average  $\epsilon\text{Hf}_i = +6.8 \pm 0.7$ . This new age is slightly older than a single-fraction zircon U-Pb age of  $103.4 \pm 0.3$  Ma (Mukasa and Dalziel, 2000). Overall, there is a general decrease in the  $\epsilon\text{Hf}_i$  from a mean of +6.5 at c. 117 Ma to +0.8 at c. 106 Ma followed by a return to +6.8 at c. 100 Ma.

Three new ages spanning the Carboniferous–Permian were determined for rocks from Thurston Island. An orthogneiss from Cape Menzel (TI 3-1, Fig. 2) yielded an igneous age of  $347 \pm 1$  Ma with  $\epsilon\text{Hf}_i = 11.0 \pm 0.6$  and an orthogneiss from King Cliffs (60-10-1, Fig. 2) provided a metamorphic age (average zircon Th/U = 0.06) of  $338 \pm 2$  Ma with  $\epsilon\text{Hf}_i = +2.1 \pm 1.2$ . A diorite from Guy Peaks (68-71-1, Fig. 2) yielded the only Permian age for Thurston

Island of  $276 \pm 1$  Ma with  $\epsilon\text{Hf}_i = 0.4 \pm 0.7$ . Three granites from Jones Mountains (61-119, 61-133, and 64-J-BS-1, Fig. 2) have Triassic ages of  $208 \pm 1$ ,  $211 \pm 1$ , and  $208 \pm 1$  Ma. Zircon Hf isotope compositions were determined for sample 61-133 and yielded  $\epsilon\text{Hf}_i = -4.8 \pm 0.7$ .

## **Discussion**

### ***Zircon record of West Antarctica (Cambrian – Cretaceous) magmatism***

The new ages reported here combined with previously reported ages indicate that basement exposures in eastern Marie Byrd Land span a longer time period than western Marie Byrd Land. The oldest igneous rock dated so far from eastern Marie Byrd Land is a  $505 \pm 5$  Ma orthogneiss from Mt. Murphy (Pankhurst et al., 1998), indicating the basement of eastern Marie Byrd Land is composed, at least, partly of plutonic rocks associated with the Ross Orogen. The oldest rock dated in this study is a Silurian granodiorite at Slater Rocks ( $420 \pm 1.8$  Ma) but an Ordovician Rb-Sr isochron age of  $446 \pm 16$  Ma (MSWD = 0.4; Pankhurst et al., 1998) for gneisses from Clark Island in Pine Island Bay indicates Ordovician rocks also exist in Marie Byrd Land. The  $420 \pm 1.8$  Ma crystallization age from Slater Rocks is contemporaneous with the Lachlan Orogen in Australia (Foster et al., 2009), Silurian (c. 435 to 422 Ma) orthogneisses from the Antarctic Peninsula (Millar et al., 2002), contemporaneous granitoids in southern Patagonia (Pankhurst et al., 2003), but older than known igneous rocks from western Marie Byrd Land (Yakymchuk et al., 2015).

The two Marie Byrd Land provinces do, however, share a record of magmatic and metamorphic activity during the Carboniferous, with a granite from Mt. McCoy ( $348 \pm 1$  Ma) and an orthogneiss from Brunner Hill ( $348 \pm 8$  Ma) falling within the age range of the Ford Granodiorite Suite (374–345 Ma) and within uncertainty of the timing of peak metamorphism in the Fosdick migmatite-granite complex (346 Ma) in western Marie Byrd Land (Siddoway and Fanning, 2009; Korhonen et al., 2010; Yakymchuk et al., 2013). Devonian–Carboniferous orthogneisses are also found on Thurston Island ( $347 \pm 1$  and  $338 \pm 2$  Ma, this study) and the Antarctic Peninsula ( $397 \pm 8$ ,  $393 \pm 1$ , and  $327 \pm 9$  Ma, Millar et al., 2002). Volcaniclastic sedimentary rocks in the central Transantarctic Mountains also contain abundant 367–328 Ma zircon thought to be sourced from West Antarctica (Elliot and Fanning, 2008; Elsner et al., 2013; Elliot et al., 2016b, 2017; Nelson and Cottle, 2017; Paulsen et al., 2017b). Mt. McCoy and Bruner Hill straddle the eastern – western Marie Byrd Land boundary and, in this study, are the closest rocks to the Ford Ranges of eastern Marie Byrd Land. Based solely on the geochronology it is unclear whether this juxtaposition of contemporaneous rocks is coincidental or indicative of a shared melting event that either extends beyond a true crustal boundary or suggests the boundary should be shifted to include Mt. McCoy within the western province. Regardless of the boundary location, the new dates presented here along with known correlative units in Zealandia (e.g., Tulloch et al., 2009b), Australia (e.g., Chappell et al., 1988), Northern Victoria Land (e.g., Borg et al., 1986), and the central Transantarctic Mountains (e.g., Nelson and Cottle, 2017) suggest that widespread magmatism occurred in the Devonian–Carboniferous consistent with an orogen-wide magmatic flare-up event.

The Permian record of arc magmatism is sparse in West Antarctica. Our new dates for Permian granites from the Walgreen Coast record a major magmatic event from 295 to 283 Ma (Fig. 2). The rock closest to this time interval is a  $276 \pm 1$  Ma diorite from Thurston Island (this study), approximately 500 km east of the Walgreen Coast. Other Permian magmatic ages have, however, been reported for a limited number of rocks from the Antarctic Peninsula (Millar et al., 2002; Riley et al., 2012). The 295–283 Ma event is also not preserved in Permian volcanoclastic sedimentary rocks of the Transantarctic Mountains (Elliot and Fanning, 2008; Elsner et al., 2013; Elliot et al., 2016b, 2017; Nelson and Cottle, 2017; Paulsen et al., 2017b). Magmatic rocks from Patagonia and detrital zircon from the Antarctic Peninsula and Patagonia do, however, have abundant ages overlapping with Walgreen Coast magmatism (e.g., Hervé et al., 2006; Pankhurst et al., 2006, 2014; Fanning et al., 2011; Castillo et al., 2015). Granites from the New England Orogen in Australia also have similar early Permian (296–288 Ma) ages (e.g., Rosenbaum et al., 2012; Kemp et al., 2009b). There are, however, very few early Permian detrital zircon U-Pb ages in sedimentary rocks from Australia and New Zealand but a prominent early Permian peak in zircon age spectra for Patagonia sedimentary rocks (see Fig. 7 of Nelson and Cottle, 2017). Zircon geochronology alone, therefore, cannot distinguish whether the Walgreen Coast event is more closely related to discrete early Permian magmatism akin to the Australian arc record, or more widespread early Permian magmatism as in South America.

The Triassic record of arc magmatism in Marie Byrd Land is limited to granite from Kinsey Ridge of the Rupert Coast (Fig. 2,  $248 \pm 1$  Ma, this study). The age of the Kinsey Ridge granite overlaps with the Permian–Triassic peak in detrital zircon U-Pb ages from Mesozoic sedimentary rocks in the Transantarctic Mountains and, therefore, is consistent

with its proposed role as the source region (Elliot and Fanning, 2008; Elsner et al., 2013; Elliot et al., 2016b, 2017; Nelson and Cottle, 2017; Paulsen et al., 2017b). Although there is a scarcity of Triassic and late Permian dates from Marie Byrd Land igneous rocks, the abundance of Triassic and late Permian aged detrital zircon in the central Transantarctic Mountains suggests that significant Permian–Triassic crust remains ice covered in Marie Byrd Land. Triassic magmatic rocks are more common in the Antarctic Peninsula, but most formed over a brief period from c. 237 to 227 Ma (Millar et al., 2002; Riley et al., 2012; Flowerdew et al., 2006). On Thurston Island, a diorite from Mount Bramhall ( $239 \pm 4$  Ma, Riley et al., 2017) is similar in age to Triassic rocks from the Antarctic Peninsula. However, our new dates for granites from Jones Mountains (215 to 208 Ma) have no identifiable plutonic correlatives in West Antarctica, other than a 208 Ma granite in the Ellsworth-Whitmore terrane (Craddock et al., 2017b). Furthermore, zircons similar in age to the Jones Mountains granite are uncommon in the detrital record of Patagonia, New Zealand, and Australia (see compilation in Nelson and Cottle, 2017).

The Early Jurassic subduction-related magmatic record in West Antarctica consists of c. 188 to 181 Ma granitoids from the Antarctic Peninsula that correlate to the subcordilleran plutonic belt of Patagonia (Riley et al., 2017). These granites appear unrelated to contemporaneous volcanic rocks of the Ferrar large igneous province (LIP) of the Transantarctic Mountains or the Chon Aike silicic LIP of Patagonia, the Ellsworth-Whitmore terrane, and Thurston Island (Pankhurst et al., 2000; Burgess et al., 2015). The emplacement of the Ferrar and Chon Aike LIPs is thought to be synchronous with the initial break-up of Gondwana in the Early Jurassic (Encarnación et al., 1996). Younger within-plate granites (c. 178–174 Ma) in the Ellsworth-Whitmore terrane are also interpreted to be related to

Gondwana break-up rather than subduction (Craddock et al., 2017b). In contrast, Early Jurassic volcanoclastic sedimentary rocks of the Hanson Formation in the central Transantarctic Mountains are inferred to be subduction-related and represent prolonged arc volcanism from c. 202 to 183 Ma with no identifiable source in West Antarctica (Elliot et al., 2016b; Nelson and Cottle, 2017).

The onset of supercontinent break-up in the Early Jurassic began a period of relative arc inactivity that persisted until the Late Jurassic. Consequently, a younger age of  $166 \pm 3$  Ma for zircon from a leucocratic dike from the Antarctic Peninsula is the only Mid-Jurassic zircon crystallization age reported for West Antarctica (Flowerdew et al., 2006). Jurassic ages have also been discovered for a mafic gneiss in western Marie Byrd Land that contains inherited  $\sim 146$  Ma zircon that could be igneous or metamorphic (Yakymchuk et al., 2013). Similar-aged magmatism in Thurston Island is represented by a  $151 \pm 2$  Ma granite (Riley et al., 2017). Other suspected Late Jurassic–Early Cretaceous granitoids occur throughout western and southern Thurston Island (Leat et al., 1993; Pankhurst et al., 1993). Late Jurassic–Early Cretaceous magmatism on the Antarctic Peninsula is absent aside from a  $141 \pm 2$  Ma granite in northwest Palmer Land (Vaughan and Millar, 1996). Overall, scattered Mid to Late Jurassic magmatic rocks in West Antarctica are contemporaneous with, and may represent an extension of, the Triassic–Cretaceous magmatic rocks of the Darran Suite in New Zealand (Mortimer et al., 2015).

Mid- to Late-Cretaceous magmatic rocks are prevalent throughout West Antarctica. Recent zircon U-Pb data for the Lassiter Coast intrusive suite from the Antarctic Peninsula indicates a magmatic flare-up event characterized by the emplacement of voluminous granitoid batholiths over three distinct episodes at  $\sim 127$  Ma,  $\sim 117$  Ma, and  $\sim 106$  Ma (Riley et

al., 2018). Both the North Patagonian Batholith and the Divisadero Group Volcanic rocks of the North Patagonian Andes share these same distinct episodes of increased magmatic flux (e.g., Pankhurst et al., 1999; Echaurren et al., 2017). In western Marie Byrd Land, 115 to 98 Ma granitoids in the Fosdick Mountains overlap in age with the proposed Cretaceous magmatic flare-up (e.g., Korhonen et al., 2010). Our new U-Pb zircon dates for Mid to Late Cretaceous magmatic rocks from eastern Marie Byrd Land are synchronous with episodic Cretaceous magmatism in both western Marie Byrd Land and the Antarctic Peninsula, indicating a major magmatic flare-up event occurred along the Antarctic margin related to major episodes of compression referred to as the Palmer Land Event (Vaughan et al., 2012; Riley et al., 2018).

### ***Zircon Hf isotopes and geodynamic evolution of the Gondwana margin***

#### *The zircon Hf isotope proxy*

The relative change in zircon  $\epsilon\text{Hf}_i$  through time in magmatic arcs has been linked to the tectonic evolution of the arc (Kemp et al., 2009). In particular, Kemp et al. (2009) argued that a relative increase in zircon  $\epsilon\text{Hf}_i$  is indicative of an extensional arc system associated with an outboard migration of subduction zone magmatism during slab rollback and associated crustal extension and thinning. Outboard migration of the arc increases zircon  $\epsilon\text{Hf}_i$  by reducing assimilation due to magma ascent through thinner possibly juvenile crust and/or melting of upwelling depleted asthenospheric mantle (e.g., Chapman et al., 2017).

Conversely, contractional arc systems produce a decrease in zircon  $\epsilon\text{Hf}_i$  during an inboard migration of magmatism due to slab shallowing and arc contraction (i.e., crustal thickening). The relative decrease in  $\epsilon\text{Hf}_i$  associated with contractional arc systems is inferred to result from increasing crustal assimilation during crustal thickening, underthrusting of fertile crust to the melt source region, and/or an inboard shift of the arc magma source region towards increased melting of ancient enriched lithospheric mantle (e.g., Chapman et al., 2017). This model for tectonic switching between extension and contraction within accretionary orogens relies on plate boundary processes that adjust the angle of the subducting slab, and include decreased convergence rates (extension) and subduction of buoyant oceanic plateaus (contraction) (Collins, 2002a, 2002b; Kemp et al., 2009).

This model of ‘tectonic switching’ or ‘accordion tectonics’ (e.g., Collins, 2002b; Aitchison and Buckman, 2012) provides one conceptual framework within which to interpret our new zircon Hf isotope data and previously published data from West Antarctica and the Transantarctic Mountains. It should be noted, however, that alternatives to the Collins (2002a) model used here have been proposed for the paleo-Pacific margin of Gondwana (Crawford, 2003; Aitchison and Buckman, 2012; Gibson et al., 2015). These models generally support “quantum tectonics” which refers to switching of subduction polarity resulting in periods of island arc formation, accretion, and a switch to continental arc formation (Aitchison and Buckman, 2012; Fergusson, 2013). These models predict that zircon Hf isotope compositions should shift rapidly to near depleted mantle values during polarity switching and associated island arc formation. Following island arc accretion, zircon Hf isotope compositions should reflect melting of the accreted juvenile island arc lithosphere and/or ancient continental arc lithosphere. For the purposes of this paper, zircon Hf isotopes

are interpreted within the framework of accretionary orogenesis because this model has been widely applied to zircon Hf isotope datasets along the paleo-Pacific margin of Gondwana (e.g., Kemp et al., 2009; Phillips et al., 2011; Li et al., 2015; del Rey et al., 2016; Pepper et al., 2016). Furthermore, our zircon Hf isotope data contain no indication that rapid formation of an island arc with near depleted mantle isotope compositions, similar to the Macquarie island arc in the Australian sector (see Aitchison and Buckman, 2012), occurred in the Antarctic sector, making it difficult to interpret our data from Antarctica within a quantum tectonics framework.

Another important consideration for the accordion tectonic model (Collins, 2002b; Aitchison and Buckman, 2012) and zircon Hf isotope proxy established by Kemp et al. (2009) is the role of internal processes such as catastrophic lithospheric thinning (e.g., foundering) rather than plate boundary processes in generating extensional collapse in accretionary orogens (Dewey, 1988). Accretionary orogens undergoing magma flare-ups during upper-plate shortening and lithospheric recycling are associated with the generation of thick (>30 km) dense granulite and garnet pyroxenite (eclogite) roots in the lower crust and lithospheric mantle (DeCelles et al., 2009; Lee and Anderson, 2015). These arc roots are significantly denser than the underlying mantle and may eventually founder into the asthenosphere (e.g., Currie et al., 2015). Catastrophic foundering or thinning of the mantle lithosphere can cause rapid uplift and a rise in the geothermal gradient leading to gravitationally driven extensional collapse of the orogen, ignimbrite flare-ups, and a shift to juvenile magmatism due to asthenospheric upwelling (e.g., Dewey, 1988; DeCelles et al., 2009; Wang and Currie, 2015). Consequently, distinctions and interrelations of arc root foundering and slab rollback are poorly constrained within the record of secular evolution of

continental arcs due in part to the two processes producing similar geological signals and the potential for them to occur simultaneously (Lister and Forster, 2009). Here we discuss periods where both plate boundary and internal processes may be driving extension.

### *Antarctic sector*

Initial subduction along the Antarctic sector during the Ross Orogeny occurred in a dominantly contractional tectonic setting and produced enriched magmas with unradiogenic initial Hf isotopic compositions sourced from an enriched continental lithospheric mantle (Hagen-Peter et al., 2015, 2016; Hagen-Peter and Cottle, 2018). Consequently, the positive zircon  $\epsilon\text{Hf}_i$  values younger than the Ordovician from West Antarctica cannot be explained without the addition of a depleted asthenospheric mantle component to the arc magma source region(s) following the Ross Orogeny (i.e., the increase in zircon  $\epsilon\text{Hf}_i$  requires juvenile mantle input) (Cawood and Buchan, 2007; Kemp et al., 2009; Chapman et al., 2017). For this reason, the markedly more juvenile zircon  $\epsilon\text{Hf}_i$  from Silurian–Triassic plutonic rocks in Marie Byrd Land and Carboniferous rocks in Thurston Island and the Antarctic Peninsula are here interpreted as a broad change in the tectonic conditions from contraction during the Ross Orogeny to extension via slab rollback and/or lithosphere removal.

The role of foundering in this tectonic switching event is unknown, but the Ross Orogeny was a dominantly advancing system undergoing lithospheric recycling with a documented magmatic flare-up capable of developing a dense arc root. Lithospheric mantle thinning/removal and asthenospheric upwelling consistent with extensional collapse perhaps

due to arc root foundering have been used to explain the emplacement of isotopically enriched lamprophyre dikes emplaced at the end of the Ross Orogeny (Rocchi et al., 2009). The period between the Ordovician and Silurian (c. 485–425 Ma) contains no identified *in-situ* magmatic rocks in West Antarctica and, therefore, the lack of age and geochemical control during the first ~60 million years following the Ross Orogeny is poor (Fig. 6). Granitic cobbles from conglomerates in the Antarctic Peninsula with c. 485–425 Ma ages record an increase in the  $\epsilon\text{Hf}_i$  immediately following the Ross Orogeny, consistent with extension (Fig. 6, Bradshaw et al., 2012). Geophysical data have identified an ~100 km thick segment of foundered lithospheric mantle at ~200 km depth beneath the Transantarctic Mountains, providing evidence for an exceptionally thick arc lithosphere at some point in the Phanerozoic (Shen et al., 2018). There are no constraints on when or why lithospheric foundering may have initiated, but it has been generally associated with previous major episodes of extension along the Antarctic margin.

Even though Ordovician–Carboniferous (c. 485–320 Ma) zircon Hf isotope data from Thurston Island, the Antarctic Peninsula, and eastern Marie Byrd Land represent increased juvenile asthenospheric mantle melting compared to the Ross Orogeny, the zircon initial  $\epsilon\text{Hf}_i$  is still far below the depleted mantle evolution line and also varies considerably (Fig. 6). The variation in zircon Hf composition during this, and later time periods, is interpreted to represent either a heterogeneous mantle source (i.e., lithospheric and asthenospheric sources) and/or variable crustal assimilation during magma ascent. Only a few of the lowest zircon  $\epsilon\text{Hf}_i$  values from the Silurian–Carboniferous (c. 420–320 Ma) from Thurston Island, the Antarctic Peninsula, and eastern Marie Byrd Land can be explained by complete recycling of Ross-aged or older crust (assuming a  $\text{Lu}/\text{Hf} = 0.0115$ , Rudnick and Gao, 2003).

Figure 6 demonstrates that almost all Devonian–Carboniferous (c. 350–340 Ma) zircon from both Thurston Island and eastern Marie Byrd Land have juvenile isotopic compositions and are viable sources for Devonian–Carboniferous zircon found within volcanoclastic sedimentary rocks in the central Transantarctic Mountains (Nelson and Cottle, 2017). However, Devonian–Carboniferous zircon from western Marie Byrd Land are more isotopically evolved than eastern Marie Byrd Land and Thurston Island and can be accounted for by remelting of Ross-aged or Grenville-aged lithosphere (e.g., Proterozoic lithospheric mantle) or sedimentary derivatives (Fig. 6). The inferred high degree of ancient lithospheric recycling in western Marie Byrd Land during a period of juvenile magmatism in eastern Marie Byrd Land is problematic (Yakymchuk et al., 2015). The isotopic difference between eastern Marie Byrd Land and western Marie Byrd Land may result from western Marie Byrd Land’s position inboard of the rest of West Antarctica during this time and, consequently, it may have been composed of thicker crust (and/or with a more ancient enriched composition) that led to increased crustal assimilation consistent with spatial isotopic trends within other Cordilleran style magmatic systems (e.g., Chapman et al., 2017). The inferred inboard shift of arc magmatism in the Devonian–Carboniferous may have been caused by an episode of contraction and arc/slab advancement in the Antarctic sector. Enriched Ross-aged or Grenville-aged lithosphere would have been melted during shortening and underthrusting and/or in regions where ancient lithospheric mantle persisted (i.e., western Marie Byrd Land). This scenario is supported by petrogenetic modeling utilizing zircon Hf and O isotopes that indicate a possible enriched lithospheric mantle source in western Marie Byrd Land and Proterozoic Os model ages for peridotite xenoliths of Marie Byrd Land (Handler et al., 2003; Yakymchuk et al., 2015).

Juvenile magmatism in eastern Marie Byrd Land identified in this study (c. 348 Ma) and by detrital zircon in the Transantarctic Mountains (Nelson and Cottle, 2017) occurs either immediately after or during the waning stages of isotopically enriched magmatism in western Marie Byrd Land (c. 375–345 Ma, Yakymchuk et al., 2015). This observation suggests that the Devonian–Carboniferous time period may represent a classic cordilleran-style cycle of contraction (early enriched inboard magmatism in western Marie Byrd Land) followed by extensional collapse (late juvenile outboard magmatism in eastern Marie Byrd Land), consistent with slab advance and subsequent rollback and/or arc root foundering (Fig. 6). This contractional episode is not observed in Thurston Island and the Antarctic Peninsula, which may reflect continued extension in those regions.

Highly positive zircon  $\epsilon\text{Hf}_i$  values persisted in eastern Marie Byrd Land through the Permian and into the Early Triassic (c. 248 Ma), consistent with a decreasing contribution of ancient lithosphere to the melt source and/or ascending magmas following Devonian–Carboniferous contraction. A second-order episode of contraction may be recorded in our Permian data with a shift in  $\epsilon\text{Hf}_i$  from +10 to +3 from c. 295 to 283 Ma. Despite this possible episode of contraction the secular trend is towards increasingly juvenile isotopic values consistent with a major extensional episode throughout the Carboniferous and Permian. However, during this same time period, Thurston Island and the Antarctic Peninsula switched to enriched  $\epsilon\text{Hf}_i$  values indicative of ancient lithosphere recycling during contraction and slab advance that continued through the Jurassic (Flowerdew et al., 2007; Riley et al., 2017). We argue that the Permian shift to enriched zircon Hf isotope compositions similar to the Ross Orogeny in Thurston Island and the Antarctic Peninsula is evidence for possible preservation of an ancient lithospheric mantle that avoided foundering. This is further supported by

mantle-like zircon oxygen isotope compositions ( $\delta^{18}\text{O} = \sim 5.3 \text{ ‰}$ ) for Permian detrital zircon with enriched Hf isotope compositions ( $\epsilon\text{Hf}_i = 0$  to  $+3$ ) from the Antarctic Peninsula (Castillo et al., 2016). The dramatic difference in zircon Hf isotopes for the Permian and Early Triassic between Marie Byrd Land / central Transantarctic Mountains (juvenile) and those for Thurston Island / Antarctic Peninsula (enriched) reflect an along arc geochemical difference and inferred geodynamic switch as previously postulated by Nelson and Cottle (2017). Our new data indicate that this along arc geodynamic change from extension to contraction was originally established in the early Permian and occurs between Thurston Island and Marie Byrd Land (Fig. 6 and 7).

Magmatic rocks of mid-Triassic to mid-Jurassic age are absent from Marie Byrd Land, but decreasing zircon  $\epsilon\text{Hf}_i$  values from the Permian–Triassic to the mid-Jurassic in detrital zircon from the cTAM may suggest Marie Byrd Land was under contraction or was a stationary arc at that time (Fig. 6). By the Late Jurassic and Cretaceous almost all zircon  $\epsilon\text{Hf}_i$  from zircon of West Marie Byrd Land can be explained by melting of juvenile crust formed after the Ross Orogeny (Fig. 6, assuming a  $\text{Lu}/\text{Hf} = 0.0115$ , Rudnick and Gao, 2003). During the Early Cretaceous in western Marie Byrd Land zircon  $\epsilon\text{Hf}_i$  undergo a dramatic isotopic pull-down or shift from relatively juvenile, or positive, compositions to highly enriched, or negative (Yakymchuk et al., 2013), signifying an episode of contraction that is also identified by an isotopic pull-down and compressional deformation in Cretaceous granites in the Antarctic Peninsula (Riley et al., 2018). Our new data from eastern Marie Byrd Land also contain a minor isotopic pull-down consistent with contraction followed by extension at c. 100 Ma, similar to that reported for western Marie Byrd Land (e.g., Korhonen et al., 2010). These observations support previous studies that report contraction-related Cretaceous

magmatic flare-ups in West Antarctic and Zealandia that likely resulted from major plate reorganization in the late Early Cretaceous (Matthews et al., 2012, 2016; Seton et al., 2012; Milan et al., 2017; Riley et al., 2018).

Eastern Marie Byrd Land again is more juvenile than western Marie Byrd Land, which we attribute to an outboard position for eastern Marie Byrd Land and a history of juvenile magmatism that has either not yet been observed or may not have occurred in western Marie Byrd Land. Therefore, Cretaceous contraction resulted in juvenile mantle melts and juvenile lithospheric recycling in eastern Marie Byrd Land (Chapman et al., 2017). This hypothesis is further supported by evidence for an enriched lithospheric mantle source for Cretaceous magmatism in western Marie Byrd Land (e.g., Saito et al., 2013). Earliest Cretaceous magmatism in western Marie Byrd Land, however, was relatively more juvenile than Devonian–Carboniferous magmatism in western Marie Byrd Land (Yakymchuk et al., 2013, 2015). This juvenile source may have resulted from lithospheric thinning prior to the onset of Cretaceous magmatism in western Marie Byrd Land.

#### *Comparisons with adjacent sectors*

New zircon U-Pb and Hf isotope compositions for West Antarctica, combined with previously published values for the Antarctic sector of the paleo-Pacific margin of Gondwana provide the first opportunity to compare the long-term evolution of Antarctica with that of adjacent arc sectors. To do so we compiled, Hf isotope data from igneous and detrital zircon, as well as igneous whole rock Hf isotope data (Figure 8, see references in caption) separated

into two regions, Australia and Zealandia (blue), and South America (red). Zircon Hf isotopes can, however, vary greatly within a single igneous rock sample ( $> 10 \epsilon\text{Hf}_i$ ) and even more so within a given arc, requiring the need for large compilations over extended periods of time ( $\sim 100$  million years or more). Even then, sampling bias, complex arc dynamics and regional variations in magmatic processes and the age of the lithosphere on which the arc was built complicate interpretations. For this reason, every attempt has been made to compile data available over a large geographic distribution and for diverse lithologies.

The Pampean Orogeny in South America and the Delamerian Orogeny in Australia are broadly synchronous with the Ross Orogeny of Antarctica and collectively represent the initial pulse of subduction along the paleo-Pacific margin of Gondwana (Cawood, 2005). The first important observation to make for initial subduction-related magmatism along the arc is that the  $\epsilon\text{Hf}_i$  values across all of these regions during this period are remarkably similar and enriched. We argue that the isotopic composition of the magmatism in these regions is representative of the ancient lithosphere (specifically enriched mantle lithosphere) upon which these different sectors of the Gondwana margin were built, similar to the interpretation for the origin of Ross Orogeny magmatism (Hagen-Peter et al., 2015; Hagen-Peter and Cottle, 2018). The regional tectonic histories of these sectors may vary, but the Hf isotopic record indicates that initial subduction across all segments occurred in a dominantly contractional arc system built on lithosphere with fairly uniform Hf isotope composition. This is an important starting point for the discussion because it provides a single reference frame to evaluate relative changes in Hf isotope composition through time in a single arc sector and also establish variations between different sectors. Significant time-dependent

changes in zircon Hf isotope compositions are therefore most likely a result of geodynamic changes rather than dramatic variations in initial ancient lithospheric Hf composition.

Following initial subduction during the Ross-Delamerian Orogeny at c. 485 Ma the Hf isotope data for Australia and Zealandia reveal a period of juvenile arc formation represented by the Macquarie arc (c. 480–443 Ma) that may have resulted from slab rollback and extension or subduction polarity switch (Aitchison and Buckman, 2012; Rosenbaum, 2018). The termination of the Macquarie arc occurred during a period of persistent contraction from c. 443 to 340 Ma during the Lachlan Orogeny (including contraction in the Thomson and Mossman Orogenesis) represented by enriched isotopic compositions that transition to juvenile compositions related to asymmetric slab rollback and extension (Kemp et al., 2009; Rosenbaum, 2018). Progressive slab rollback culminated in a major widespread period of extension in the early Permian (c. 300–270 Ma, Rosenbaum, 2018) corresponding to a dramatic secular shift from enriched isotopic compositions to juvenile isotopic compositions (Kemp et al., 2009). Following major early Permian extension, juvenile isotopic compositions persist during contractional episodes (e.g., Permian Hunter-Bowen Orogeny) excluding a major contractional episode during formation of Cordillera Zealandia in the Cretaceous (e.g., Milan et al., 2017). Extensional collapse this contractional episode may have been responsible for emplacement of voluminous ignimbrite deposits of the Whitsunday Volcanic Province that have uniformly juvenile isotopic compositions (Tucker et al., 2016). Our new data for eastern Marie Byrd Land combined with data from the central Transantarctic Mountains and western Marie Byrd Land share a similar zircon Hf isotopic history and provide strong evidence for a shared geochemical and geodynamic history

throughout the Phanerozoic for the Australian sector and the Marie Byrd Land and Transantarctic Mountains components of the Antarctic sector (Fig. 9).

In contrast, the South American sector maintains evolved  $\epsilon\text{Hf}_i$  values (primarily negative) similar to that of the Pampean Orogeny from the Ordovician to early Permian reflecting crustal recycling in a dominantly advancing or contractional arc system. Limited zircon Hf isotope data from c. 450 to 360 Ma may be associated with a magmatic lull during accretion of exotic terranes or flat slab subduction in the early and middle Paleozoic (Cawood, 2005; Ramos, 2009; Dahlquist et al., 2018). A minor early Carboniferous (c. 359–322 Ma) episode of slab rollback related extension is recorded by a brief increase in the zircon Hf isotope composition (Dahlquist et al., 2018). The most pronounced period of sustained extension in South America's tectonic history, however, occurred from the late Permian to Early Cretaceous (c. 250 to 140 Ma, Horton, 2018 and references therein). This period is considered to include a major extensional collapse of the proto-Andean arc (San Rafael Orogen) attributed to changing convergence rates generating slab rollback (Ramos, 2009) and is recorded in the zircon Hf record of South America as a shift from enriched Hf isotopic compositions to juvenile isotopic compositions (del Rey et al., 2016; Pepper et al., 2016; Balgord, 2017). Importantly, the shift from enriched to juvenile Hf isotopic compositions occurs in the late Permian in the central Andes (del Rey et al., 2016) and the Jurassic in the southern Andes (Pepper et al., 2016; Balgord, 2017; Castillo et al., 2017b). Both isotopic and tectonic shifts are contemporaneous with large ignimbrite flare-ups, the Choiyoi Province in the central Andes and the Chon Aike in Patagonia (e.g., Kay et al., 1989; Pankhurst et al., 1998a; Rocha-Campos et al., 2011). When contraction is resumed during the initial stage of arc advancement at c. 100 Ma (Ramos, 2009) the zircon Hf isotopes do not

return to enriched compositions. The central Andes do, however, return to ancient lithosphere Hf isotope compositions in the Neogene due to shallow slab subduction and eastward migration of the arc possibly towards regions with more preserved ancient lithospheric mantle (Pepper et al., 2016; Chapman et al., 2017).

The Thurston Island and the Antarctic Peninsula Hf isotope record matches well with the trend for the southern Andes, indicating a coupling of these arc segments, particularly that of the Southern Andes. The mismatch between these records in the Ordovician–Devonian suggests these arc segments may have experienced an uncoupling, perhaps caused by regional tectonics in South America such as terrane accretion or flat slab subduction. However, the shared zircon Hf isotopic history in the early Permian among Antarctic Peninsula, Thurston Island, and South America highlights a geochemical and inferred geodynamic switch along the entire paleo-Pacific margin from enriched compositions during contraction in South America to depleted compositions during extension in Australia at c. 300–270 Ma. The limited data for *in situ* rocks from West Antarctica and Zealandia don't allow us to determine whether this transition is gradual or abrupt, but the locus of the switch is constrained to somewhere between Thurston Island and Marie Byrd Land (Fig. 7, Nelson and Cottle, 2017).

### ***Implications for Phanerozoic accretionary orogens***

The Hf isotopic records for the Antarctic, Australian, and South American sectors of the Gondwana margin are different but contain broadly similar patterns. For instance, the

Permian to Cretaceous (c. 250 to 140 Ma) record of extension in South America is comparable to extension and the isotopic shift observed from c. 430 to 270 Ma in Australia, Zealandia, and Antarctica. Evidence for the propagation of major extension along the Gondwana margin has also been documented using zircon Th/U (McKay et al., 2018). Collectively, these periods of extension in which the continental arc shifts to persistently juvenile isotopic compositions exemplify the process of lithosphere rejuvenation and continental crustal growth characteristic of accretionary orogens (Collins et al., 2011). Our compilation indicates that lithosphere rejuvenation along the Gondwana margin is not necessarily an ongoing process that occurred progressively throughout the Phanerozoic but instead occurred during episodes of major extensional orogenic collapse.

Regional models for extensional orogenic collapse invoke plate boundary processes, i.e., slab rollback (e.g., Kemp et al., 2009; del Rey et al., 2016; Mckibbin et al., 2017), as the driving mechanism. In the Chilean Frontal Andes, however, the shift from enriched to juvenile magmatism (c. 300 to 250 Ma) does not correlate with an outboard migration of arc magmatism that may be expected for slab rollback (Aitchison and Buckman, 2012; del Rey et al., 2016). Numerous models for extensional collapse of other active margins have been suggested as alternatives to slab rollback including slab detachment and lithospheric removal (i.e., foundering) (e.g., Platt et al., 2003). Slab detachment may be unlikely to produce a secular change to juvenile isotopic compositions considering it is often associated with a shallowing of the subducting slab that may lead to contraction (Haschke et al., 2002). In South America, persistently enriched zircon Hf isotopes related to prolonged lithospheric melting during contraction throughout most of the Paleozoic, a shift to juvenile isotopic compositions without outboard arc migration, and the presence of ignimbrite flare-ups during

extensional collapse, could be evidence of ancient catastrophic root removal (Dewey, 1988; DeCelles et al., 2009). Collins et al. (2011) considered lithospheric mantle removal to occur in the backarc due to mantle flow-induced gravitational instability of a normal thickness lithosphere (Currie et al., 2008). However, the fate of overthickened dense arc roots and their relationship to secular evolution of continental margins remains underexplored. We speculate that catastrophic root foundering may have played a critical role in major extensional collapse episodes of the middle Paleozoic to middle Mesozoic in Antarctica, Australia, and South America.

There is the possibility that slab rollback may induce lithospheric mantle foundering or vice-a-versa. For instance, slab rollback could create a step change in density between mantle lithosphere and upwelling asthenosphere that may trigger gravitational instability (Stern et al., 2013). Ramos (2009) described extensional collapse of an Andean-type orogenic cycle as an initial period of slab rollback followed by lithospheric root removal. In contrast, the model of extensional collapse driven initially by lithosphere removal, gravitational forces, and an elevated thermal gradient may occur independent of, or be enhanced by, subsequent plate boundary driven extension (Dewey, 1988; Lister and Forster, 2009). There remains no clear distinction between the roles of plate boundary and internal processes during major middle Paleozoic–middle Mesozoic lithospheric rejuvenation of Phanerozoic accretionary orogens and limits our understanding of the secular evolution of accretionary orogens (Collins et al., 2011).

There are numerous possible explanations for why South America, and Antarctica and Australia, underwent major extensional collapse and lithosphere rejuvenation at different times. In the case of changing plate boundary processes, extensional collapse is dependent on

the timing of major plate reorganization and the absolute motion of Gondwana (and Pangea) that established varied convergence rates along the Gondwana margin (Lallemand et al., 2005; Matthews et al., 2016; Riel et al., 2018). If catastrophic root foundering is responsible for extensional collapse, then differences in the timing of extension would have been controlled primarily by magma addition rates and the rheology of the arc root and mantle that may have varied along the margin (Jull and Kelemen, 2001; Behn et al., 2007; Currie et al., 2015).

Our evaluation of the zircon Hf isotope record of Gondwana margin identifies broad characteristics of the secular evolution of accretionary orogens through geologic time. Initial subduction along the entire paleo-Pacific margin of Gondwana was well established by the Cambrian and occurred during contraction with an enriched lithospheric mantle source and high amounts of supracrustal assimilation. The early to middle Paleozoic history is fairly complicated for all segments of the Gondwana margin with short-term or second-order processes occurring, such as possible polarity switching, retreat and advance, terrane accretion, etc., however, the first-order secular evolution of the arc chemistry maintains an enriched composition due to melting of ancient lithosphere. During the middle Paleozoic to middle Mesozoic the entire Gondwana margin undergoes a major segmented extensional collapse, perhaps caused by slab rollback and/or catastrophic root foundering that begins a secular shift in arc geochemistry towards more juvenile compositions. As contraction is reestablished, the arc maintains a juvenile composition except during major magma flare-ups associated with underthrusting, shallow subduction, and/or arc advancement (i.e., isotopic pulldowns). Importantly, this secular isotopic evolution is also observed in a compilation of zircon Hf isotopes from the western margin of North America, indicating that a global

change in external plate boundary forces during the middle Paleozoic to middle Mesozoic and/or gravity driven catastrophic extensional collapse is an inherent result of over-thickened accretionary orogens.

## **Conclusions**

Zircon geochronology and Hf isotope compositions of magmatic rocks in eastern Marie Byrd Land and Thurston Island provide new constraints on the age and geochemical development of West Antarctica. Both eastern Marie Byrd Land and Thurston Island record crustal growth and extension from the termination of the Ross Orogeny through to the Carboniferous. In eastern Marie Byrd Land, extension may have initiated in the early Carboniferous and continued until the Permian–Triassic following Late Devonian contraction documented in Forge Ranges of western Marie Byrd Land. A switch to contraction is indicated by more negative zircon  $\epsilon\text{Hf}_i$  through the Cretaceous in the central Transantarctic Mountains and western Marie Byrd Land. In contrast, Thurston Island switched to enriched  $\epsilon\text{Hf}_i$  values and contraction in early Permian through Jurassic time followed by an increase in  $\epsilon\text{Hf}_i$  and extension in the Cretaceous.

Comparing these records to zircon Hf isotope compilations from adjacent sectors of the arc demonstrates a shared geochemical and tectonic history for Marie Byrd Land, Australia, and Zealandia that contrasts with the history of Thurston Island, the Antarctic Peninsula, and South America. Our compilation also demonstrates the presence of a significant along arc geochemical and inferred geodynamic switch from enriched isotopic

compositions and contraction in South America, the Antarctic Peninsula, and Thurston Island to depleted isotopic compositions and extension in Marie Byrd Land during the early Permian. This variation highlights the difference in timing of major extensional collapse and lithospheric rejuvenation between Australia and Marie Byrd Land (c. 430–270) and South America (c. 250–140) that is evidenced by a shift to persistent juvenile zircon Hf isotopic compositions during these times. Plate boundary processes related to plate reconfiguration (e.g., slab rollback) and/or internal processes (e.g., lithospheric foundering, gravitational collapse, and heating) may have driven extensional collapse and lithospheric rejuvenation of Phanerozoic accretionary orogens. We conclude that Phanerozoic accretionary orogens have undergone comparable secular Hf isotope evolutionary histories.

### **Acknowledgements**

This material is based upon work supported by the National Science Foundation Graduate Research Fellowship under Grant No. 1650114 and support from NSF—ANT—1443296, NSF—ANT—1043152. This research used samples and/or data provided by the Polar Rock Repository (PRR). The PRR is sponsored by the National Science Foundation Office of Polar Programs. We are grateful to Anne Grunow and the PRR for providing samples and assisting with sample selection. We also acknowledge the original sample collectors: C. Craddock, I. Dalziel, V. DiVenere, P. Schmidt, B. Sporli, and C. White. Special thanks to S. Mukasa and F. Fahnestock for providing zircon separates. Constructive reviews from M. McKay and two anonymous reviewers greatly improved this manuscript. Additional

analytical details and data tables are available in the Supplementary Information and Datasets.



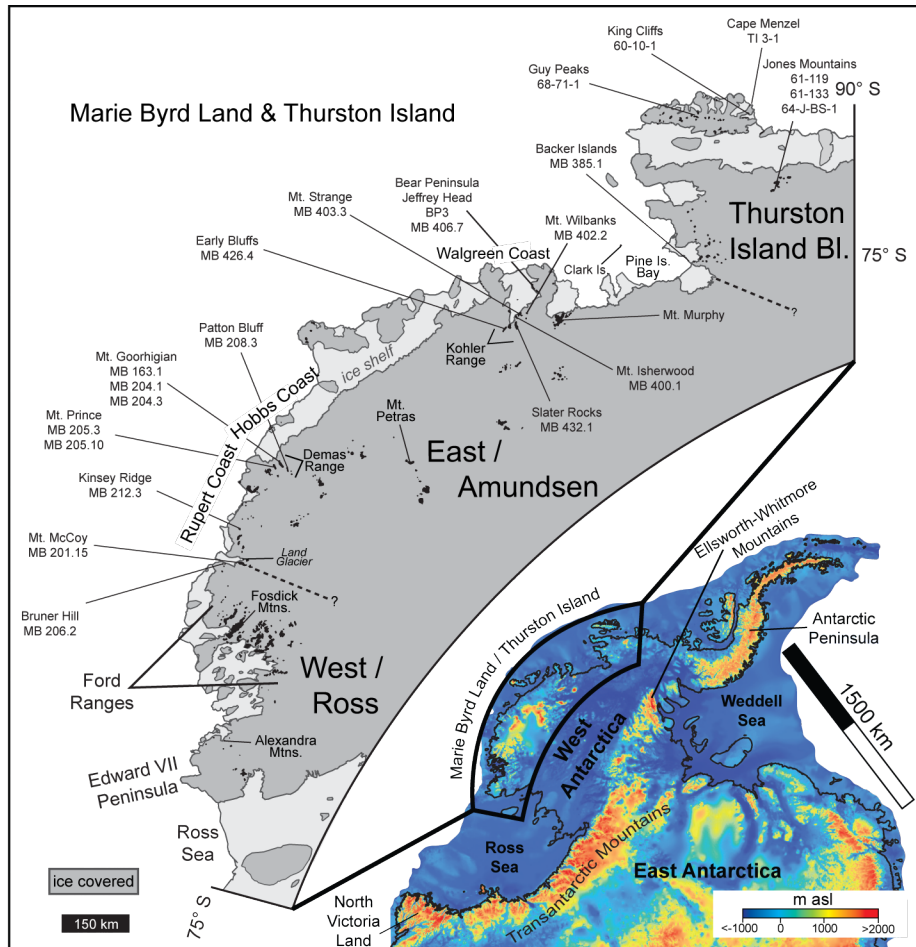


Figure 2. (Color map) Subice topographic DEM of Antarctica (BEDMAP2) with major crustal blocks and localities identified; asl—above sea level (Fretwell et al., 2013). (B&W map) Enlarged map of Marie Byrd Land and Thurston Island showing sample locations (Pankhurst et al., 1998b).

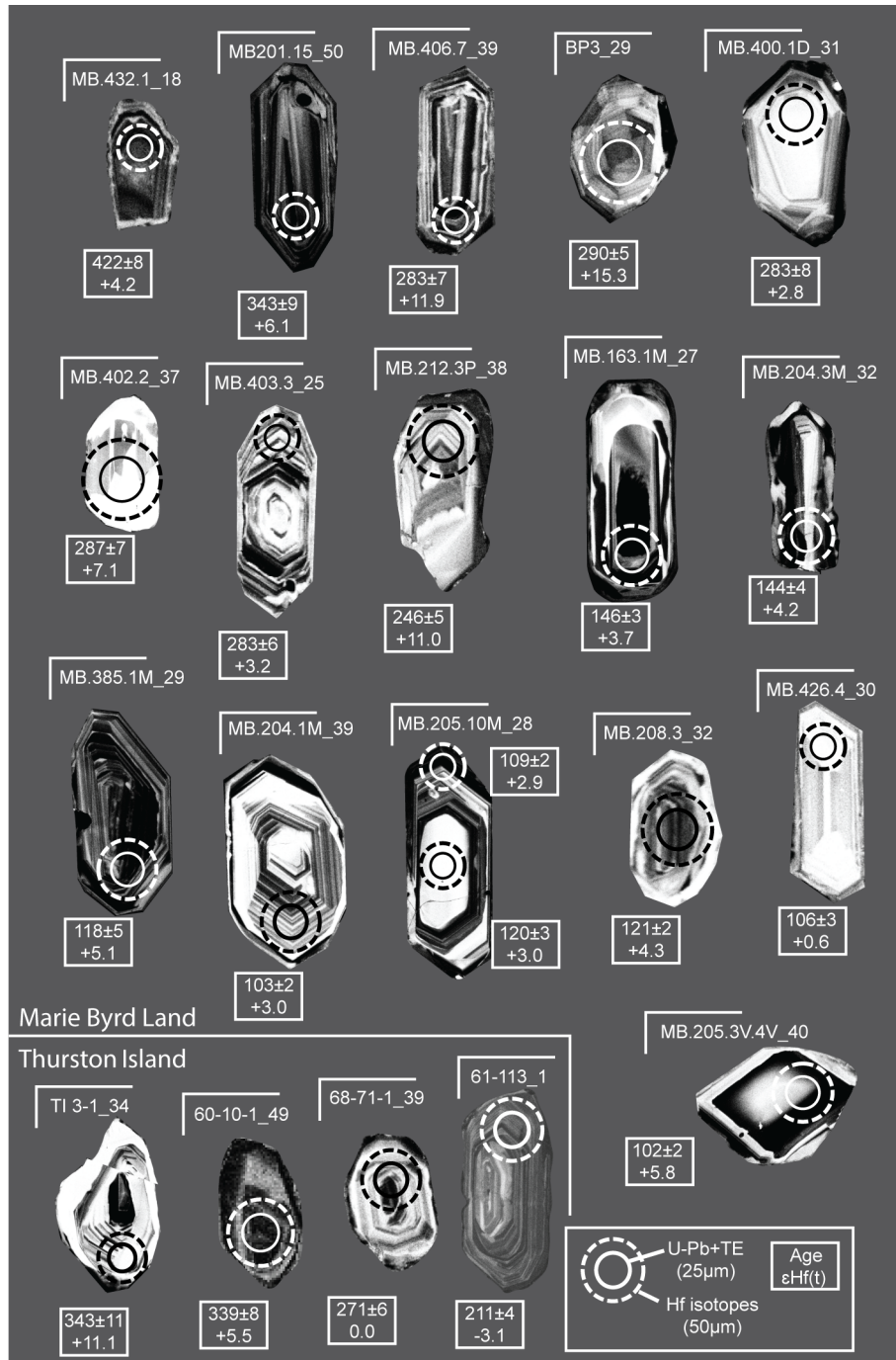


Figure 3. Representative zircon cathodoluminescence images for each sample showing the location of U-Pb and Hf isotopic analyses with the correlated single spot age and epsilon Hf.

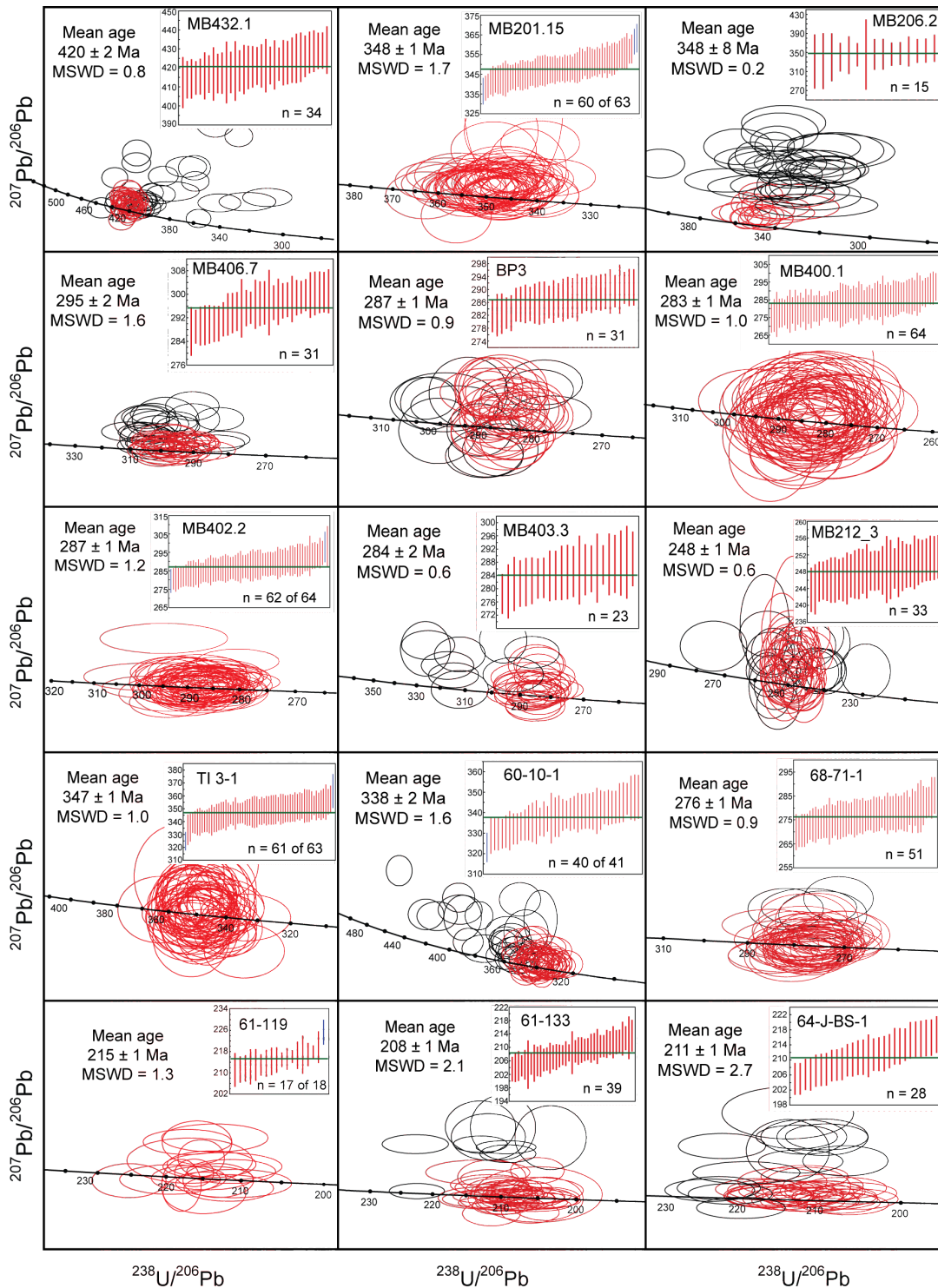


Figure 4. Zircon U-Pb geochronology data for Silurian to Triassic aged samples of East Marie Byrd Land and Thurston Island in Tera-Wasserburg Concordia plots.  $^{207}\text{Pb}$  corrected  $^{206}\text{Pb}/^{238}\text{U}$  ages (inset) are provided for select ellipses in red and used to calculate weighted mean ages. See Dataset S1 for full zircon U-Pb dataset.

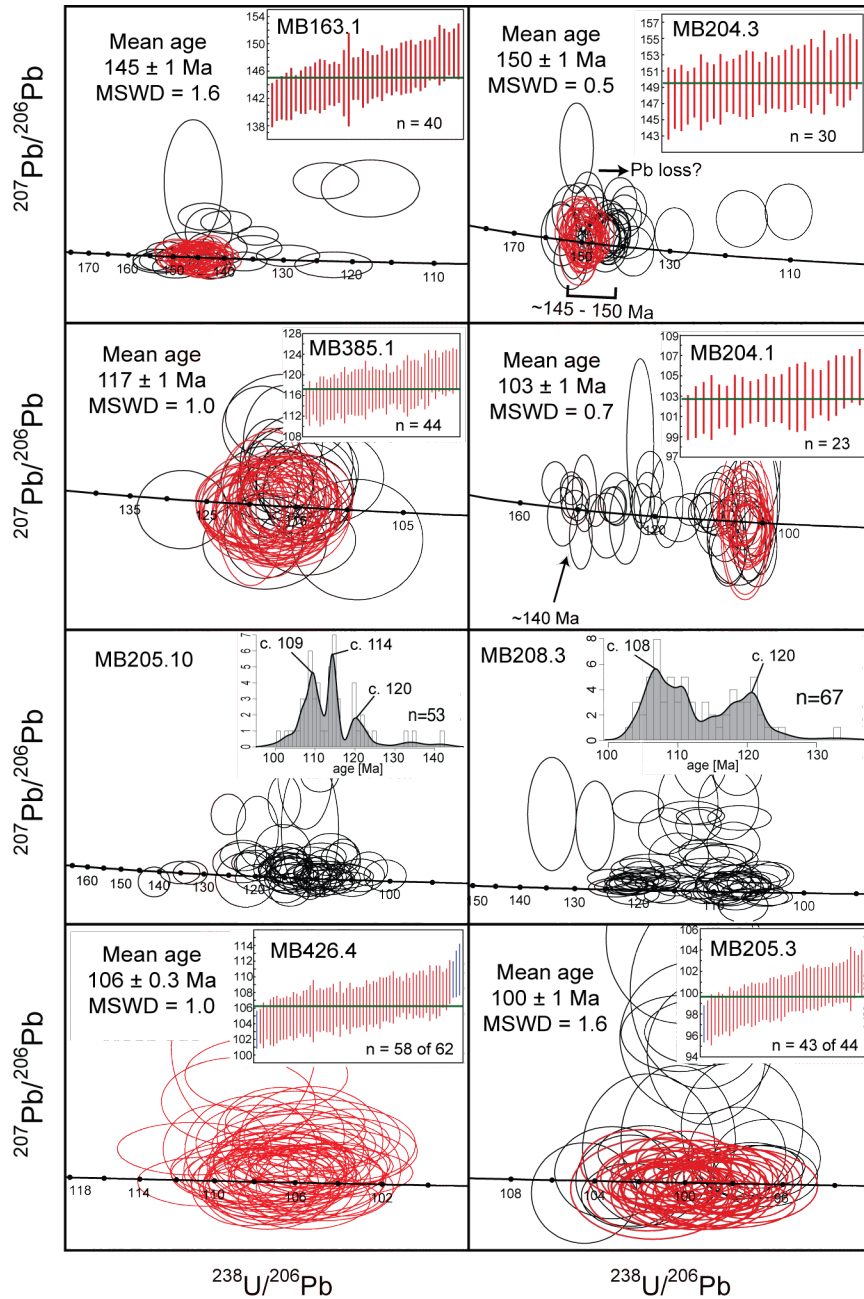


Figure 5. Zircon LASS U-Pb geochronology data for Late Jurassic to Cretaceous aged samples of eastern Marie Byrd Land in Tera-Wasserburg Concordia plots.  $^{207}\text{Pb}$  corrected- $^{206}\text{Pb}/^{238}\text{U}$  ages (inset) are provided for select ellipses in red and used to calculate weighted mean ages. Normal kernel density estimates with a bandwidth of 1 and histograms are provided when no single age is dominant (Vermeesch, 2012). See Dataset S1 for full zircon U-Pb dataset.

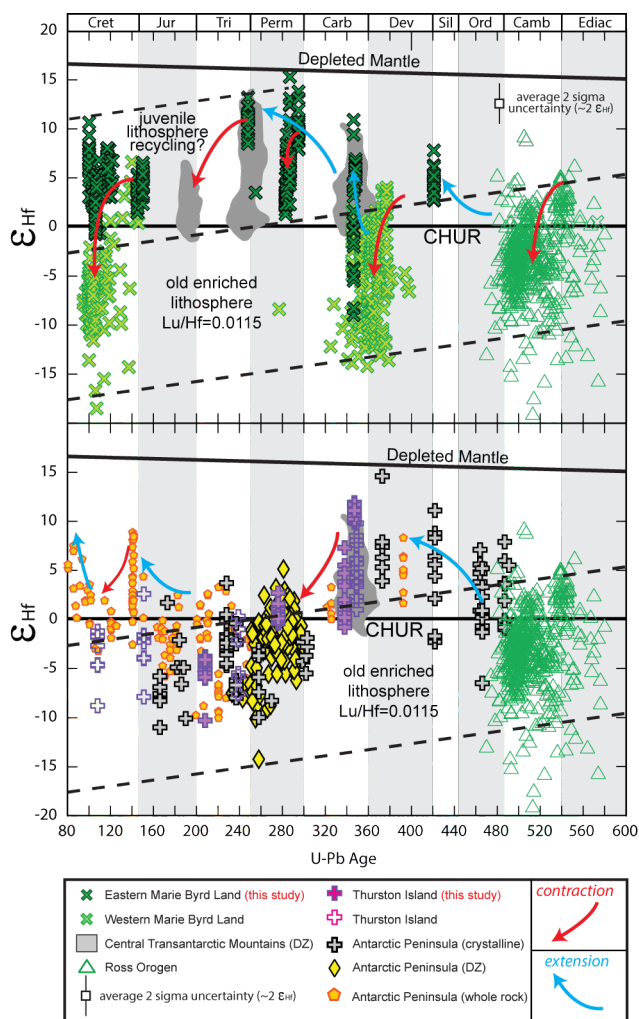


Figure 6. Zircon age versus initial  $\epsilon_{\text{Hf}}$  plot summarizing all Hf isotopic data from this study combined with available data for the Ross Orogen (Hagen-Peter et al., 2015; Yakymchuk et al., 2015; Hagen-Peter and Cottle, 2018), the central Transantarctic Mountains (Nelson and Cottle, 2017), western Marie Byrd Land (Yakymchuk et al., 2013, 2015), Thurston Island (Riley et al., 2017), and the Antarctic Peninsula (Millar et al., 2001; Fanning et al., 2011; Bradshaw et al., 2012; Castillo et al., 2016). Dashed lines outline fields of crustal recycling assuming a  $\text{Lu}/\text{Hf} = 0.0115$  (Rudnick and Gao, 2003). Colored arrows correspond to geodynamic interpretations of extension or contraction based on relative increases and decreases in zircon  $\epsilon_{\text{Hf}}$ . Hf isotopic values for depleted mantle is from Vervoort and Blichert-Toft (1999). CHUR—chondritic uniform reservoir. DZ = detrital zircon and CZ = zircon from crystalline rocks. Whole rock Hf isotope data from were converted from Nd isotope data (Millar et al. 2001) using the terrestrial array equation of (Vervoort et al., 1999). See Dataset S2 for full zircon Hf isotope dataset.

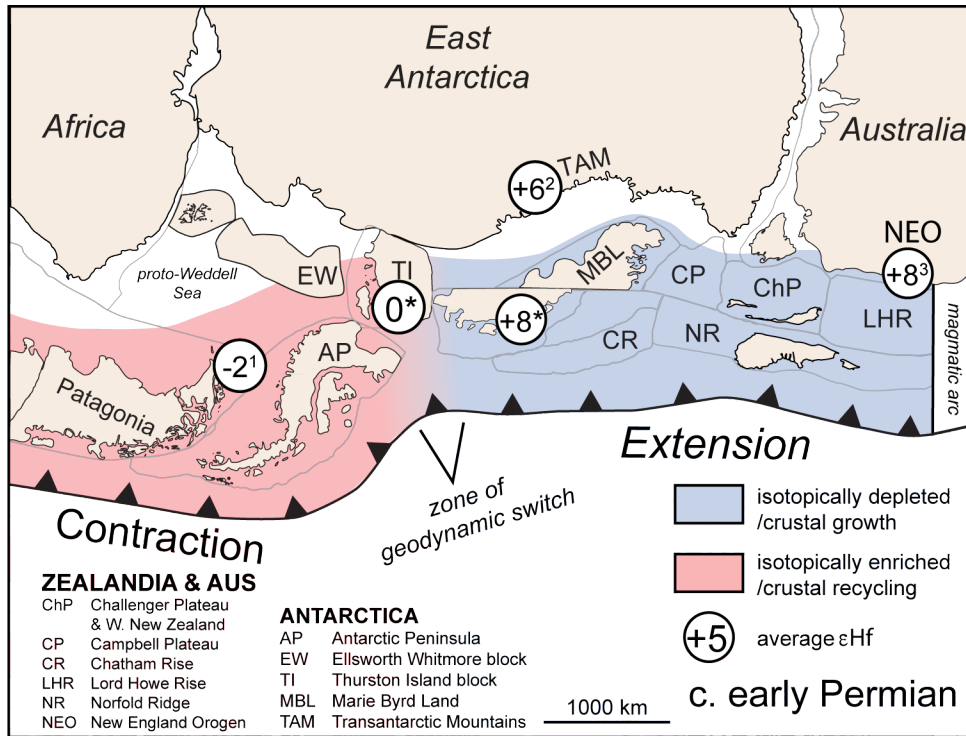


Figure 7. Reconstruction of the Gondwana plate margin, c. Permian (Elliot, 2013). Shown are the inferred limits of the isotopically depleted and extensional arc (red) and the isotopically enriched and contractional arc (blue). Average Hf isotope compositions are calculated using Permian aged zircon Hf isotope data from: \*this study, <sup>1</sup>Antarctic Peninsula and Patagonia (Castillo et al., 2016), <sup>2</sup>central Transantarctic Mountains (Nelson and Cottle, 2017), and <sup>3</sup>New England Orogen (Kemp et al., 2009; Phillips et al., 2011; Shaw et al., 2011). These data suggest a zone of geochemical and geodynamic switch occurs in the region between the Thurston Island block and Marie Byrd Land in the early Permian.

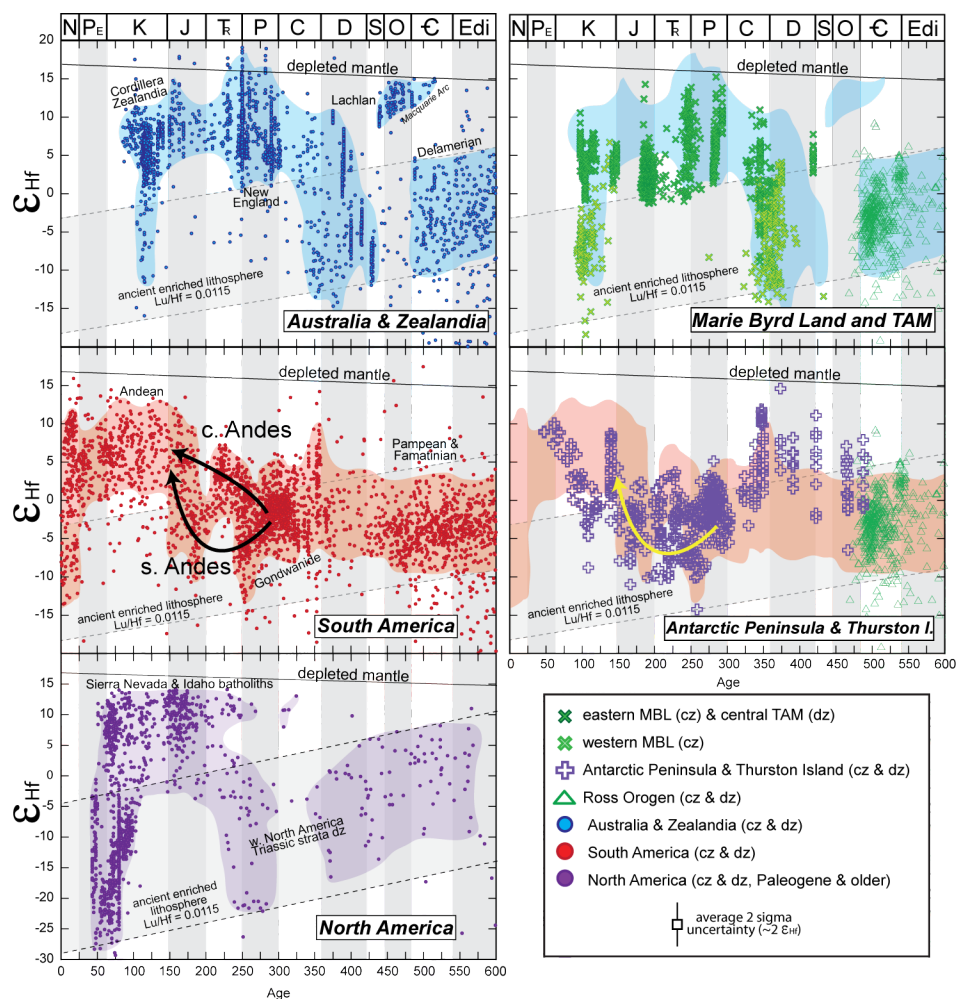


Fig. 8. Compilation of zircon Hf isotope data from (A) Australia–Zealandia (red), (B) South America (blue), and (C) North America with hand drawn fields to outline dominant geochemical envelopes. Data for Australia–Zealandia are from: (Belousova et al., 2005; Kemp et al., 2005; Veevers et al., 2006; Kemp et al., 2007; Murgulov et al., 2007; Nebel et al., 2007; Kemp et al., 2009; Allibone et al., 2009; Nebel-Jacobsen et al., 2011; Phillips et al., 2011; Shaw et al., 2011; Glen et al., 2011; Jeon et al., 2014; Hiess et al., 2015; Li et al., 2015; Purdy et al., 2016; Tucker et al., 2016; Martin et al., 2017; Milan et al., 2017; Schwartz et al., 2017; Decker et al., 2017). Data from South America are from: (Flowerdew et al., 2006; Munizaga et al., 2008; Willner et al., 2008; Bahlburg et al., 2009; Mišković and Schaltegger, 2009; Fanning et al., 2011; Bradshaw et al., 2012; Hervé et al., 2013, 2014, 2016; Augustsson et al., 2016; Pankhurst et al., 2016; Pepper et al., 2016; Canile et al., 2016; Castillo et al., 2016, 2017; del Rey et al., 2016; Ortiz et al., 2017; Balgord, 2017; Dahlquist et al., 2018). Data from North America are from: (Cecil et al., 2011; Lackey et al., 2012; Gaschnig et al., 2013; Gehrels and Pecha, 2014; Garver and Davidson, 2015; Barth et al., 2016; Sauer et al., 2017). Paleozoic and Triassic data from Gehrels and Pecha (2014) are from Triassic strata in British Columbia through Sonora in North America. D and E compare Antarctica data presented in Figure 6 with compilations from A and B. Dashed lines outline fields of crustal recycling assuming a Lu/Hf = 0.0115 ((Rudnick and Gao, 2003). Hf isotopic values for depleted mantle and new crust are from Vervoort and Blichert-Toft (1999). CHUR—chondritic uniform reservoir. CZ refers to crystalline rock zircon and DZ refers to detrital zircon.

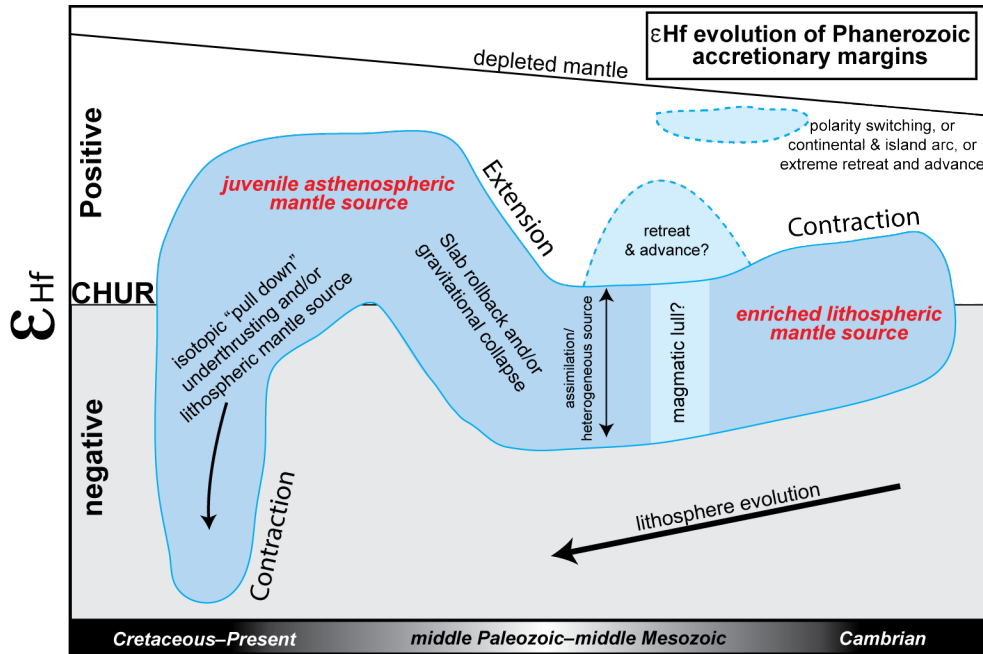


Figure 9. Generalized zircon Hf isotope evolution curve for Phanerozoic accretionary orogens. All orogens record c. Cambrian magmatism with an enriched lithospheric mantle source and an inferred contractional tectonic regime. Early Paleozoic records vary with episodes of extension and contraction, terrane accretion, magmatic lulls, etc. All orogens, however, undergo a profound isotopic shift from enriched to juvenile compositions during major extensional collapse in the middle Paleozoic to middle Mesozoic that may be caused by plate boundary processes (i.e., slab rollback) and/or internal processes (i.e., gravitational collapse related to root foundering). In the Cretaceous, major isotopic pull-downs occur during major contractional episodes.

Table 1: Summary of zircon geochronology and geochemistry

Sample #	Rock Type	Location	Lat (S) <sup>a</sup>	Long (W) <sup>a</sup>	Age ± 2σ (Ma)	MSWD	Inherited (Ma)	Mean εHf <sub>i</sub> (2SE)
<b>Thurston Island</b>								
61-133	Granite	Jones Mtns	73.50	94.40	208 ± 1	2.1		- 4.8 (0.7)
64-J-BS-1	Granite	Jones Mtns	73.50	94.37	211 ± 1	2.7	c. 1131 & 1433	n.d.
61-119	Granite	Jones Mtns	73.50	94.37	215 ± 1	1.3		n.d.
68-71-1	Diorite	Guy Peaks	72.15	98.90	276 ± 1	0.9		0.4 (0.7)
60-10-1	Orthogneiss	King Cliffs	72.30	96.02	338 ± 2	1.6		2.1 (1.2)
TI 3-1	Orthogneiss	Cape Menzel	72.06	95.76	347 ± 1	1.0		11.0 (0.6)
<b>Marie Byrd Land</b>								
MB 205.3V	Dike Swarm	Mt. Prince	74.97	134.17	100 ± 1	1.6		6.8 (0.7)
MB 205.10M	Granite	Mt. Prince	74.97	134.17	108–120			4.2 (0.7)
MB 208.3	Granite	Patton Bluff	75.22	133.68	110–120			4.7 (0.5)
MB 204.1M	Granite	Mt. Goorhigian	75.05	133.80	103 ± 1	1.0	c. 140 & 247	3.7 (0.5)
MB 426.4	Monzogranite	Early Bluff	75.19	113.97	106 ± 1	1.0	c. 412	0.8 (0.5)
MB 385.1M	Granite	Backer Island	74.47	102.39	117 ± 1	1.0		6.5 (0.9)
MB 163.1M	Granite	Mt. Goorhigian	75.05	133.72	145 ± 1	1.6		3.5 (0.5)
MB 204.3M	Orthogneiss	Mt. Goorhigian	75.05	133.80	150 ± 1	0.5		4.7 (0.5)
MB 212.3P	Granite	Kinsey Ridge	75.37	139.15	248 ± 1	0.6	c. 1089	10.9 (0.6)
MB 400.1D	Granodiorite	Mt. Isherwood	74.98	113.70	283 ± 1	1.0		3.0 (0.5)
MB 403.3	Quartz Diorite	Mt. Strange	74.96	113.52	284 ± 2	0.6		6.0 (0.8)
BP3	Granodiorite	Bear Peninsula	74.55	111.89	287 ± 1	0.9		9.0 (1.1)
MB 402.2	Quartz Diorite	Mt. Wilbanks	75.00	112.88	287 ± 1	1.2		5.8 (0.5)
MB 406.7	Granite	Jeffrey Head	74.55	111.90	295 ± 2	1.6		10.2 (0.7)
MB 201.15	Granite	Mt. McCoy	75.80	141.00	348 ± 1	1.7	c. 572	5.3 (0.4)
MB 206.2	Orthogneiss	Bruner Hill	75.65	142.40	348 ± 8	0.2		0.2 (2.0)
MB 432.1	Granodiorite	Slater Rocks	75.08	113.88	420 ± 2	0.8		4.7 (0.5)

<sup>a</sup>Reported by the Polar Rock Repository

### **III. Tracking voluminous Permian volcanism of the Choiyoi Province into central Antarctica**

#### **Abstract**

Permian volcanic deposits are widespread throughout southwestern Gondwana and record voluminous silicic continental arc volcanism (e.g., Choiyoi Province) that may have contributed to Permian global warming and environmental degradation. Many Permian volcanic deposits of southwestern Gondwana, however, have not been accurately correlated to magmatic source regions along the active paleo-Pacific margin of Gondwana, limiting our understanding of the timing and distribution of voluminous volcanism. Here we present detrital zircon U-Pb and Hf isotope data for Permian volcanoclastic sedimentary rocks from the Ellsworth Mountains, Pensacola Mountains, and the Ohio Range of central Antarctica in southwestern Gondwana and use it to determine their volcanic source along the paleo-Pacific margin of Gondwana. Rocks in central Antarctica record Permian volcanism between c. 277 to 260 Ma with a weighted mean  $\epsilon\text{Hf}_i -0.2 \pm 0.5$  (2SE) for all Permian zircon. Comparison of these zircon age and Hf data with compilations for adjacent regions along the Gondwana margin suggest derivation from a major episode of Permian explosive arc volcanism that is broadly synchronous with, and geochemically similar to, the voluminous Choiyoi Province in South America. The data indicate that volcanoclastic deposits in the Karoo Basin, South Africa, are also sourced from this high magma flux event, but contain zircon with higher Gd/Yb and U/Yb suggestive of a thicker arc crust in the source for volcanoclastic deposits of

the Karoo Basin. In aggregate, Permian zircon in central Antarctica support an along-arc variation in geochemistry, geodynamics, and crustal thickness, with isotopically enriched high-flux magmatism and thickened crust during contraction in South America and isotopically depleted magmatism and thinned crust during extension in Australia. The timing of Choiyoi-related explosive volcanism recorded in central Antarctica and the Karoo Basin is contemporaneous with a documented increase in global arc flux, an increase in atmospheric CO<sub>2</sub>, a decrease in  $\delta^{13}\text{C}$  of benthic marine fossils, and mass extinction events. We suggest that the Choiyoi Province contributed to increased global arc flux in the Permian, leading to elevated background levels of atmospheric CO<sub>2</sub> conducive to producing an environmental crisis during large igneous province emplacement, and may serve as an example of continental arc outgassing exerting a first order control on climate.

## **Introduction**

There is evidence for widespread explosive continental arc volcanism during the Permian throughout southwestern Gondwana (Fig. 1, Rocha-Campos et al., 2011; Sato et al., 2015; Castillo et al., 2016; Elliot et al., 2016, 2017; McKay et al., 2016). In South America, Permian arc volcanism resulted in exceptionally high volume silicic volcanism in the Choiyoi Province (estimated volume of  $\sim 1.3 \text{ Mkm}^3$ ) that may have contributed to global climate change, Permian mass extinctions and biotic crises (e.g., Henry et al., 2009; Hermann et al., 2011; Henry, 2013; Limarino et al., 2014; Kimbrough et al., 2016; Spalletti and Limarino, 2017; Luppó et al., 2018). Correctly correlating Permian volcanic deposits in southwestern

Gondwana to the Choiyoi Province, therefore, is critical to determining the distribution and timing of one of the largest silicic provinces along the paleo-Pacific margin of Gondwana and its relationship to Permian global warming and environmental degradation.

Constraints on the timing and geochemistry of regional Permian volcanism in the proto-Weddell Sea segment of the paleo-Pacific margin have been greatly improved by the application of zircon geochronology and geochemistry (i.e., petrochronology) in studies of detrital zircons in volcanoclastic sediments (Fanning et al., 2011; Canile et al., 2016; Castillo et al., 2016; McKay et al., 2016b; Kylander-Clark, 2017; Nelson and Cottle, 2017). In particular, detrital zircon U-Pb geochronology and Hf isotopic investigations of sedimentary rocks from the Paraná Basin and accretionary complexes of the Antarctic Peninsula and Patagonia (Fig. 1) have identified Permian volcanic detritus that may be directly sourced from the Choiyoi Province or correlative continental arc magmatism (Fanning et al., 2011; Canile et al., 2016; Castillo et al., 2016). In contrast, distal volcanic deposits in the Karoo Basin of South Africa (Fig. 2), although synchronous with the Choiyoi Province, have instead been correlated to volcanic deposits and detrital zircon in the Ellsworth and Transantarctic mountains (Fig. 1 and 2) of Antarctica, based on detrital zircon Th/U ratios (McKay et al., 2016b). Sedimentary facies comparisons of Permian successions in the Ellsworth and Transantarctic mountains with the Karoo Basin, however, suggest deposition in two separate and distinct basins that may not contain correlative volcanic detritus (Elliot et al., 2016a). Thus, it remains unclear whether explosive volcanic deposits correlative to the Choiyoi Province extend into South Africa and the Ellsworth and Transantarctic mountains of Antarctica. This limits our understanding of the volume and distribution of distal ashes from one of the largest silicic volcanic provinces in Earth's history.

Combined zircon geochronology and geochemistry, e.g., trace elements and Hf isotopes, provide an ideal opportunity to investigate volcanic provenance along the paleo-Pacific margin (Kylander-Clark, 2017). Comprehensive zircon geochemistry data does not exist for Permian volcanic deposits of the Ellsworth and southern Transantarctic mountains (TAM), referred to here as central Antarctica (Fig. 2). An advantage of combined geochronology and geochemical data for accessory minerals such as zircon (i.e., petrochronology) is the ability to stitch together a fragmented temporal, geochemical, and geodynamic history of a convergent margin using both igneous and sedimentary rocks. Furthermore, the addition of geochemical tracers provides increased reliability to provenance studies that otherwise rely solely on geochronologic data. A petrochronologic approach, therefore, is particularly useful in Antarctica where the tectonic evolution is highly fragmented due to inaccessibility and poor exposure (Fig. 2). For this reason, we focus on key sections of Permian strata in central Antarctica, i.e., Ellsworth Mountains and southern TAM (Fig. 2, Elliot et al., 2016, 2017), with the goal of characterizing the age and geochemistry of Permian-aged zircon. These data are compared with a new compilation of zircon Hf data for surrounding crustal blocks to determine potential temporal and geochemical correlations with other Permian-aged rocks along the Gondwana margin. The data support the contention that Permian volcanic strata from central Antarctica and the Karoo Basin represent distal components of continental arc volcanism temporally and geochemically characteristic of South America and the Choiyoi Province.

## **Geological Background**

The source of widespread Permian distal volcanic ash deposits and detrital zircon within the proto-Weddell Sea region is generally considered to be the outboard active continental paleo-Pacific margin of Gondwana, including the Choiyoi Province (Fig. 1, Sato et al., 2015; Canile et al., 2016; Elliot et al., 2016). However, this segment of the Gondwana margin has been highly dissected due to supercontinent breakup in the Jurassic through Cretaceous and, consequently, reconstructing the pre-breakup arrangement of the various crustal blocks has been considered the “problem child” of paleo-Pacific margin tectonics (Dalziel and Elliot, 1982; Grunow et al., 1987; Storey et al., 1988). This problem has been further complicated by the inaccessibility and poor exposure of areas of interest in southern Patagonia and ice-covered regions in West Antarctica (Fig. 2). For these reasons, potential sources of Permian-aged detrital zircon in volcanogenic sediments in the Paraná Basin, southern Patagonia, West Antarctica, and South Africa have been limited to abundant Permian subduction-related magmatic and volcanic rocks of the Choiyoi Province, or sparse occurrences of subduction-related Permian granites in the crustal blocks of West Antarctica (e.g., Antarctic Peninsula, Marie Byrd Land, Thurston Island, Fig. 2) (Fanning et al., 2011; Canile et al., 2016; Castillo et al., 2016; Elliot et al., 2016a, 2017; McKay et al., 2016b).

The Choiyoi Province (Fig. 1) is principally characterized by widespread Permian subduction-related andesitic to rhyolitic volcanic rocks (primarily ignimbrites) erupted over an area of  $\sim 1.7$  Mkm<sup>2</sup> of Chile and Argentina, with an average thickness of 700 m emplaced between c. 282 to 251 Ma with a major flare-up at 269 to 263 Ma (e.g., Rocha-Campos et al., 2011; Kimbrough et al., 2016; Spalletti and Limarino, 2017). The plutonic components of the Choiyoi are broadly defined as tonalities-granodiorites to granites emplaced between 286 to 247 Ma (e.g., Sato et al., 2015). Plutonic and volcanic rocks of the Choiyoi Province are

distributed across the Chilean Coastal Cordillera, the Chilean Precordillera, the Principal and the Frontal Andean Cordillera, the Argentinian Precordillera, the San Rafael-Las Matras-Chadileuvú Blocks and northern Patagonia, including the North Patagonian Massif. Contemporaneous Permian plutonic rocks have also been discovered in Tierra del Fuego (Fig. 1). Proposed distal volcanic ashes of the Choiyoi Province are found throughout Late Paleozoic Gondwana basins in South America and South Africa including the Paraná and Karoo basins, respectively (Fig. 1). Voluminous calc-alkaline volcanism and magmatism of the early stage of the Choiyoi Province at c. 280 to 265 Ma is generally syntectonic with transpression during the San Rafael compressional event and Gondwanide Orogeny (e.g., Kleiman and Japas, 2009). The later stage of Choiyoi Province is characterized by anorogenic magmatism from c. 265 to 250 Ma associated with extensional collapse of the San Rafael event and Gondwanide Orogeny at c. 265 Ma (Kleiman and Japas, 2009; Rocha-Campos et al., 2011; Sato et al., 2015).

Definitive volume estimates for the Choiyoi Province, volcanic and plutonic, are lacking but there is broad consensus that the Choiyoi Province represents the largest silicic magmatic event in southwestern Gondwana (e.g., Rocha-Campos et al., 2011; Sato et al., 2015; Kimbrough et al., 2016; Spalletti and Limarino, 2017). The age of the Choiyoi Province (c. 286 to 247 Ma) overlaps with the Permian–Triassic and End Guadalupian mass extinction events, carbon isotope excursions, and a shift from icehouse to greenhouse conditions associated with increases in atmospheric greenhouse gases (Spalletti and Limarino, 2017). For these reasons, the Choiyoi Province has been proposed as a major source of volcanogenic greenhouse gases (e.g., CO<sub>2</sub>) during volcanism and magmatism that heated organic-rich Paleozoic sedimentary rocks, releasing additional greenhouse gases and

contributing to Permian global warming and environmental crises (Henry et al., 2009; Hermann et al., 2011; Henry, 2013; Limarino et al., 2014; Kimbrough et al., 2016; Spalletti and Limarino, 2017; Luppó et al., 2018).

Recent work has utilized zircon geochronology and geochemistry to unlock the history of Permian magmatism and volcanism in southwestern Gondwana contemporaneous with the Choiyoi Province. U-Pb and Hf isotopes of detrital zircon within volcanoclastic rocks from the Paraná Basin are reported to be temporally and geochemically comparable to the Choiyoi Province (Canile et al., 2016). Similarly, Fanning et al. (2011) and Castillo et al. (2016) utilized zircon Hf-O isotopes to demonstrate a correlation in Permian detrital zircon Hf isotope compositions between the Antarctic Peninsula, Patagonia, and the Choiyoi Province. They argue that similarities in age and zircon Hf isotope composition for detrital zircon from the Antarctic Peninsula and Patagonia suggest they may be sourced directly from the Choiyoi Province or a temporally and geochemically related southern extension of the Permian magmatic arc into southern Patagonia and the Antarctic Peninsula.

Distal volcanic tuffs from the Karoo Basin, South Africa (Fig. 1), overlap in age with Permian zircon from South America and may represent distal ash deposits of the Choiyoi Province (e.g., McKay et al., 2016). Whole-rock geochemistry for Karoo Basin tuffs indicate a possible intraplate magmatic source consistent with back-arc magmatism rather than continental arc magmatism (McKay et al., 2016b). Whole-rock data for Karoo Basin tuff samples, however, are contaminated by admixed detritus consisting of possibly multiple geochemically distinct signatures and require zircon geochemistry for reliable time-integrated geochemical interpretations. Similarities in zircon Th/U ratios were interpreted to indicate that Karoo Basin tuffs are genetically related to volcanogenic sediments in the

Ellsworth Mountains and TAM, Antarctica (Fig. 1 and 2), rather than Permian zircon from South America, i.e., Choiyoi Province (McKay et al., 2016b). Zircon Th/U ratios, however, may vary greatly within a single magma system due to temperature variations and differentiation, which make Th/U a potentially unreliable geochemical tracer for zircon provenance (e.g., Kirkland et al., 2015; Yakymchuk et al., 2018). Instead, Hf isotopes provide a more reliable geochemical signature of the magma source because Hf isotopic ratios do not vary with magma temperature and fractionation. Zircon Hf isotopic data, unfortunately, do not currently exist for Permian zircon from either the Karoo Basin or Permian strata of central Antarctica (Elliot et al., 2016a, 2017; McKay et al., 2016b). In this contribution, we investigate the geochronology, trace elements, and Hf isotopic composition of Permian zircon from Permian strata (Fig. 2 and 3, >500 km between each locality) of the Ellsworth Mountains (Polarstar Formation), and the Ohio Range (Mt. Glossopteris Formation) and Pensacola Mountains (Pecora Formation) of the southern TAM to clarify correlations with the Karoo Basin, Choiyoi flare-up in South America, or petrogenetically distinct magmatism recorded in the CTAM, Marie Byrd Land, Zealandia, and Australia. Our data, combined with a new compilation for adjacent regions along the Gondwana margin, demonstrate that Permian zircon from central Antarctica and the Karoo Basin have a strong temporal and geochemical similarity to South America and the Choiyoi Province.

***Polarstar Formation, Ellsworth Mountains***

The Polarstar Formation is the youngest formation of the Paleozoic strata in the Ellsworth Mountains (Fig. 2 and 3, Elliot et al., 2016; Castillo et al., 2017a; Craddock et al., 2017). A minimum thickness of 1.2 km for the intensely folded strata of the Polarstar Formation has been estimated by combining several measured sections. The Polarstar Formation has been divided into a lower Argillite Facies, middle volcanoclastic Sandstone–Argillite Facies, and upper *Glossopteris*–bearing Coal Measures Facies (Collinson et al., 1992; Elliot et al., 2016a). Our sample is from the middle volcanoclastic sandstone facies (Fig. 3). Comparable Permian strata to the Polarstar Formation have been identified in eastern Ellsworth Land, the Karoo Basin of South Africa, the Falkland Islands, and central TAM (Elliot et al., 2016). Based on geochronology and facies comparisons, the Polarstar Formation has been interpreted as an extension of the Permo–Triassic Transantarctic Basin and is separate from the Karoo Basin of South Africa and Permian deposits in the Falkland Islands (Elliot et al., 2016a). Volcanogenic Permian detrital zircon for volcanoclastic sandstones of the Polarstar Formation generally range in age from 270 to 260 Ma and three zircon U-Pb dates have been determined for tuff beds:  $258 \pm 2$  Ma,  $263 \pm 2$  Ma, and  $263 \pm 1$  Ma (Elliot et al., 2016a; Craddock et al., 2017a).

### ***Mt. *Glossopteris* Formation, Ohio Range***

The Permian Mt. *Glossopteris* Formation is the youngest formation in the Ohio Range of the Transantarctic Mountains (Fig. 2 and 3, Elliot et al., 2017). It is comprised of a lower marine succession (shale and siltstone) and a thick upper fluvial succession consisting of

sandstones and coal (Collinson et al., 1994). The Mt. Glossopteris Formation is a member of the Beacon Supergroup that comprises Devonian-Triassic sediments of the TAM and correlates with the Buckley and Fairchild formations in the central TAM and the Weller Formation in south Victoria Land (Elliot et al., 2017). Recent detrital zircon geochronology for the Mt. Glossopteris Formation reported high proportions of air fall volcanic detritus and Permian zircon ranging in age from 280 to 245 Ma that were derived from the outboard active Gondwana margin. We selected a sample from a stratigraphic position close to the reported volcanoclastic sandstone in order to target Permian zircon (Fig. 3).

### ***Pecora Formation, Pensacola Mountains***

The Pecora Escarpment, the type locality for the Permian Pecora Formation, is the southernmost extension of the Pensacola Mountains (Fig. 2 and 3, Williams, 1969; Barrett et al., 1986; Collinson et al., 1994). Rocks of the Pecora Formation include abundant sandstones, siltstones, and shales. Minor coal beds contain Permian Glossopteris fossil leaves indicative of a Permian age for the Pecora Formation (Paul L. Williams, 1969). The Pecora Formation of the Pensacola Mountains has been correlated to Beacon Supergroup sediments of the Transantarctic Mountains, including the Mt. Glossopteris Formation in the Ohio Range and the Buckley Formation in the central TAM (Barrett et al., 1986; Collinson et al., 1994). Detrital zircon studies have not previously reported Permian zircon in the Pecora Formation and no radiometric dates are available.

## Analytical Methods

One sample from each Permian unit, the Mt. Glossopteris Formation, Pecora Formation, and Polarstar Formation (Fig. 2 and 3) were selected from the Polar Rock Repository (Repository, 2018) to determine the age and geochemistry of Permian zircon. Zircons were separated using standard mineral separation techniques (i.e., disk milling, water table, magnetic separation, and heavy liquids), mounted in epoxy, and polished to expose equatorial sections. Prior to isotopic analysis, zircons were imaged via Cathodoluminescence (CL) on an FEI Quanta400f scanning electron microscope (SEM) and used to guide selection of locations for LASS (U–Pb and trace elements) and Lu–Hf measurements.

Zircon U–Pb isotopes and trace element concentrations were obtained simultaneously with using the ‘split stream’ approach (Kylander–Clark et al., 2013) at the University of California Santa Barbara under standard operating conditions (McKinney et al., 2015). Instrumentation consists of a 193 nm ArF excimer laser ablation (LA) system coupled to Nu Plasma high–resolution multi collector–inductively coupled plasma mass spectrometer (MC–ICP–MS) for U/Pb and a Agilent 7700S Quadrupole ICPMS for trace elements. A selection of 64 zircon grains were measured for U–Pb and trace element analysis from each sample. Subsequent Lu–Hf analyses were performed by LA–MC–ICPMS exclusively on zircon younger than Ordovician ( $n = \sim 25$  per sample) to better characterize the geochemistry of post–Ross–aged zircon. All data reduction was performed using Iolite v2.5 (Paton et al., 2010, 2011) and  $^{207}\text{Pb}$  corrected  $^{206}\text{Pb}/^{238}\text{U}$  ages were calculated for zircon younger than c. 800 Ma using the method of Andersen (2002) and ISOPLOT/EX (Ludwig, 2003). Detailed analytical methods, data reduction protocols and results of reference zircon analyses and

unknown data are in the Supplementary Information, and Datasets S1 and S2 provided in the Appendix (Patchett and Tatsumoto, 1980, 1981, Wiedenbeck et al., 1995, 2004; Chu et al., 2002; Jackson et al., 2004; Thirlwall and Anczkiewicz, 2004; Woodhead and Hergt, 2005; Blichert-Toft, 2008; Sláma et al., 2008; Liu et al., 2010).

## Results

All zircon U-Pb and geochemical data are provided in Supplementary Datasets 1 and 2. Zircon U-Pb Tera-Wasserburg concordia,  $^{207}\text{Pb}$ -corrected weighted mean  $^{206}\text{Pb}/^{238}\text{U}$  crystallization ages, representative cathodoluminescence (CL) images of zircon, and kernel density/histogram plots for Permian-aged zircon are provided in Figure 4. Permian zircons from all formations have euhedral prismatic and elongate morphologies showing both oscillatory and sector zoning in CL. Histograms of zircon Hf isotope data are given in Figure 5. Zircon trace-element concentrations fall within the range of continental arc zircon and have ‘igneous’ Th/U ratios ( $> 0.1$ ) (Rubatto, 2002; Grimes et al., 2015). Calculated weighted mean crystallization ages with two sigma uncertainties and mean squared weighted deviation (MSWD) for samples from this study are discussed below. Calculated weighted mean  $\epsilon\text{Hf}_i$  values are provided alongside their two standard error uncertainties below. All  $\epsilon\text{Hf}_i$  values were calculated using chondritic uniform reservoir (CHUR) parameters of Bouvier et al. (2008) and  $^{176}\text{Lu}$  decay constant from (Söderlund et al., 2004).

A sandstone from the Mt. Glossopteris Formation (PRR-11683, Fig.4) of the Ohio Range yielded Permian-aged zircon with a weighted mean of  $265.5 \pm 0.8$  Ma (MSWD = 1.5

for  $n = 55$ ). The kernel density plot indicates two sub-populations (probability peaks) at c. 264 and 267.5 Ma. The zircon  $\epsilon\text{Hf}_i$  ranges from  $-3.2$  to  $0.7$  with a unimodal distribution and a weighted mean of  $-0.5 \pm 0.3$  (2SE) (Fig. 5). Only one zircon within this sample yielded a concordant U-Pb age older than the Permian (c. 508 Ma). Permian zircons from the Mt. Glossopeteris Formation have an average  $\text{Th}/\text{U} = 0.62$ ,  $\text{Gd}/\text{Yb} = 0.07$ , and  $\text{U}/\text{Yb} = 0.58$ .

A sandstone sample from the Pecora Formation (PRR-33218, Fig. 4) in the Pensacola Mountains contained Permian zircon with a weighted mean age of  $267.4 \pm 1.2$  Ma (MSWD = 1.2 for  $n = 36$ ). The kernel density plot looks very similar to that for the Mt. Glossopeteris sample with two probability peaks at c. 263.5 and 269 Ma. The zircon  $\epsilon\text{Hf}_i$  ranges from  $-4.2$  to  $+5.6$  with a weighted mean of  $+0.3 \pm 1.0$  (2SE). The zircon  $\epsilon\text{Hf}_i$  histogram plot demonstrates a bimodal distribution of  $\epsilon\text{Hf}_i$  with peaks at  $\sim -0.5$  and  $+3$  (Fig. 5). Concordant ages for PRR-33218 older than the Permian include four Carboniferous ages, a c. 512-489 Ma ( $n = 11$ ), and a single age of c. 632 Ma. Permian zircon from the Pecora Formation have an average  $\text{Th}/\text{U} = 0.93$ ,  $\text{Gd}/\text{Yb} = 0.08$ , and  $\text{U}/\text{Yb} = 0.60$ .

A sandstone from the Polarstar Formation (PRR-299, Fig. 4) of the Ellsworth Mountains yielded a population of Permian-aged zircon with a weighted mean of  $270.3 \pm 1.3$  Ma (MSWD = 1.5 for  $n = 36$ ). The kernel density plot for PRR-299 has an older age, c. 273 Ma, for the highest probability sub-population than other samples from this study. Two minor peaks at c. 264 and 267.5 Ma match with peaks in kernel density plots for samples from the Ohio Range and Pensacola Mountains. The zircon  $\epsilon\text{Hf}_i$  ranges from  $-5.4$  to  $+4.5$  with a weighted mean of  $-0.3 \pm 1.1$  (2SE) (Fig. 5). Concordant dates for PRR-33218 older than the Permian include a single date of c. 308 Ma, an age range of c. 520-486 Ma ( $n = 9$ ),

and seven Proterozoic dates from c. 1735 to 541 Ma. Permian zircon from the Pecora Formation have an average  $\text{Th/U} = 0.75$ ,  $\text{Gd/Yb} = 0.06$ , and  $\text{U/Yb} = 0.54$ .

## **Discussion**

### ***Regional Temporal Correlations of Permian Volcanism***

Our new detrital zircon data for Polarstar, Mt. Glossopteris, and Pecora formations indicate a period of Permian volcanism between c. 277 and 260 Ma (Fig. 6), consistent with previous detrital zircon data published for the Polarstar and Mt. Glossopteris formations (Elliot et al., 2016a, 2017; Craddock et al., 2017a). The age range for zircon from these formations (c. 277-260) is contemporaneous with volcanic units of the Choiyoi Province (c. 281-252 Ma, Fig. 6) and weighted mean ages for all samples are within uncertainty of a major peak in Choiyoi volcanic activity at 269–263 Ma (Rocha-Campos et al., 2011; Kimbrough et al., 2016). Distal tuffs from the Karoo Basin, South Africa, have a broad peak in zircon ages of c. 282 to 250 Ma (Fig. 6), with the highest age probability between c. 275 and 260 Ma (McKay et al., 2016b), demonstrating a strong age correlation with both the Choiyoi Province and detrital zircon from central Antarctica. Detrital zircon from the Paraná Basin (Canile et al., 2016) and accretionary complexes in Patagonia (Hervé et al., 2014b; Castillo et al., 2016) contain polymodal distributions with abundant Permian-aged zircon contemporaneous with Permian zircon from central Antarctica, Karoo Basin, and the Choiyoi Province (Fig. 6). Importantly, the Paraná Basin and Patagonia sediments preserve evidence

for Carboniferous–Permian zircon sources from ash fall and erosion of crystalline basement (Canile et al., 2016; Castillo et al., 2016).

In Antarctica, detrital zircon from the Antarctic Peninsula record a broad Permian age peak with subpopulation probability peaks at c. 266 and c. 272 Ma (Castillo et al., 2016), similar to central Antarctica, South America, and South Africa (Fig. 6). Magmatic ages for basement rocks of the Antarctic Peninsula and Thurston Island (c. 280 to 255 Ma) also overlap in age with Permian zircon from central Antarctica (Millar et al., 2002; Riley et al., 2012, 2017). In contrast, detrital zircon ages from late Paleozoic–Mesozoic volcanoclastic sedimentary rocks in the central TAM yield a broad Permian–Triassic age probability peak (c. 265 to 240 Ma, Fig. 6) that is slightly younger than Permian zircon ages recorded in other regions within the proto-Weddell Sea sector discussed above as well as our data from central Antarctica (Elliot et al., 2017; Nelson and Cottle, 2017). Instead, the age of Permian–Triassic zircon from the central TAM are comparable to detrital zircon ages from Australia and New Zealand, demonstrating a broad difference in the timing of Permian arc magmatism between Australia / Zealandia and South America (see compilation in Nelson and Cottle, 2017). In summary, detrital zircon ages for Mt. Glossopferis, Polarstar, and Pecora formations in central West Antarctica are contemporaneous with the Choiyoi igneous province, Patagonia, the Antarctica Peninsula and South Africa, and are generally older than Permian arc magmatism recorded in the cTAM that is itself contemporaneous with arc activity in Zealandia and Australia. Consequently, central Antarctica defines the southernmost distal component of widespread Permian volcanism contemporaneous with the Choiyoi Province along the Gondwana margin and may have been directly sourced from a major high-flux period of Choiyoi volcanic activity (Kimbrough et al., 2016).

### ***Hf Isotopic Constraints On Provenance***

The Hf isotopic composition of zircon from the central Antarctica samples exhibit similarly enriched  $\epsilon\text{Hf}_i$  values that overlap within uncertainty and have a combined  $\epsilon\text{Hf}_i$  range of c.  $-5$  to  $+5$  (Fig. 5), reinforcing a shared geochemical and temporal history for these rocks. At least two geologically feasible scenarios can explain the lack of juvenile Hf isotopic compositions ( $\epsilon\text{Hf}_i > +5$ ) in central Antarctica samples. The evolved signature may result from contamination of depleted mantle melts by assimilation of enriched Cambrian (e.g., Ross Orogen) and/or Proterozoic (Grenville-aged cratonic basement) crustal reservoirs (Hagen-Peter et al., 2015; Hagen-Peter and Cottle, 2018) that are ubiquitous along the Gondwana margin (Chapter 2). Alternatively, enriched compositions may have resulted from enriched lithospheric mantle melting followed by crustal assimilation. Permian zircon from the Antarctic Peninsula contain enriched Hf isotope compositions ( $\epsilon\text{Hf}_i = -1.3$  to  $+5.2$ ), similar to those of central Antarctica, and mantle-like oxygen isotope compositions ( $\delta^{18}\text{O} = 4.5$  to  $6.4\%$ ) (Castillo et al., 2016), consistent with a shared enriched lithospheric mantle source for central Antarctica and the Antarctic Peninsula. Evidence for proximal magmatism with an enriched lithospheric mantle source recorded in Permian zircon from the Antarctic Peninsula and the absence of zircon  $\epsilon\text{Hf}_i > +5$  in central Antarctica suggest an enriched lithospheric mantle source for central Antarctica.

### *Regional Detrital Zircon Hf Isotope Comparisons*

Here we compile detrital zircon Hf isotope data to test whether Permian zircons in central Antarctica have geochemical affinities with Permian detrital zircon in the Antarctic Peninsula and South America or the central TAM (Fig. 7). Permian detrital zircon from the Paraná Basin, Patagonia, and Antarctic Peninsula all contain enriched Hf isotope compositions and lack juvenile Hf isotope compositions, similar to central Antarctica (Fig. 7, Fanning et al., 2011; Canile et al., 2016; Castillo et al., 2016). Intermediate Hf compositions ( $\epsilon\text{Hf}_i = 0$  to  $+5$ ) for middle Permian zircon are more common in central Antarctica than the Paraná Basin, Patagonia, and Antarctic Peninsula, however, the uniformly enriched compositions ( $\epsilon\text{Hf}_i < +5$ ) for all of these regions are consistent with derivation from temporally and geochemically related magmatic sources. Limited early to middle Permian zircon Hf isotope data exist for the central TAM, but late Permian and Early Triassic Hf isotope compositions are significantly more juvenile ( $\epsilon\text{Hf}_i$  up to c.  $+14$ ) and there is only a minor amount of zircon with  $\epsilon\text{Hf}_i < 0$  (Fig. 7, Nelson and Cottle, 2017). The data from central TAM, therefore, suggest zircon derived from a magmatic arc that is temporally and geochemically distinct (i.e., Marie Byrd Land, Zealandia, and Australia) from the source of central Antarctica, Paraná Basin, Patagonia, and Antarctic Peninsula (Nelson and Cottle, 2017).

### *Zircon Hf Isotope Composition of Permian Magmatic Rocks*

We also compiled zircon Hf isotope data from plutonic rocks across the Gondwana margin to better constrain potential source regions for Permian zircons in central Antarctica (Fig. 8). In South America, magmatic rocks of the Frontal Andes, Coastal Batholith, North Patagonian Massif, and Tierra del Fuego generally have enriched zircon Hf isotope compositions ( $\epsilon\text{Hf}_i < c. +5$ ) similar to those of central Antarctica (Fig. 8, Fanning et al., 2011; del Rey et al., 2016; Castillo et al., 2017b). A comprehensive study of the zircon Hf isotope composition of volcanic rocks of the Choiyoi Province is unavailable, but limited data from Choiyoi volcanic rocks and plutonic rocks from the North Patagonian Massif indicate the Choiyoi Province has an  $\epsilon\text{Hf}_i = c. -7$  to  $+5$  (Fig 8, Fanning et al., 2011; Castillo et al., 2017b). The lack of zircon with  $\epsilon\text{Hf}_i > c. +5$  in South America may be due to melting of an enriched lithospheric mantle, or extensive crustal contamination of depleted mantle melts. Evidence for an enriched lithospheric mantle is preserved in Permian zircon with enriched Hf isotope compositions and mantle-like O isotope compositions from Frontal Andes batholiths and the North Patagonian Massif (Fig. 8, del Rey et al., 2016; Castillo et al., 2017b). Re/Os data from Patagonian mantle xenoliths demonstrate the existence of a Proterozoic enriched lithospheric mantle that was likely present in the Permian and related to ancient lithosphere reported in South Africa and the Shackleton Range of Antarctica (Schilling et al., 2008, 2017; Mundl et al., 2015). Together these observations provide strong evidence for a lithospheric mantle source for contemporaneous Permian magmatism in South America, including the Choiyoi Province, and are consistent with the Choiyoi Province or temporally and geochemically correlative arc magmatism as the source for Permian zircon from central Antarctica.

Zircon Hf isotope compositions for crystalline basement in the Antarctic Peninsula and the adjacent crustal block of Thurston Island are limited (Fig. 8, Flowerdew et al., 2006; Riley et al., 2017, Chapter 2). The available data suggest they both record enriched Hf isotopic compositions in the Permian–Triassic and, therefore, may have been sourced from an enriched lithospheric mantle similar to that observed in South America. A Permian diorite from Thurston Island ( $276 \pm 1$  Ma) is contemporaneous with the Permian zircon age peak for central Antarctica (c. 277–260 Ma) and has similarly enriched zircon Hf isotope compositions (mean  $\epsilon_{\text{Hf}_i} = +0.4 \pm 0.7$  (2SE)) suggesting Thurston Island as a potential source for Permian zircon from central Antarctica (Fig. 8, Nelson and Cottle, in review). In contrast, there are no Permian magmatic rocks from Marie Byrd Land contemporaneous with the central Antarctica Permian zircon age (c. 277–260 Ma) (Fig. 8, Pankhurst et al., 1998; Mukasa and Dalziel, 2000; Yakymchuk et al., 2013, 2015; Nelson and Cottle, in review). Older Permian magmatic rocks (c. 295–283 Ma) and a Triassic granite (c 248 Ma) from Marie Byrd Land have zircon Hf isotopic compositions that are generally more depleted than those of central Antarctica (Fig. 8) and record unambiguous evidence for a depleted mantle source (Nelson and Cottle, in review). In summary, there is currently no evidence to support Marie Byrd Land as a likely source region for Permian zircon in central Antarctica.

### ***Along Arc Geochemical Variation***

The depleted zircon Hf isotope compositions from Marie Byrd Land are comparable to Permian–Triassic zircon from the central TAM and compiled zircon Hf isotope data from

Zealandia and Australia (Fig. 8, Nelson and Cottle, in review). These observations have previously been used to argue for an along arc geochemical variation from depleted in Australia, Zealandia, and Marie Byrd Land to enriched in South America, Antarctic Peninsula, and Thurston Island (Nelson and Cottle, 2017; Nelson and Cottle, in review). This along arc variation is likely caused at least in part by a depleted asthenospheric mantle source in Australia, Zealandia, and Marie Byrd Land and an ancient enriched lithospheric mantle source in South America, Antarctic Peninsula, and Thurston Island. These differences may have developed due to varied tectonic (i.e., geodynamic) histories of these two broad segments of the Gondwana margin. In particular, Australia, Zealandia, and Marie Byrd Land likely underwent lithosphere rejuvenation during slab rollback and/or lithospheric foundering (i.e., extensional collapse) earlier, c. mid to late Paleozoic, than in South America, which did not undergo major extension and lithospheric rejuvenation until later, c. late Permian to Jurassic (Nelson and Cottle, in review).

The difference in tectonic history along the Gondwana margin is particularly pronounced during the early Permian, when the margin of Australia was undergoing widespread extension, leading to the opening of the Sydney and Bowen basins (e.g., Rosenbaum, 2018) while the margin of South America was undergoing contraction during the San Rafael compressional event associated with the Gondwanide Orogeny (e.g., Kleiman and Japas, 2009; Sato et al., 2015). Permian volcanic and plutonic rocks of the Choiyoi Province were emplaced during contraction of the San Rafael event and continued through the initial stage of extension at c. 265 Ma (Kleiman and Japas, 2009; Rocha-Campos et al., 2011; Sato et al., 2015; Spalletti and Limarino, 2017). The temporal and geochemical signature of this event is present in our data from central Antarctica and indicates they are

sourced from the Choiyoi Province or correlative rocks of Patagonia, Antarctic Peninsula, and/or Thurston Island. We therefore suggest that Permian volcanic and magmatic rocks in Patagonia, Antarctic Peninsula, and Thurston Island define a southern extension of the Choiyoi Province (Fanning et al., 2011; Castillo et al., 2016) and volcanic deposits in central Antarctica represent the distal expression of this southern extension of the Choiyoi Province (Fig. 9). Paleogeographic reconstructions indicate that the location of the Karoo Basin was between the Paraná Basin and central Antarctica and constrain the source for Karoo Basin tuffs to Choiyoi-related magmatism (Fig. 9). Our data from central Antarctica also support the notion that an early-Permian along arc geochemical switch occurred in the vicinity of Thurston Island and Marie Byrd Land (Nelson and Cottle, 2017; Nelson and Cottle, in review) based on the difference in Permian zircon Hf isotopes of central Antarctica and central TAM.

### ***Zircon Trace Element Constraints On Source***

Key zircon trace element ratios (Gd/Yb, U/Yb, Th/U) have been established as proxies for magmatic arc systems (e.g., Barth et al., 2013; McKay et al., 2018) and provide an opportunity to compare the source of Permian zircon from central Antarctica to Permian zircon from the Karoo Basin (Fig. 10). In continental arcs, fractionation of garnet and/or melting of garnet-bearing lower crust produces heavy rare earth element depletion, i.e., a high Gd/Yb “garnet-signature”, in magmas and crystallizing zircon that is indicative of thickened crust (Barth et al., 2013). Similarly, addition of U-rich slab-derived fluids to

continental arc melts generates magmas and crystallizing zircon with high U/Yb ratios (Barth et al., 2013). Permian zircon from the Karoo Basin (McKay et al., 2016b) have markedly higher average Gd/Yb (0.09) and U/Yb (1.23) ratios than central Antarctica (Gd/Yb = 0.07 and U/Yb = 0.57) (Fig. 10) and, therefore, indicate that Karoo Basin tuffs had a source with a thicker arc crust and higher ingress of slab-derived fluids, both of which are consistent with high arc magma flux (Ducea and Barton, 2007; Barth et al., 2013). The zircon Gd/Yb and U/Yb data imply the existence of thickened arc crust in South America that underwent a progressive or step-wise transition to thinner crust towards Patagonia and West Antarctica (Fig. 9). This along arc variation in crustal thickness and slab fluid addition is consistent with early Permian along arc variation from contraction and crustal thickening during the San Rafael event and Choiyoi magmatism in South America (e.g., Kleiman and Japas, 2009) to extension and thinning in the Australian margin and the opening of the Sydney-Bowen basin (e.g., Rosenbaum, 2018) (Fig. 9).

High zircon Th/U ratios have been used as proxies for both crustal input (e.g., Barth et al., 2013) and extension (e.g., McKay et al., 2018). As a crustal input proxy, high Th/U results from high Th content in old lithosphere and, therefore, corresponds to periods of increased ancient fertile crust contribution during high magma flux episodes favored during upper plate contraction (Barth et al., 2013). Alternatively, high Th/U has been interpreted to result from high magma temperatures, increased fractionation, and more primitive mafic melts common during extension (McKay et al., 2018). These contrasting applications of zircon Th/U to studies of ancient arc systems highlight the necessity for combining traditional zircon U-Th-Pb isotope and concentration measurements with supplemental zircon trace element and Hf isotope measurements. For example, average Permian zircon

Th/U ratios from the Karoo Basin (0.71) and central Antarctica (0.75) are nearly indistinguishable and elevated, similar to documented arc flare-up events in the Sierra Nevada Batholith and the Ross Orogen, Antarctica, which have average zircon Th/U ratios >0.7 during peak magma flux (Barth et al., 2013; Paulsen et al., 2016). In both the Sierra Nevada Batholith and the Ross Orogen, high Th/U correlates with high Gd/Yb and U/Yb interpreted to reflect upper plate thickening during contraction (Ducea and Barton, 2007; DeCelles et al., 2009; Barth et al., 2013; Ducea et al., 2015; Paulsen et al., 2016). We assert, therefore, that the high zircon Th/U, Gd/Yb, and U/Yb in Permian zircon from the Karoo Basin, combined with our zircon Hf isotope compilation that indicates pervasive enriched isotopically enriched compositions during the Permian, are consistent with a thick Andean style arc source undergoing a high magma flux event during contraction rather than extension. In contrast, high Th/U Permian zircon from central Antarctica with enriched Hf isotopes, but relatively lower Gd/Yb and U/Yb, were sourced from the fringe of this arc flare-up where the crust was thinner owing to an early Permian transition from thick crust in South America (e.g., Kleiman and Japas, 2009) during contraction to thin crust in Australia due to extension (e.g., Rosenbaum, 2018) (Fig. 9).

### ***Environmental Impacts of the Choiyoi Flare-up***

Previous workers have asserted that the Choiyoi flare-up may have contributed significantly to an increase in atmospheric CO<sub>2</sub> during the Permian, which is associated with the end-Permian and end Guadalupian mass extinction events and a transition from icehouse

to greenhouse conditions (Henry et al., 2009; Hermann et al., 2011; Henry, 2013; Limarino et al., 2014; Kimbrough et al., 2016; Spalletti and Limarino, 2017; Luppó et al., 2018). Our new geochronology data, combined with that from the Karoo Basin (McKay et al., 2016b), provide an opportunity to assess correlations between peak Choiyoi-related volcanism (inferred as peaks in distal zircon ages) with major shifts in global continental arc flux (McKenzie et al., 2016; Cao et al., 2017), atmospheric CO<sub>2</sub> (Berner and Kothavala, 2001), large igneous provinces, mass extinction events (Bond and Wignall, 2014), and marine fossil  $\delta^{13}\text{C}$  (Veizer et al., 1999), to evaluate the relationship between Choiyoi-related volcanism and possible environmental change (Fig. 11). Detrital zircon data and global granite surface area addition rates have been established as proxies for global arc flux through time and a correlation between high global arc flux and elevated atmospheric CO<sub>2</sub> suggests continental arc volcanism may be the principle driver of atmospheric CO<sub>2</sub> (e.g., McKenzie et al., 2016; Cao et al., 2017). In particular, there is a general increase in global arc flux beginning in the Permian and continuing through the Cretaceous that aligns with an increase in atmospheric CO<sub>2</sub> (Fig. 11, Berner and Kothavala, 2001; McKenzie et al., 2016; Cao et al., 2017). Furthermore, this increased global arc flux is broadly correlated with a shift to lighter  $\delta^{13}\text{C}$  values in brachiopod, belemnite, oyster, and foraminifera shells (Fig. 11, Veizer et al., 1999) that may be the result of addition of light mantle carbon through prolonged increased volcanic outgassing that began in the Permian (e.g., Paulsen et al., 2017).

Our data for the Choiyoi flare-up is synchronous with the initial increase in global arc flux in the Permian and suggests that the Choiyoi contributed to a dramatic increase in global continental arc flux that elevated background CO<sub>2</sub> (Fig. 11). Approximately 10<sup>22</sup> g of CO<sub>2</sub> is estimated to have been released over ~30 million years during the emplacement of the

Choiyoi Province, corresponding to a minimum CO<sub>2</sub> volcanic outgassing flux of  $\sim 10^{14}$  g/myr (Henry et al., 2009; Henry, 2013). Significant additional CO<sub>2</sub> and CH<sub>4</sub> may have been released due to heating of Paleozoic organic-rich shales, peat and carbonates (decarbonation) by Choiyoi magmas and volcanic rocks (Spalletti and Limarino, 2017). Constraints on global continental arc CO<sub>2</sub> flux in the Permian are lacking, but modern continental arc CO<sub>2</sub> flux estimates of 150 Tg/year (on the order of  $10^{20}$  g/myr) suggest that the Choiyoi Province may have only represented a small component of the global arc CO<sub>2</sub> flux (Lee and Lackey, 2015). However, emplacement of the Siberian Traps large igneous province associated with the end-Permian mass extinction released  $\sim 30,000$  Gt CO<sub>2</sub> (Bond and Wignall, 2014) over  $\sim 800$  kyrs (Burgess and Bowring, 2015), corresponding to a volcanic CO<sub>2</sub> flux on the order of  $10^{13}$  g/myr – comparable to the Choiyoi Province. Estimates for the Choiyoi and Siberian Traps igneous provinces do not incorporate release of CO<sub>2</sub> from decarbonation of crustal carbonates due to carbonate-magma interaction that may radically increase CO<sub>2</sub> flux during magmatism (e.g., Lee and Lackey, 2015). We suggest, therefore, that decarbonation of crustal carbonates during emplacement of the Choiyoi Province, combined with global increases in continental arc flux (both volcanic outgassing and decarbonation), elevated background atmospheric CO<sub>2</sub> levels, creating environmental degradation and global warming in the Permian (Lee and Lackey, 2015; McKenzie et al., 2016; Cao et al., 2017; Spalletti and Limarino, 2017). Punctuated mafic LIP emplacement, e.g., Siberian Traps and Emeishan, caused additional CO<sub>2</sub> input and environmental stress leading to mass extinction events (Bond and Wignall, 2014). These combined effects may have occurred numerous times throughout the Phanerozoic. Better constraints on the timing and volume of continental arc flare-ups and the amount of volcanic and decarbonation CO<sub>2</sub> outgassing throughout the Phanerozoic will

enable determination of the relationship between continental arc flare-up events, global warming, and mass extinctions (e.g., Cao et al., 2017).

## **Conclusions**

New zircon U-Pb and Hf isotopic data for Permian detrital zircon from volcanoclastic sedimentary rocks in central Antarctica record a major episode of explosive continental arc volcanism at c. 277 to 260 Ma. Hf isotopes indicate that Permian volcanism in central Antarctica is consistent with derivation from temporally and geochemically correlative rocks in South America, Antarctic Peninsula, and Thurston Island, that likely represent a continental arc flare-up related to the Choiyoi Province. Central Antarctica therefore represents the southernmost documented extension of this broad volcanic and magmatic province that is distinct from continental arc activity recorded in central TAM, Marie Byrd Land, Zealandia, and Australia. Volcanic rocks in the Karoo Basin, South Africa, must also be sourced from Choiyoi-related igneous activity but Permian zircon from the Karoo Basin have higher average zircon Gd/Yb and U/Yb than central Antarctica, indicative of thicker arc crust in their source. Zircon Hf isotopes and trace elements suggest an along arc shift from voluminous isotopically enriched arc magmatism, thickened crust, and contraction in South America to lower volume isotopically depleted magmatism, thinned crust, and extension in eastern Australia during the early to middle Permian. The timing of voluminous volcanism and magmatism associated with the Permian Choiyoi Province, recorded in central Antarctica and the Karoo Basin, is broadly synchronous with a shift from icehouse to greenhouse

conditions, decreased  $\delta^{13}\text{C}$  in benthic marine fossils, increased atmospheric  $\text{CO}_2$ , mass extinction events, large igneous provinces, and increased global arc flux. Consequently, we suggest the Choiyoi Province was a major contributor to increased global arc flux and volcanic outgassing and decarbonation of crustal carbonates in the Permian that produced a background level of atmospheric  $\text{CO}_2$  conducive to climatic and biotic crises during mafic large igneous province emplacement.

### **Acknowledgements**

This material is based upon work supported by the National Science Foundation Graduate Research Fellowship under Grant No. 1650114 and support from NSF—ANT—1443296, NSF—ANT—1043152. This research used samples and/or data provided by the Polar Rock Repository (PRR). The PRR is sponsored by the National Science Foundation Office of Polar Programs. We are grateful to Anne Grunow and the PRR for providing samples and assisting with sample selection. We also acknowledge the original sample collectors: C. Craddock, I. Dalziel, and W. Long.



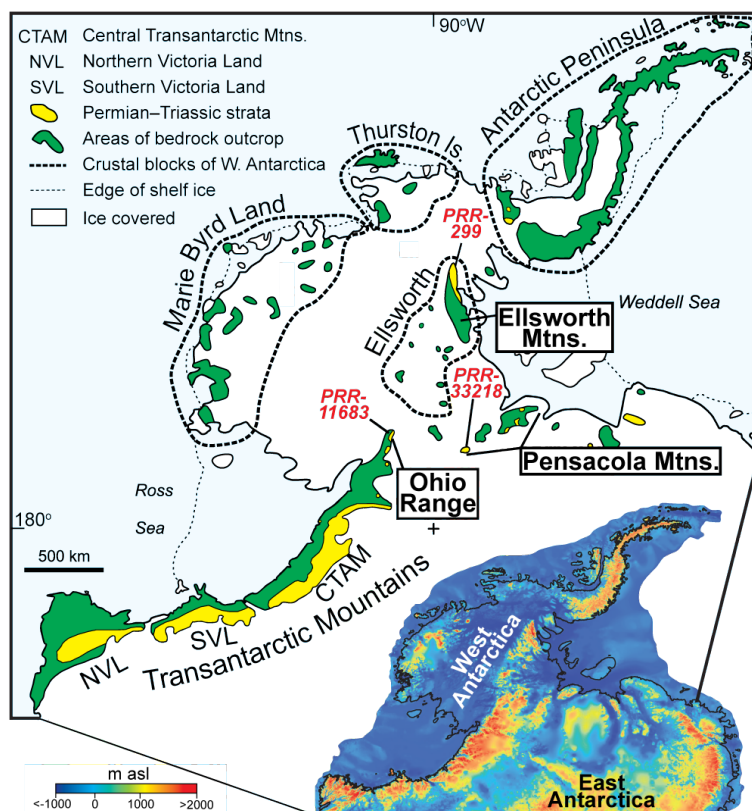


Figure 2. (Inset map) Subice topographic DEM of Antarctica (BEDMAP2) with major crustal blocks and localities identified; asl—above sea level (Fretwell et al., 2013). (Enlarged map) Map of western Antarctica outlining major bedrock outcrops, crustal blocks of West Antarctica, and sample locations in central Antarctica (modified from Elliot et al., 2016).

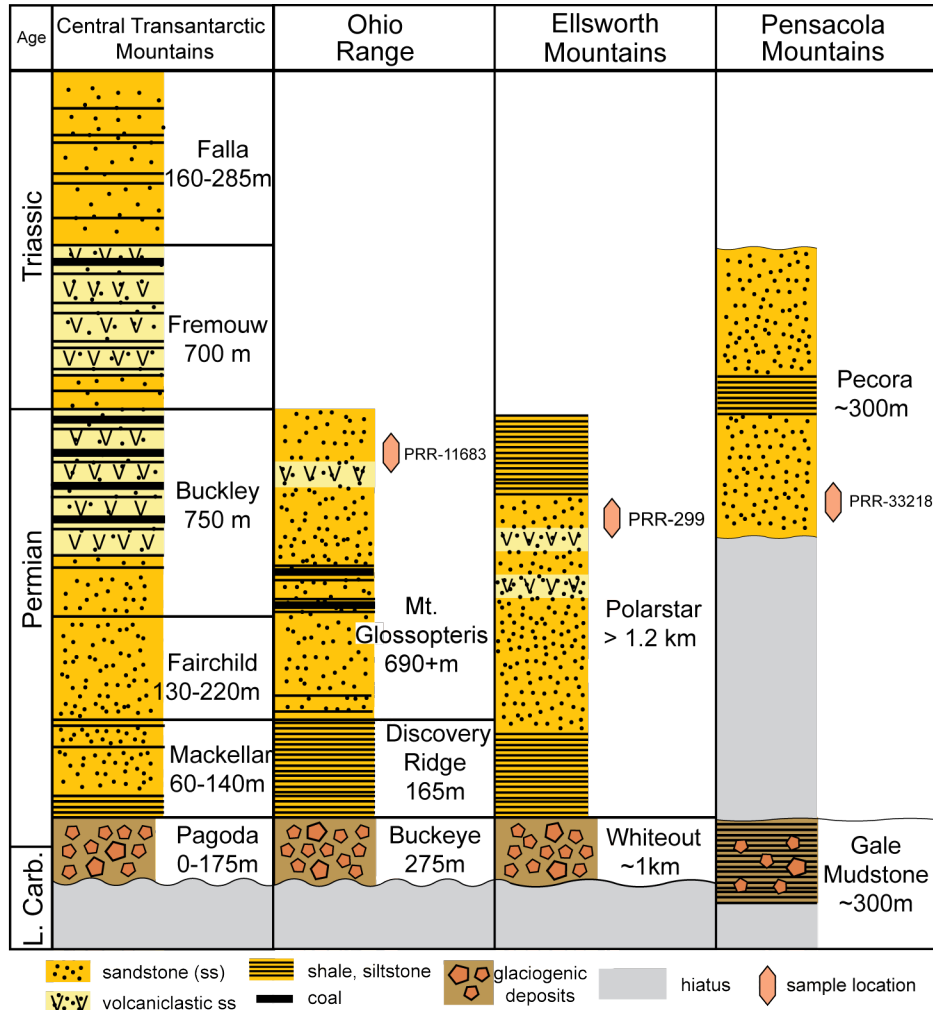


Figure 3. Simplified geologic columns for Carboniferous to Triassic strata in central Antarctica and central Transantarctic Mountains with the stratigraphic positions of samples (modified from Storey and Macdonald, 1996; Elliot et al., 2016, 2017).

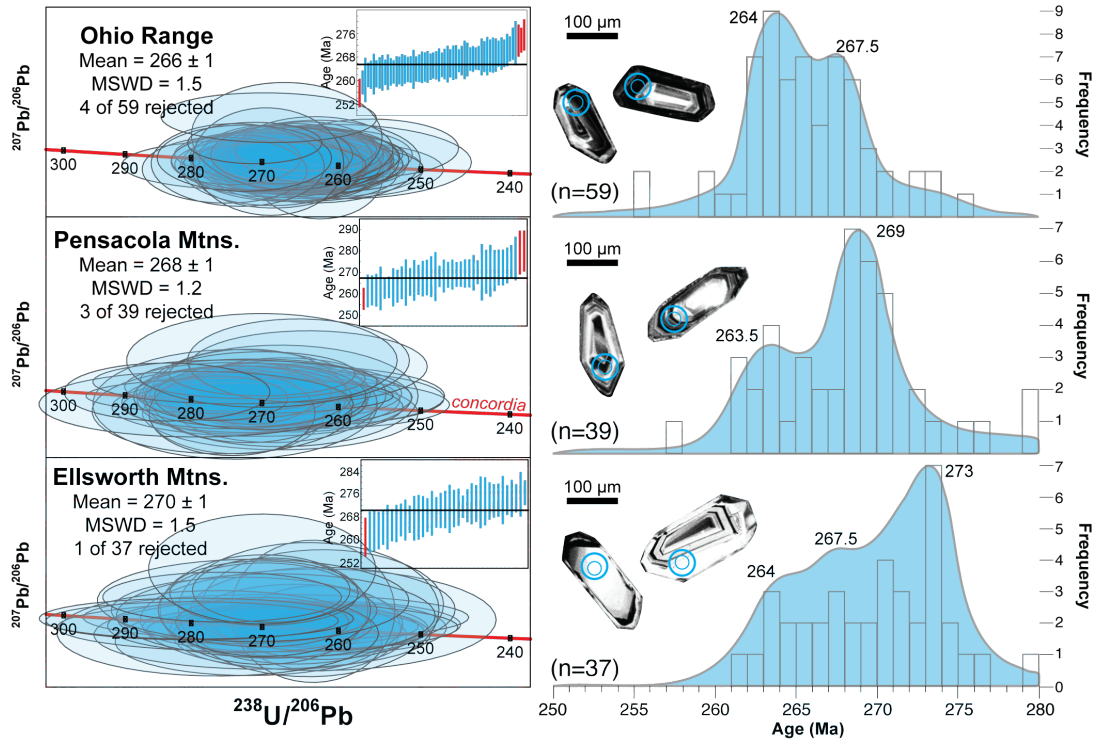


Figure 4. Zircon U-Pb geochronology data illustrated in Tera-Wasserburg Concordia plots, calculated weighted mean  $^{207}\text{Pb}$  corrected- $^{206}\text{Pb}/^{238}\text{U}$  ages, kernel density estimations and histograms, and representative Permian zircon cathodoluminescent images with the locations of U-Pb (small circles) and Hf isotope (large circles) measurements. Normal adaptive kernel density estimates with a bandwidth of 2 were used (Vermeesch, 2012). See Dataset S1 for full zircon U-Pb dataset.

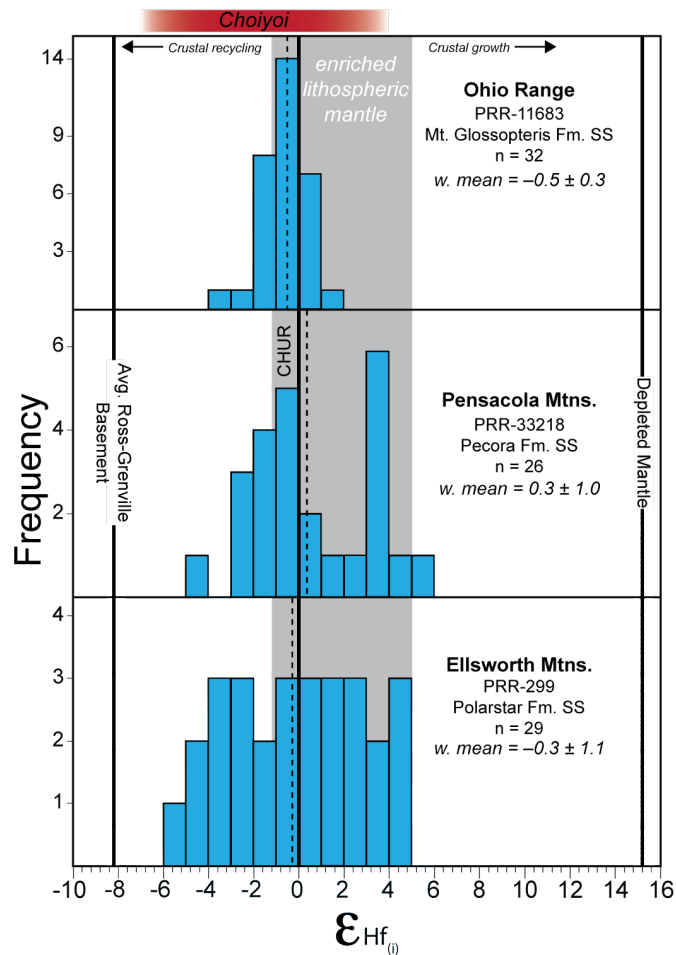


Figure 5. Histograms of initial  $\epsilon_{\text{Hf}}$  values for central Antarctica Permian zircon and calculated weighted mean initial  $\epsilon_{\text{Hf}}$  values including the 2 standard error uncertainties. Also included is the average  $\epsilon_{\text{Hf}}$  of the basement represented by zircon Hf data for the Ross Orogen and Grenville-aged zircon recalculated to 275 Ma (Hagen-Peter et al., 2015; Hagen-Peter and Cottle, 2018), the composition of enriched lithospheric mantle estimated from Permian zircon from the Antarctic Peninsula with enriched Hf isotopic compositions and mantle like O isotope compositions (Castillo et al., 2016). The range of  $\epsilon_{\text{Hf}}$  values for the Choiyoi Province are from the Northern Patagonian Massif and unpublished data for Choiyoi Province volcanic rocks (Fanning et al., 2011; Castillo et al., 2017b). Hf isotopic values for depleted mantle is from Vervoort and Blichert-Toft (1999). CHUR—chondritic uniform reservoir. See Dataset S2 for full zircon Hf isotope dataset.

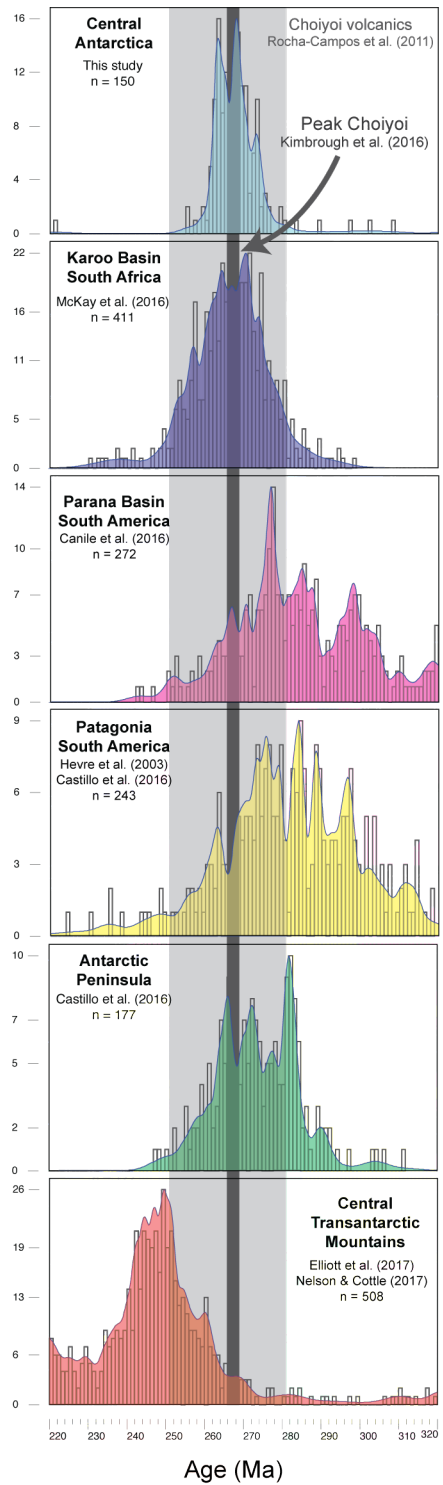


Figure 6. Kernel density estimations and histograms of detrital zircon data from central Antarctica and major Gondwana margin basins compared to the age range of volcanic rocks from the Choiyoi Province (Rocha-Campos et al., 2011) and the timing of peak Choiyoi Province volcanism (c. 269–266 Ma) (Kimbrough et al., 2016). Normal adaptive kernel density estimates with a bandwidth of 2 were used (Vermeesch, 2012).

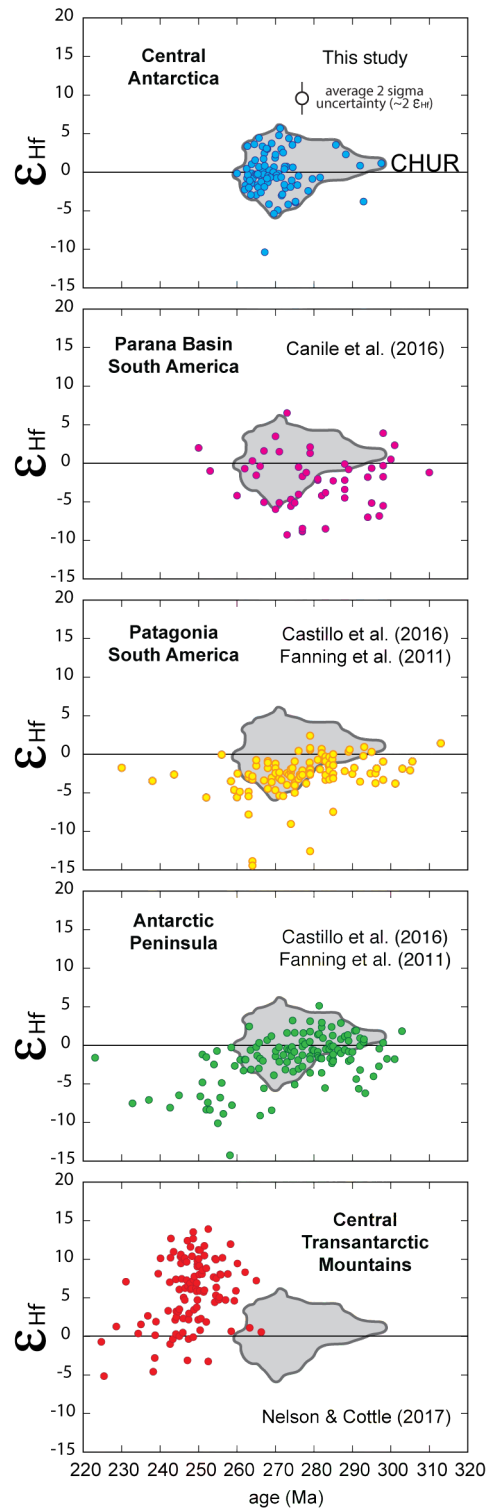


Figure 7. Detrital zircon Hf isotope compositions from central Antarctica and major Gondwana margin basins. CHUR-chondritic uniform reservoir.

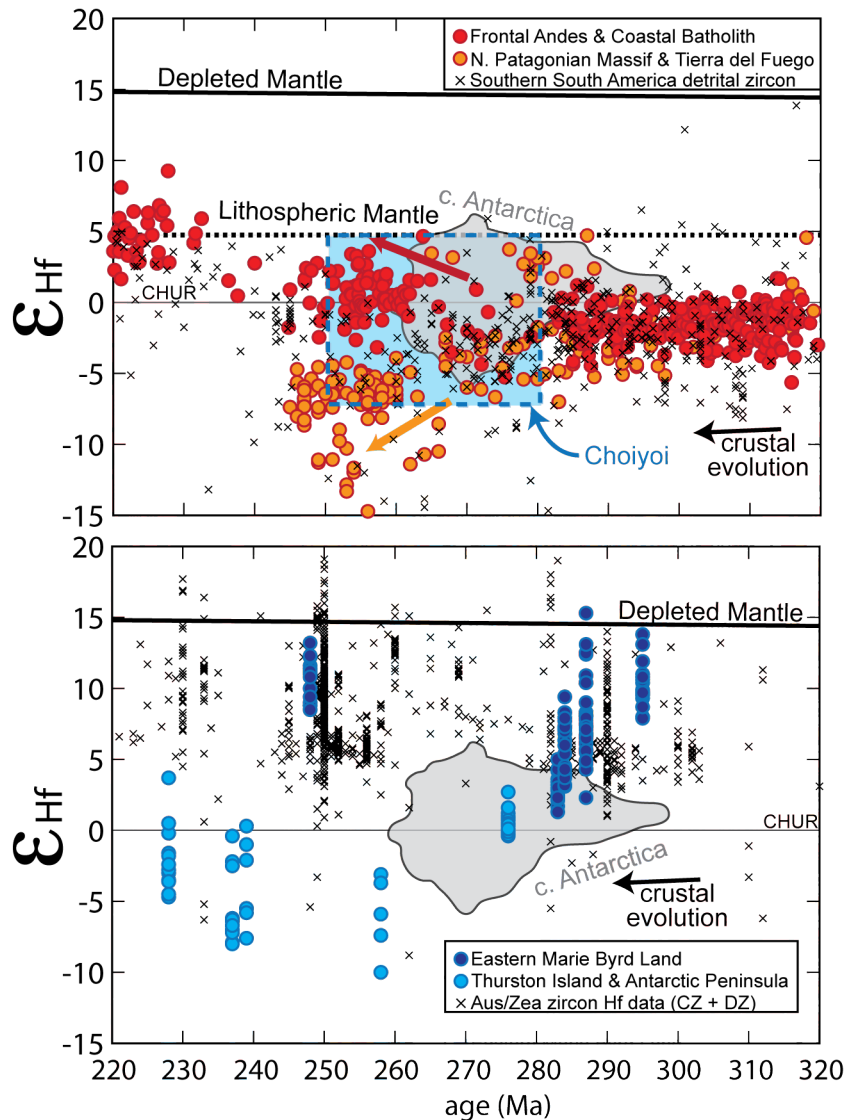


Figure 8. (Top) Zircon Hf isotope compositions for magmatic rocks of South America including the Frontal Andes and Coastal Batholith (Deckart et al., 2014; Hervé et al., 2014; del Rey et al., 2016), Northern Patagonian Massif (Fanning et al., 2011; Castillo et al., 2017b), and an envelope for the Choiyoi Province (Fanning et al., 2011; Rocha-Campos et al., 2011; Castillo et al., 2017b) compare with detrital zircon of southern South America (Fanning et al., 2011; Hervé et al., 2013; Canile et al., 2016; Castillo et al., 2016; Pepper et al., 2016; Balgord, 2017). The Hf isotope composition of enriched lithospheric mantle is estimated from enriched Permian zircon with mantle like O isotope compositions reported by Castillo et al., 2016, 2017b; del Rey et al., 2016). (Bottom) Zircon Hf compositions for magmatic rocks of Marie Byrd Land, Thurston Island, and the Antarctic Peninsula (Flowerdew et al., 2006; Riley et al., 2017; Nelson and Cottle, in review). A compilation of Hf isotope compositions of detrital zircon (DZ) and zircon from crystal-line rocks (CZ) from Australia and Zealandia are provided for comparison (Belousova et al., 2005; Kemp et al., 2005, 2007, 2009; Veevers et al., 2006; Murgulov et al., 2007; Nebel et al., 2007; Allibone et al., 2009; Phillips et al., 2011; Shaw et al., 2011; Nebel-Jacobsen et al., 2011; Jeon et al., 2014; Li et al., 2015). Hf isotopic values for depleted mantle is from Vervoort and Blichert-Toft (1999). CHUR-chondritic uniform reservoir. Crustal evolution line assumes a Lu/Hf = 0.0115 (Rudnick and Gao, 2003).

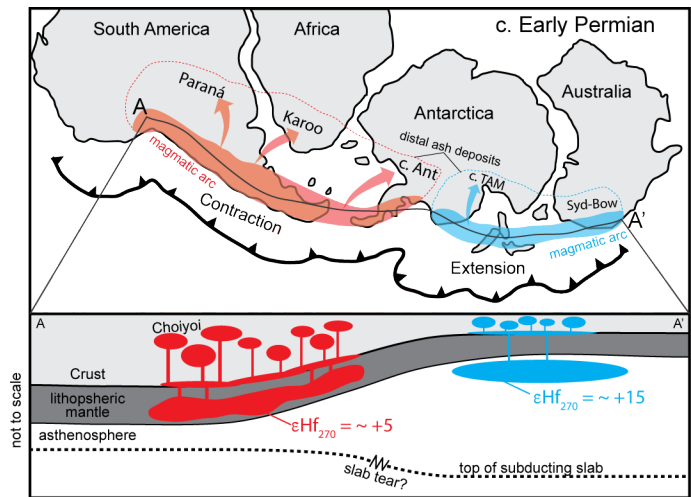


Figure 9. Paleogeographic reconstruction of supercontinent Gondwana and a cross section of Permian arc crust of South America, West Antarctica, Zealandia, and Australia summarizing the conclusions of this study (modified from Meert and Lieberman, 2008).



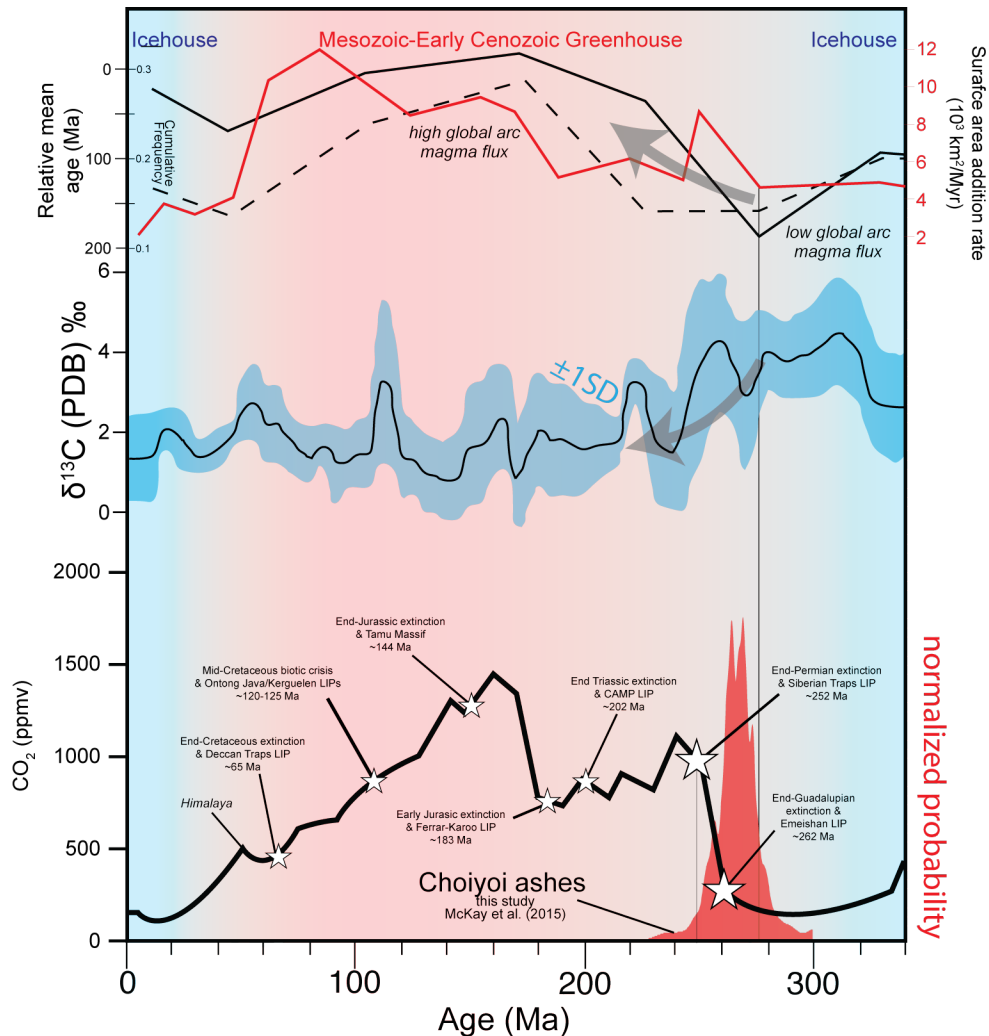


Figure 11. Compilation of Phanerozoic global arc flux proxy data (McKenzie et al., 2016; Cao et al., 2017),  $\delta^{13}\text{C}$  data from benthic marine fossils (Veizer et al., 1999), and atmospheric  $\text{CO}_2$  (Bernier and Kothavala, 2001) compared with the timing of peak Choiyoi-related volcanism recorded in the Karoo Basin and central Antarctica, large igneous provinces and mass extinction events (Kidder and Worsley, 2010; Bond and Wignall, 2014). Global arc flux is inferred from compilations of global surface area addition rates of granitoids (red), global compilation of proportion of young detrital zircon ages within 200 million years of minimum deposition age (dashed), and global compilation of detrital zircon relative mean age calculated from difference between youngest zircon population and minimum deposition age (McKenzie et al., 2016; Cao et al., 2017). Age data for the Karoo Basin and central Antarctica are presented as a normal kernel density estimation with a bandwidth of 1 (Vermeesch, 2012).

## Appendix: Supplementary Information

### Zircon U-Pb geochronology

U-Pb measurements were made on a Nu Plasma high-resolution multi collector-inductively-coupled plasma-mass spectrometer (MC-ICP-MS) (Nu Instruments, Wrexham, UK) at the University of California, Santa Barbara. A 193 nm ArF excimer laser (Teledyne Cetac, USA) was used to ablate domains 25  $\mu\text{m}$  in diameter, and  $^{238}\text{U}$ ,  $^{232}\text{Th}$ ,  $^{208}\text{Pb}$ ,  $^{207}\text{Pb}$ ,  $^{206}\text{Pb}$ , and  $^{204}(\text{Pb} + \text{Hg})$  were measured. Laser energy was typically 3—4 mJ and the ablation repetition rate 4 Hz. Analyses were conducted over 30 second ablation periods with 20 second washout periods between measurements to return signal to background. Isotopes  $^{204}\text{Pb}$ ,  $^{206}\text{Pb}$ ,  $^{207}\text{Pb}$ , and  $^{208}\text{Pb}$  were measured on secondary electron multipliers, while  $^{232}\text{Th}$  and  $^{238}\text{U}$  were measured on Faraday cups equipped with  $10^{11}$  ohm resistors.

U-Pb data were collected during two analytical sessions. A primary reference material, ‘91500’ zircon ( $1065.4 \pm 0.3$  Ma  $^{207}\text{Pb}/^{206}\text{Pb}$  ID-TIMS age and  $1062.4 \pm 0.4$  Ma  $^{206}\text{Pb}/^{238}\text{U}$  ID-TIMS age, Wiedenbeck et al., 1995, 2004) was used to monitor and correct for mass bias as well as Pb/U fractionation. To assess data accuracy, two secondary reference zircon ‘GJ-1’ ( $608.5 \pm 0.4$  Ma  $^{207}\text{Pb}/^{206}\text{Pb}$  ID-TIMS age; Jackson et al., 2004 and  $601.7 \pm 1.3$  Ma  $^{206}\text{Pb}/^{238}\text{U}$  ID-TIMS age; Condon, personal commun.) and ‘Plešovice’ ( $337.13 \pm 0.37$  Ma  $^{206}\text{Pb}/^{238}\text{U}$  ID-TIMS age Sláma et al., 2008) were analyzed concurrently (typically once every 8-10 unknowns) and mass bias- and fractionation- corrected based on measured isotopic ratios of the primary reference material. Analyses of the GJ-1 and Plešovice

secondary reference zircon over all of the analytical sessions yield a mean  $^{206}\text{Pb}/^{238}\text{U}$  age within uncertainty of the reported values. Data reduction, including corrections for baseline subtraction, instrumental drift, mass bias, down-hole fractionation, and primary-reference normalization was carried out using Iolite v2.5. Full details of the data reduction methodology can be found in Paton et al. (2010, 2011).

Uncertainties on individual analyses are quoted at the 95% confidence or  $2\sigma$  level and include contributions from the external reproducibility of the secondary reference material for the  $^{207}\text{Pb}/^{206}\text{Pb}$  and  $^{206}\text{Pb}/^{238}\text{U}$  ratios. Weighted  $^{206}\text{Pb}/^{238}\text{U}$  averages were calculated using Isoplot version 3.00 (Ludwig, 2003). Uncertainties on weighted mean ages are quadratic additions of the internal precision on the measurements and the long-term external reproducibility of GJ-1 and Plešovice ( $\sim 1.7\%$  2 SE).

### **Zircon Hf isotopes**

Hf isotopes in zircon were measured *in situ* by LA-MC-ICP-MS at UCSB. Methods used in this study are similar to those used by Hagen-Peter et al. (2015). Ablation spots were placed over the original U–Pb analysis spots to obtain Hf compositions that correspond to the measured U–Pb date of the zircon. A laser spot size of 50  $\mu\text{m}$ , 4 mJ laser energy at 100%, and a pulse rate of 8 Hz were used to ablate samples for 50 s, with a 30 s delay between analyses to allow washout. Masses 171–180 inclusive were measured on 10 Faraday cups at 1 a.m.u. spacing.

Data were reduced using Iolite v2.31 (Paton et al., 2011). Natural ratios of  $^{176}\text{Yb}/^{173}\text{Yb} = 0.786847$  (Thirlwall and Anczkiewicz, 2004) and  $^{176}\text{Lu}/^{175}\text{Lu} = 0.02656$  (Chu et al., 2002) were used to subtract isobaric interferences of  $^{176}\text{Yb}$  and  $^{176}\text{Lu}$  on  $^{176}\text{Hf}$ . The Yb mass bias factor was calculated using a natural  $^{173}\text{Yb}/^{171}\text{Yb}$  ratio of 1.123575 (Thirlwall and Anczkiewicz, 2004) and was used to correct for both Yb and Lu mass bias. A natural  $^{179}\text{Hf}/^{177}\text{Hf}$  ratio of 0.7325 (Patchett and Tatsumoto, 1980, 1981) was used to calculate the Hf mass bias factor.

To assess accuracy and precision, natural reference material zircons ‘91500’ ( $^{176}\text{Hf}/^{177}\text{Hf} = 0.282308 \pm 6$ ; Blichert-Toft, 2008), and ‘Plešovice’ ( $^{176}\text{Hf}/^{177}\text{Hf} = 0.282482 \pm 13$ ; Sláma *et al.*, 2008), and ‘MunZirc1’ ( $^{176}\text{Hf}/^{177}\text{Hf} = 0.282135 \pm 7$ ; Fisher et al., 2011) were analyzed between every 8 sample analyses. The weighted mean corrected  $^{176}\text{Hf}/^{177}\text{Hf}$  values ( $\pm 2\text{SD}$ ) obtained for the secondary reference materials 91500, Plešovice, and MunZirc were within uncertainty of reported values.

**Dataset S1.** Zircon U-Pb and trace elements for zircon.

**Dataset S2.** Zircon Hf isotope data for zircon.

## References Cited

- Adams, C.J., Barley, M.E., Maas, R., Doyle, M.G., 2002. Provenance of Permian - Triassic volcanoclastic sedimentary terranes in New Zealand: Evidence from their radiogenic isotope characteristics and detrital mineral age patterns. *New Zeal. J. Geol. Geophys.* 45, 221–242. <https://doi.org/10.1080/00288306.2002.9514970>
- Adams, C.J., Campbell, H.J., Griffin, & W.L., 2007. Provenance comparisons of Permian to Jurassic tectonostratigraphic terranes in New Zealand: perspectives from detrital zircon age patterns. *Geol. Mag* 144, 701–729. <https://doi.org/10.1017/S0016756807003469>
- Adams, C.J., Korsch, R.J., Griffin, W.L., 2013. Provenance comparisons between the Nambucca Block, Eastern Australia and the Torlesse Composite Terrane, New Zealand: connections and implications from detrital zircon age patterns. *Aust. J. Earth Sci.* 60, 241–253. <https://doi.org/10.1080/08120099.2013.767282>
- Adams, C.J., Korsch, R.J., Griffin, W.L., Division, N.H., Box, G.P.O., Sciences, P., Sciences, E., Papers, S., Dpxx, R., Road, A.S., 2013a. Provenance comparisons between the Nambucca Block , Eastern Australia and the Torlesse Composite Terrane , New Zealand : connections and implications from detrital zircon age patterns GNS Science , Private Bag 1930 , Dunedin 9054 , New Zealand . GEMOC and.
- Adams, C.J., Mortimer, N., Campbell, H.J., Griffin, W.L., 2013b. Detrital zircon geochronology and sandstone provenance of basement Waipapa Terrane (Triassic–Cretaceous) and Cretaceous cover rocks (Northland Allochthon and Houhora Complex) in northern North Island, New Zealand. *Geol. Mag.* 150, 89–109. <https://doi.org/10.1017/s0016756812000258>

- Aitchison, J.C., Buckman, S., 2013. Reply to comment on “Accordion vs. quantum tectonics: Insights into continental growth processes from the Paleozoic of eastern Gondwana.” *Gondwana Res.* 22, 674–680. <https://doi.org/10.1016/j.gr.2012.05.013>
- Aitchison, J.C., Buckman, S., 2012. Accordion vs. quantum tectonics: Insights into continental growth processes from the Paleozoic of eastern Gondwana. *Gondwana Res.* 22, 674–680. <https://doi.org/10.1016/j.gr.2012.05.013>
- Allibone, A.H., Jongens, R., Scott, J.M., Tulloch, A.J., Turnbull, I.M., Cooper, A.F., Powell, N.G., Ladley, E.B., King, R.P., Rattenbury, M.S., 2009. Plutonic rocks of the Median Batholith in eastern and central Fiordland, New Zealand: Field relations, geochemistry, correlation, and nomenclature. *New Zeal. J. Geol. Geophys.* 52, 101–148. <https://doi.org/10.1080/00288300909509882>
- Andersen, T., 2002. Correction of common lead in U–Pb analyses that do not report  $^{204}\text{Pb}$ . *Chem. Geol.* 192, 59–79. [https://doi.org/10.1016/S0009-2541\(02\)00195-X](https://doi.org/10.1016/S0009-2541(02)00195-X)
- Bahlburg, H., Vervoort, J.D., Du Frane, S.A., Bock, B., Augustsson, C., Reimann, C., 2009. Timing of crust formation and recycling in accretionary orogens: Insights learned from the western margin of South America. *Earth-Science Rev.* 97, 215–241. <https://doi.org/10.1016/j.earscirev.2009.10.006>
- Balgord, E.A., 2017. Triassic to Neogene evolution of the south-central Andean arc determined by detrital zircon U-Pb and Hf analysis of Neuquén Basin strata, central Argentina (34°S–40°S). *Lithosphere* 9, 453–462. <https://doi.org/10.1130/L546.1>
- Barham, M., Kirkland, C.L., Reynolds, S., O’Leary, M.J., Evans, N.J., Allen, H., Haines, P.W., Hocking, R.M., McDonald, B.J., Belousova, E., Goodall, J., 2016. The answers are blowin’ in the wind: Ultra-distal ashfall zircons, indicators of Cretaceous super-

eruptions in eastern Gondwana. *Geology* 44, 643–646.

<https://doi.org/10.1130/G38000.1>

Barrett, P.J., Elliot, D.H., Lindsay, J.F., 1986. The Beacon Supergroup (Devonian-Triassic) and Ferrar Group (Jurassic) in the Beardmore Glacier Area, Antarctica. *Geol. Cent. Transantarctic Mt., Antarctic Research Series* 36, 339–428.

<https://doi.org/10.1029/AR036>

Barth, A.P., Wooden, J.L., Jacobson, C.E., Economos, R.C., 2013. Detrital zircon as a proxy for tracking the magmatic arc system: The California arc example. *Geology* 41, 223–226. <https://doi.org/10.1130/G33619.1>

Behn, M.D., Hirth, G., Kelemen, P.B., 2007. Trench-parallel anisotropy produced by foundering of arc lower crust. *Science* 317, 108–111.

<https://doi.org/10.1126/science.1141269>

Belousova, E., Griffin, W., O'Reilly, S.Y., Fisher, N., 2002a. Igneous zircon: trace element composition as an indicator of source rock type. *Contrib. to Mineral. Petrol.* 143, 602–622. <https://doi.org/10.1007/s00410-002-0364-7>

Belousova, E., Griffin, W., O'Reilly, S.Y., Fisher, N., 2002b. Igneous zircon: trace element composition as an indicator of source rock type. *Contrib. to Mineral. Petrol.* 143, 602–622. <https://doi.org/10.1007/s00410-002-0364-7>

Berner, R.A., Kothavala, Z., 2001. GEOCARB III: A revised model of atmospheric CO<sub>2</sub> over Phanerozoic time. *Am. J. Sci.* 301, 182–204. <https://doi.org/10.2475/ajs.301.2.182>

Blichert-Toft, J., 2008. The Hf isotopic composition of zircon reference material 91500. *Chem. Geol.* 253, 252–257. <https://doi.org/10.1016/j.chemgeo.2008.05.014>

Bond, D.P.G., Wignall, P.B., 2014. Large igneous provinces and mass extinctions: An

update, in: Keller, G., Kerr, A.C. (Eds.), *Volcanism, Impacts, and Mass Extinctions: Causes and Effects: Geological Society of America Special Paper 505*. pp. 29–55.  
[https://doi.org/10.1130/2014.2505\(02\)](https://doi.org/10.1130/2014.2505(02))

Borg, S.G., Stump, E., Holloway, J.R., 1986. Granitoids of northern Victoria Land, Antarctica: A reconnaissance study of field relations, petrography, and geochemistry. pp. 115–188. <https://doi.org/10.1029/AR046p0115>

Bouvier, A., Vervoort, J.D., Patchett, P.J., 2008. The Lu-Hf and Sm-Nd isotopic composition of CHUR: Constraints from unequilibrated chondrites and implications for the bulk composition of terrestrial planets. *Earth Planet. Sci. Lett.* 273, 48–57.  
<https://doi.org/10.1016/j.epsl.2008.06.010>

Bradshaw, J.D., Vaughan, a. P.M., Millar, I.L., Flowerdew, M.J., Trouw, R. a. J., Fanning, C.M., Whitehouse, M.J., 2012. Permo-Carboniferous conglomerates in the Trinity Peninsula Group at View Point, Antarctic Peninsula : sedimentology, geochronology and isotope evidence for provenance and tectonic setting in Gondwana. *Geol. Mag.* 149, 626–644. <https://doi.org/10.1017/S001675681100080X>

Brown, C.R., Yakymchuk, C., Brown, M., Fanning, C.M., Korhonen, F.J., Piccoli, P.M., Siddoway, C.S., 2016. From Source to Sink: Petrogenesis of Cretaceous Anatectic Granites from the Fosdick Migmatite–Granite Complex, West Antarctica. *J. Petrol.* 57, 1241–1278. <https://doi.org/10.1093/petrology/egw039>

Burgess, S.D., Bowring, S.A., 2015. High-precision geochronology confirms voluminous magmatism before, during, and after Earth’s most severe extinction. *Sci. Adv.* 1, e1500470–e1500470. <https://doi.org/10.1126/sciadv.1500470>

Burgess, S.D., Bowring, S.A., Fleming, T.H., Elliot, D.H., 2015. High-precision

geochronology links the Ferrar large igneous province with early-Jurassic ocean anoxia and biotic crisis. *Earth Planet. Sci. Lett.* 415, 90–99.

<https://doi.org/10.1016/j.epsl.2015.01.037>

Canile, F.M., Babinski, M., Rocha-Campos, A.C., 2016. Evolution of the Carboniferous–Early Cretaceous units of Paraná Basin from provenance studies based on U–Pb, Hf and O isotopes from detrital zircons. *Gondwana Res.* 40, 142–169.

<https://doi.org/10.1016/j.gr.2016.08.008>

Cao, W., Lee, C.-T.A., Lackey, J.S., 2017. Episodic nature of continental arc activity since 750 Ma: A global compilation. *Earth Planet. Sci. Lett.* 461, 85–95.

<https://doi.org/10.1016/J.EPSL.2016.12.044>

Castillo, P., Fanning, C.M., Fernandez, R., Poblete, F., Hervé, F., 2017a. Provenance and age constraints of Paleozoic siliciclastic rocks from the Ellsworth Mountains in West Antarctica, as determined by detrital zircon geochronology. *GSA Bull.* 129121, 1568–1584. <https://doi.org/10.1130/B31686.1>

Castillo, P., Fanning, C.M., Hervé, F., Lacassie, J.P., 2016. Characterisation and tracing of Permian magmatism in the south-western segment of the Gondwanan margin; U–Pb age, Lu–Hf and O isotopic compositions of detrital zircons from metasedimentary complexes of northern Antarctic Peninsula and western Patagonia. *Gondwana Res.* 36, 1–13. <https://doi.org/10.1016/j.gr.2015.07.014>

Castillo, P., Fanning, C.M., Hervé, F., Lacassie, J.P., 2015. Characterisation and tracing of Permian magmatism in the south-western segment of the Gondwanan margin; U–Pb age, Lu–Hf and O isotopic compositions of detrital zircons from metasedimentary complexes of northern Antarctic Peninsula and western Patagonia. *Gondwana Res.* 1–13.

<https://doi.org/10.1016/j.gr.2015.07.014>

- Castillo, P., Fanning, C.M., Pankhurst, R.J., Hervé, F., Rapela, C., 2017b. Zircon O- and Hf-isotope constraints on the genesis and tectonic significance of Permian magmatism in Patagonia. *J. Geol. Soc. London*. 174, 803–816. <https://doi.org/10.1144/jgs2016-152>
- Cawood, P.A., 2005. Terra Australis Orogen: Rodinia breakup and development of the Pacific and Iapetus margins of Gondwana during the Neoproterozoic and Paleozoic. *Earth-Science Rev.* 69, 249–279. <https://doi.org/10.1016/j.earscirev.2004.09.001>
- Cawood, P.A., Buchan, C., 2007. Linking accretionary orogenesis with supercontinent assembly. *Earth-Science Rev.* 82, 217–256. <https://doi.org/10.1016/j.earscirev.2007.03.003>
- Cawood, P.A., Hawkesworth, C.J., Dhuime, B., 2012. Detrital zircon record and tectonic setting. *Geology* 40, 875–878. <https://doi.org/10.1130/G32945.1>
- Cawood, P.A., Kröner, A., Collins, W.J., Kusky, T.M., Mooney, W.D., Windley, B.F., 2009. Accretionary orogens through Earth history. *Geol. Soc. London, Spec. Publ.* 318, 1–36. <https://doi.org/10.1144/SP318.1>
- Cawood, P.A., Leitch, E.C., Merle, R.E., Nemchin, A.A., 2011. Orogenesis without collision: Stabilizing the terra australis accretionary Orogen, Eastern Australia. *Bull. Geol. Soc. Am.* 123, 2240–2255. <https://doi.org/10.1130/B30415.1>
- Cawood, P.A., Nemchin, A.A., Leverenz, A., Saeed, A., Ballance, P.F., 1999. U/Pb dating of detrital zircons: Implications for the provenance record of Gondwana margin terranes. *Bull. Geol. Soc. Am.* 111, 1107–1119. [https://doi.org/10.1130/0016-7606\(1999\)111<1107:UPDODZ>2.3.CO;2](https://doi.org/10.1130/0016-7606(1999)111<1107:UPDODZ>2.3.CO;2)
- Chapman, J.B., Ducea, M.N., Kapp, P., Gehrels, G.E., Decelles, P.G., 2017. Spatial and

- temporal radiogenic isotopic trends of magmatism in Cordilleran orogens. *Gondwana Res.* 48, 189–204. <https://doi.org/10.1016/J.GR.2017.04.019>
- Chapman, J.B., Gehrels, G.E., Ducea, M.N., Giesler, N., Pullen, A., 2016. A new method for estimating parent rock trace element concentrations from zircon. *Chem. Geol.* 439, 59–70. <https://doi.org/10.1016/j.chemgeo.2016.06.014>
- Chappell, B.W., White, A.J.R., Hine, R., 1988. Granite provinces and basement terranes in the Lachlan Fold Belt, southeastern Australia. *Aust. J. Earth Sci.* 35, 505–521. <https://doi.org/10.1080/08120098808729466>
- Chu, N.-C., Taylor, R.N., Chavagnac, V., Nesbitt, R.W., Boella, R.M., Milton, J.A., German, C.R., Bayon, G., Burton, K., 2002. Hf isotope ratio analysis using multi-collector inductively coupled plasma mass spectrometry: an evaluation of isobaric interference corrections. *J. Anal. At. Spectrom.* 17, 1567–1574. <https://doi.org/10.1039/b206707b>
- Collins, W.J., 2002a. Hot orogens, tectonic switching, and creation of continental crust. *Geology* 30, 535–538. [https://doi.org/10.1130/0091-7613\(2002\)030<0535:HOTSAC>2.0.CO;2](https://doi.org/10.1130/0091-7613(2002)030<0535:HOTSAC>2.0.CO;2)
- Collins, W.J., 2002b. Nature of extensional accretionary orogens. *Tectonics* 21, 6-1-6–12. <https://doi.org/10.1029/2000TC001272>
- Collins, W.J., Belousova, E.A., Kemp, A.I.S., Murphy, J.B., 2011. Two contrasting Phanerozoic orogenic systems revealed by hafnium isotope data. *Nat. Geosci.* 4, 333–337. <https://doi.org/10.1038/ngeo1127>
- Collinson, J.W., Elliot, D.H., 1984. Triassic stratigraphy of the Shackleton Glacier area. American Geophysical Union, pp. 103–117. <https://doi.org/10.1029/AR036p0103>
- Collinson, J.W., Isbell, J.L., Elliot, D.H., Miller, M.F., Miller, J.M.G., Veevers, J.J., 1994.

- Permian-Triassic Transantarctic basin, in: Geological Society of America Memoirs. pp. 173–222. <https://doi.org/10.1130/MEM184-p173>
- Collinson, J.W., Vavra, C.L., Zawiskie, J.M., 1992. Chapter 5: Sedimentology of the Polarstar Formation (Permian), Ellsworth Mountains, West Antarctica, in: Webers, G.F., Craddock, C., Spletstoesser, J.F. (Eds.), *Geology and Paleontology of the Ellsworth Mountains, West Antarctica*. pp. 63–79. <https://doi.org/10.1130/MEM170-p63>
- Couzinié, S., Laurent, O., Moyen, J.-F., Zeh, A., Bouilhol, P., Villaros, A., 2016. Post-collisional magmatism: Crustal growth not identified by zircon Hf–O isotopes. *Earth Planet. Sci. Lett.* 456, 182–195. <https://doi.org/10.1016/j.epsl.2016.09.033>
- Cox, S.C., Parkinson, D.L., Allibone, A.H., Cooper, A.F., 2000. Isotopic character of Cambro - Ordovician plutonism, southern Victoria Land, Antarctica. *New Zeal. J. Geol. Geophys.* 43, 501–520. <https://doi.org/10.1080/00288306.2000.9514906>
- Craddock, J.P., Fitzgerald, P., Konstantinou, A., Nereson, A., Thomas, R.J., 2017a. Detrital zircon provenance of upper Cambrian-Permian strata and tectonic evolution of the Ellsworth Mountains, West Antarctica. *Gondwana Res.* 45, 191–207. <https://doi.org/10.1016/j.gr.2016.11.011>
- Craddock, J.P., Schmitz, M.D., Crowley, J.L., Larocque, J., Pankhurst, R.J., Juda, N., Konstantinou, A., Storey, B., 2017b. Precise U-Pb zircon ages and geochemistry of Jurassic granites, Ellsworth-Whitmore terrane, central Antarctica. *Geol. Soc. Am. Bull.* 129, 118–136. <https://doi.org/10.1130/B31485.1>
- Crawford, A., 2003. 120 to 0 Ma tectonic evolution of the southwest Pacific and analogous geological evolution of the 600 to 220 Ma Tasman Fold Belt System. *Geol. Soc. Aust. Spec. Publ.* 22, 377–397. <https://doi.org/10.1130/0-8137-2372-8.383>

- Currie, C.A., Ducea, M.N., Decelles, P.G., Beaumont, C., 2015. Geodynamic models of Cordilleran orogens: Gravitational instability of magmatic arc roots. *Geol. Soc. Am. Mem.* 212, 1–22. [https://doi.org/10.1130/2015.1212\(01\)](https://doi.org/10.1130/2015.1212(01))
- Currie, C.A., Huisman, R.S., Beaumont, C., 2008. Thinning of continental backarc lithosphere by flow-induced gravitational instability. *Earth Planet. Sci. Lett.* 269, 436–447. <https://doi.org/10.1016/J.EPSL.2008.02.037>
- Dahlquist, J.A., Alasino, P.H., Basei, M.A.S., Morales Cámara, M.M., Macchioli Grande, M., da Costa Campos Neto, M., 2018. Petrological, geochemical, isotopic, and geochronological constraints for the Late Devonian–Early Carboniferous magmatism in SW Gondwana (27–32°LS): an example of geodynamic switching. *Int. J. Earth Sci.* 1–29. <https://doi.org/10.1007/s00531-018-1615-9>
- Dalziel, I.W.D., Elliot, D.H., 1982. West Antarctica: Problem child of Gondwanaland. *Tectonics* 1, 3–19. <https://doi.org/10.1029/TC001i001p00003>
- Decelles, P.G., Ducea, M.N., Kapp, P., Zandt, G., 2009. Cyclicality in Cordilleran orogenic systems. *Nat. Geosci.* 2, 251–257. <https://doi.org/10.1038/ngeo469>
- del Rey, A., Deckart, K., Arriagada, C., Martínez, F., 2016. Resolving the paradigm of the late Paleozoic–Triassic Chilean magmatism: Isotopic approach. *Gondwana Res.* 37, 172–181. <https://doi.org/10.1016/j.gr.2016.06.008>
- Dewey, J.F., 1988. Extensional collapse of orogens. *Tectonics* 7, 1123–1139.
- Dhuime, B., Hawkesworth, C., Cawood, P.A., 2011. When Continents Formed. *Science* (80-.). 331, 154–155. <https://doi.org/10.1126/science.1201245>
- DiVenere, V., Kent, D. V., Dalziel, I.W.D., 1995. Early Cretaceous paleomagnetic results from Marie Byrd Land, West Antarctica: Implications for the Weddellia collage of

crustal blocks. *J. Geophys. Res. Solid Earth* 100, 8133–8151.

<https://doi.org/10.1029/95JB00042>

Ducea, M.N., Barton, M.D., 2007. Igniting flare-up events in Cordilleran arcs. *Geology* 35, 1047. <https://doi.org/10.1130/G23898A.1>

Ducea, M.N., Paterson, S.R., Decelles, P.G., 2015. High-Volume Magmatic Events in Subduction Systems. *Elements* 11, 99–104. <https://doi.org/10.2113/gselements.11.2.99>

Echaurren, A., Oliveros, V., Folguera, A., Ibarra, F., Creixell, C., Lucassen, F., 2017. Early Andean tectonomagmatic stages in north Patagonia: insights from field and geochemical data. *J. Geol. Soc. London*. 174, 405–421. <https://doi.org/10.1144/jgs2016-087>

Elliot, D.H., 2013. The geological and tectonic evolution of the Transantarctic Mountains: a review. *Geol. Soc. London, Spec. Publ.* 381, 7–35. <https://doi.org/10.1144/SP381.14>

Elliot, D.H., 2000. Stratigraphy of Jurassic pyroclastic rocks in the Transantarctic Mountains. *J. African Earth Sci.* 31, 77–89. [https://doi.org/10.1016/S0899-5362\(00\)00074-9](https://doi.org/10.1016/S0899-5362(00)00074-9)

Elliot, D.H., 1996. The Hanson Formation: a new stratigraphical unit in the Transantarctic Mountains, Antarctica. *Antarct. Sci.* 8. <https://doi.org/10.1017/S0954102096000569>

Elliot, D.H., Fanning, C.M., 2008. Detrital zircons from upper Permian and lower Triassic Victoria Group sandstones, Shackleton Glacier region, Antarctica: Evidence for multiple sources along the Gondwana plate margin. *Gondwana Res.* 13, 259–274. <https://doi.org/10.1016/j.gr.2007.05.003>

Elliot, D.H., Fanning, C.M., Fleming, T.H., Foland, K. a, Raymond, C.E., International Symposium on Antarctic Earth, S., 2007. Jurassic silicic volcanism in the Transantarctic Mountains; was it related to plate margin processes or to Ferrar magmatism? Open-File Rep. - U. S. Geol. Surv. Short Research Paper 051. <https://doi.org/10.3133/of2007->

1047.srp051

Elliot, D.H., Fanning, C.M., Hulett, S.R.W., 2015. Age provinces in the Antarctic craton: Evidence from detrital zircons in Permian strata from the Beardmore Glacier region, Antarctica. *Gondwana Res.* 28, 152–164. <https://doi.org/10.1016/j.gr.2014.03.013>

Elliot, D.H., Fanning, C.M., Isbell, J.L., Hulett, S.R.W., 2017. The Permo-Triassic Gondwana sequence, central Transantarctic Mountains, Antarctica: Zircon geochronology, provenance, and basin evolution. *Geosphere* 13, 155–178. <https://doi.org/10.1130/GES01345.1>

Elliot, D.H., Fanning, C.M., Laudon, T.S., 2016a. The Gondwana Plate margin in the Weddell Sea sector: Zircon geochronology of Upper Paleozoic (mainly Permian) strata from the Ellsworth Mountains and eastern Ellsworth Land, Antarctica. *Gondwana Res.* 29, 234–247. <https://doi.org/10.1016/j.gr.2014.12.001>

Elliot, D.H., Fleming, T.H., 2004. Occurrence and Dispersal of Magmas in the Jurassic Ferrar Large Igneous Province, Antarctica. *Gondwana Res.* 7, 223–237. [https://doi.org/10.1016/S1342-937X\(05\)70322-1](https://doi.org/10.1016/S1342-937X(05)70322-1)

Elliot, D.H., Larsen, D., Fanning, C.M., Fleming, T.H., Vervoort, J.D., 2016b. The Lower Jurassic Hanson Formation of the Transantarctic Mountains: implications for the Antarctic sector of the Gondwana plate margin. *Geol. Mag.* 154, 777–803. <https://doi.org/10.1017/S0016756816000388>

Elsner, M., Schöner, R., Gerdes, A., Gaupp, R., 2013. Reconstruction of the early Mesozoic plate margin of Gondwana by U–Pb ages of detrital zircons from northern Victoria Land, Antarctica. *Geol. Soc. London, Spec. Publ.* 383, 211–232. <https://doi.org/10.1144/SP383.5>

- Encarnación, J., Fleming, T.H., Elliot, D.H., Eales, H. V., 1996. Synchronous emplacement of Ferrar and Karoo dolerites and the early breakup of Gondwana. *Geology* 24, 535–538. [https://doi.org/10.1130/0091-7613\(1996\)024<0535](https://doi.org/10.1130/0091-7613(1996)024<0535)
- Fanning, C.M., Hervé, F., Pankhurst, R.J., Rapela, C.W., Kleiman, L.E., Yaxley, G.M., Castillo, P., 2011. Lu–Hf isotope evidence for the provenance of Permian detritus in accretionary complexes of western Patagonia and the northern Antarctic Peninsula region. *J. South Am. Earth Sci.* 32, 485–496. <https://doi.org/10.1016/j.jsames.2011.03.007>
- Fergusson, C.L., 2013. Comment on “Accordion vs. quantum tectonics: Insights into continental growth processes from the Paleozoic of eastern Gondwana” by Jonathan C. Aitchison, *Solomon Buckman Gondwana Research*, Volume 22, Issue 2, September 2012, Pages 674-680. *Gondwana Res.* 23, 1646–1649. <https://doi.org/10.1016/j.gr.2012.12.013>
- Fielding, C.R., Frank, T.D., Birgenheier, L.P., Rygel, M.C., Jones, A.T., Roberts, J., 2008. Stratigraphic imprint of the Late Palaeozoic Ice Age in eastern Australia: a record of alternating glacial and nonglacial climate regime. *J. Geol. Soc. London.* 165, 129–140. <https://doi.org/10.1144/0016-76492007-036>
- Flowerdew, M.J., Millar, I.L., Curtis, M.L., Vaughan, A.P.M., Horstwood, M.S.A., Whitehouse, M.J., Fanning, C.M., 2007. Combined U-Pb geochronology and Hf isotope geochemistry of detrital zircons from early Paleozoic sedimentary rocks, Ellsworth-Whitmore Mountains block, Antarctica. *Bull. Geol. Soc. Am.* 119, 275–288. <https://doi.org/10.1130/B25891.1>
- Flowerdew, M.J., Millar, I.L., Vaughan, A.P.M., Horstwood, M.S.A., Fanning, C.M., 2006.

- The source of granitic gneisses and migmatites in the Antarctic Peninsula: a combined U–Pb SHRIMP and laser ablation Hf isotope study of complex zircons. *Contrib. to Mineral. Petrol.* 151, 751–768. <https://doi.org/10.1007/s00410-006-0091-6>
- Foden, J., Elburg, M.A., Dougherty -Page, J., Burt, A., 2006. The Timing and Duration of the Delamerian Orogeny: Correlation with the Ross Orogen and Implications for Gondwana Assembly. *J. Geol.* 114, 189–210. <https://doi.org/10.1086/499570>
- Foster, D.A., Gray, D.R., Spaggiari, C., Kamenov, G., Bierlein, F.P., 2009. Palaeozoic Lachlan orogen, Australia; accretion and construction of continental crust in a marginal ocean setting: isotopic evidence from Cambrian metavolcanic rocks. *Geol. Soc. London, Spec. Publ.* 318, 329–349. <https://doi.org/10.1144/SP318.12>
- Fruchter, J.S., Robertson, D.E., Evans, J.C., Olsen, K.B., Lepel, E.A., Laul, J.C., Abel, K.H., Sanders, R.W., Jackson, P.O., Wogman, N.S., Perkins, R.W., Van Tuyl, H.H., Beauchamp, R.H., Shade, J.W., Daniel, J.L., Erikson, R.L., Sehmel, G.A., N., L.R., Robinson, A. V., Moss, O.R., Briant, J.K., Cannon, W.C., 1980. Mount St. Helens Ash from the 18 May 1980 Eruption: Chemical, Physical, Mineralogical, and Biological Properties. *Science* (80-. ). 209, 1116–1125. <https://doi.org/10.1126/science.209.4461.1116>
- Gibson, G.M., Champion, D.C., Ireland, T.R., 2015. Preservation of a fragmented late Neoproterozoic-earliest Cambrian hyper-extended continental-margin sequence in the Australian Delamerian Orogen. *Geol. Soc. London, Spec. Publ.* 269–299. <https://doi.org/10.1144/SP413.8>
- Gibson, G.M., Ireland, T.R., 1996. Extension of delamerian (ross) orogen into western New Zealand: Evidence from zircon ages and implications for crustal growth along the

pacific margin of Gondwana. *Geology* 24, 1087–1090. [https://doi.org/10.1130/0091-7613\(1996\)024<1087:EODROI>2.3.CO;2](https://doi.org/10.1130/0091-7613(1996)024<1087:EODROI>2.3.CO;2)

Goodge, J.W., Fanning, C.M., 2016. Mesoarchean and Paleoproterozoic history of the Nimrod Complex, central Transantarctic Mountains, Antarctica: Stratigraphic revisions and relation to the Mawson Continent in East Gondwana. *Precambrian Res.* 285, 242–271. <https://doi.org/10.1016/j.precamres.2016.09.001>

Goodge, J.W., Fanning, C.M., Norman, M.D., Bennett, V.C., 2012. Temporal, isotopic and spatial relations of early paleozoic gondwana-margin arc magmatism, Central Transantarctic Mountains, Antarctica. *J. Petrol.* 53, 2027–2065. <https://doi.org/10.1093/petrology/egs043>

Grimes, C.B., Wooden, J.L., Cheadle, M.J., John, B.E., 2015. “Fingerprinting” tectono-magmatic provenance using trace elements in igneous zircon. *Contrib. to Mineral. Petrol.* 170, 46. <https://doi.org/10.1007/s00410-015-1199-3>

Grunow, A.M., Kent, D.V., Dalziel, I.W.D., 1987. Mesozoic evolution of West Antarctica and the Weddell Sea Basin: new paleomagnetic constraints. *Earth Planet. Sci. Lett.* 86, 16–26. [https://doi.org/10.1016/0012-821X\(87\)90184-1](https://doi.org/10.1016/0012-821X(87)90184-1)

Gunn, B.M., Warren, G., 1962. Geology of Victoria Land between the Mawson and Mullock Glaciers, Antarctica. *New Zeal. Geol. Surv. Bull.* 71, 157.

Hacker, B.R., Kelemen, P.B., Behn, M.D., 2011. Differentiation of the continental crust by relamination. *Earth Planet. Sci. Lett.* 307, 501–516. <https://doi.org/10.1016/J.EPSL.2011.05.024>

Hagen-Peter, G., Cottle, J., 2018. Evaluating the relative roles of crustal growth versus reworking through continental arc magmatism: A case study from the Ross orogen,

- Antarctica. *Gondwana Res.* 55, 153–166. <https://doi.org/10.1016/j.gr.2017.11.006>
- Hagen-Peter, G., Cottle, J.M., Smit, M., Cooper, A.F., 2016. Coupled garnet Lu-Hf and monazite U-Pb geochronology constrain early convergent margin dynamics in the Ross orogen, Antarctica. *J. Metamorph. Geol.* 34, 293–319. <https://doi.org/10.1111/jmg.12182>
- Hagen-Peter, G., Cottle, J.M., Tulloch, A.J., Cox, S.C., 2015. Mixing between enriched lithospheric mantle and crustal components in a short-lived subduction-related magma system, Dry Valleys area, Antarctica: Insights from U-Pb geochronology, Hf isotopes, and whole-rock geochemistry. *Lithosphere* 7, 174–188. <https://doi.org/10.1130/L384.1>
- Handler, M.R., Wysoczanski, R.J., Gamble, J.A., 2003. Proterozoic lithosphere in Marie Byrd Land, West Antarctica: Re–Os systematics of spinel peridotite xenoliths. *Chem. Geol.* 196, 131–145. [https://doi.org/10.1016/S0009-2541\(02\)00410-2](https://doi.org/10.1016/S0009-2541(02)00410-2)
- Haschke, M.R., Scheuber, E., Gunther, A., Reutter, K.-J., 2002. Evolutionary cycles during the Andean orogeny: repeated slab breakoff and flat subduction? *Terra Nov.* 14, 49–55. <https://doi.org/10.1046/j.1365-3121.2002.00387.x>
- Henry, L.C., 2013. Late Paleozoic Glaciation and Ice Sheet Collapse Over Western and Eastern Gondwana: Sedimentology and Stratigraphy of Glacial to Post- Glacial Strata in Western Argentina and Tasmania, Australia [Ph.D. thesis]. University of Wisconsin-Milwaukee.
- Henry, L.C., Limarino, C.O., Fraiser, M.L., Isbell, J.L., 2009. Potential environmental consequences of Panthalassan margin volcanism in the late Paleozoic. *Geol. Soc. Am. Abstr. with Programs* 41, 360.
- Hermann, E., Hochuli, P.A., Bucher, H., Brühwiler, T., Hautmann, M., Ware, D., Roohi, G.,

2011. Terrestrial ecosystems on North Gondwana following the end-Permian mass extinction. *Gondwana Res.* 20, 630–637. <https://doi.org/10.1016/j.gr.2011.01.008>
- Hervé, F., Calderon, M., Fanning, C.M., Pankhurst, R.J., Fuentes, F., Rapela, C.W., Correa, J., Quezada, P., Marambio, C., 2016. Devonian magmatism in the accretionary complex of southern Chile. *J. Geol. Soc. London.* 173, 587–602. <https://doi.org/10.1144/jgs2015-163>
- Hervé, F., Fanning, C.M., Calderón, M., Mpodozis, C., 2014a. Early Permian to Late Triassic batholiths of the Chilean Frontal Cordillera (28°–31°S): SHRIMP U–Pb zircon ages and Lu–Hf and O isotope systematics. *Lithos* 184–187, 436–446. <https://doi.org/10.1016/j.lithos.2013.10.018>
- Hervé, F., Fanning, C.M., Calderón, M., Mpodozis, C., 2014b. Early Permian to Late Triassic batholiths of the Chilean Frontal Cordillera (28°–31°S): SHRIMP U–Pb zircon ages and Lu–Hf and O isotope systematics. *Lithos* 184–187, 436–446. <https://doi.org/10.1016/J.LITHOS.2013.10.018>
- Hervé, F., Miller, H., Pimpirev, C., 2006. Patagonia — Antarctica Connections before Gondwana Break-Up, in: *Antarctica*. Springer-Verlag, Berlin/Heidelberg, pp. 217–227. [https://doi.org/10.1007/3-540-32934-X\\_26](https://doi.org/10.1007/3-540-32934-X_26)
- Hinkley, T.K., Smith, K.S., Taggart, J.E., Brown, J.T., 1980. Chemical and mineralogical aspects of the observed fractionation of ash from the May 18, 1980 eruption of Mount St. Helens. *U.S. Geol. Surv. Prof. Pap.* 1397–A, 73.
- Horton, B.K., 2018. Sedimentary record of Andean mountain building. <https://doi.org/10.1016/j.earscirev.2017.11.025>
- Hoskin, P.W.O., Ireland, T.R., 2000. Rare earth element chemistry of zircon and its use as a

provenance indicator. *Geology* 28, 627. [https://doi.org/10.1130/0091-7613\(2000\)28<627:REECOZ>2.0.CO;2](https://doi.org/10.1130/0091-7613(2000)28<627:REECOZ>2.0.CO;2)

Jackson, S.E., Pearson, N.J., Griffin, W.L., Belousova, E.A., 2004. The application of laser ablation-inductively coupled plasma-mass spectrometry to in situ U–Pb zircon geochronology. *Chem. Geol.* 211, 47–69. <https://doi.org/10.1016/j.chemgeo.2004.06.017>

Jeon, H., Williams, I.S., Bennett, V.C., 2014. Uncoupled O and Hf isotopic systems in zircon from the contrasting granite suites of the New England Orogen, eastern Australia: Implications for studies of Phanerozoic magma genesis. *Geochim. Cosmochim. Acta* 146, 132–149. <https://doi.org/10.1016/j.gca.2014.09.042>

Jull, M., Kelemen, P.B., 2001. On the conditions for lower crustal convective instability. *J. Geophys. Res. Solid Earth* 106, 6423–6446. <https://doi.org/10.1029/2000JB900357>

Kay, S.M., Ramos, V.A., Mpodozis, C., Sruoga, P., 1989. Late Paleozoic to Jurassic silicic magmatism at the Gondwana margin: Analogy to the Middle Proterozoic in North America? *Geology* 17, 324. [https://doi.org/10.1130/0091-7613\(1989\)017<0324:LPTJSM>2.3.CO;2](https://doi.org/10.1130/0091-7613(1989)017<0324:LPTJSM>2.3.CO;2)

Kemp, A.I.S., Hawkesworth, C.J., Collins, W.J., Gray, C.M., Blevin, P.L., 2009. Isotopic evidence for rapid continental growth in an extensional accretionary orogen: The Tasmanides, eastern Australia. *Earth Planet. Sci. Lett.* 284, 455–466. <https://doi.org/10.1016/j.epsl.2009.05.011>

Kimbrough, D.L., Mahoney, J.B., Mescua, J.F., Giambiagi, L.B., Grove, M., 2016. The Choiyoi silicic large igneous province of Argentina and Chile and its possible influence on Permian environmental degradation and mass extinction, in: Geological Society of

- America Abstracts with Programs. <https://doi.org/10.1130/abs/2016AM-287712>
- Kimbrough, D.L., Tulloch, A.J., Coombs, D.S., Landis, C. a., Johnston, M.R., Mattinson, J.M., 1994. Uranium lead zircon ages from the Median Tectonic Zone, New Zealand. *New Zeal. J. Geol. Geophys.* 37, 393–419.  
<https://doi.org/10.1080/00288306.1994.9514630>
- Kirkland, C.L., Smithies, R.H., Taylor, R.J.M., Evans, N., McDonald, B., 2015. Zircon Th/U ratios in magmatic environs. *Lithos* 212–215, 397–414.  
<https://doi.org/10.1016/j.lithos.2014.11.021>
- Kleiman, L.E., Japas, M.S., 2009. The Choiyoi volcanic province at 34°S–36°S (San Rafael, Mendoza, Argentina): Implications for the Late Palaeozoic evolution of the southwestern margin of Gondwana. *Tectonophysics* 473, 283–299.  
<https://doi.org/10.1016/j.tecto.2009.02.046>
- Korhonen, F.J., Brown, M., Grove, M., Siddoway, C.S., Baxter, E.F., Inglis, J.D., 2012. Separating metamorphic events in the Fosdick migmatite-granite complex, West Antarctica. *J. Metamorph. Geol.* 30, 165–192. <https://doi.org/10.1111/j.1525-1314.2011.00961.x>
- Korhonen, F.J., Saito, S., Brown, M., Siddoway, C.S., Day, J.M.D., 2010. Multiple generations of granite in the Fosdick Mountains, Marie Byrd Land, West Antarctica: Implications for polyphase intracrustal differentiation in a continental margin setting. *J. Petrol.* 51, 627–670. <https://doi.org/10.1093/petrology/egp093>
- Kylander-Clark, A.R.C., 2017. Petrochronology by Laser-Ablation Inductively Coupled Plasma Mass Spectrometry. *Rev. Mineral. Geochemistry* 83, 183–198.  
<https://doi.org/10.2138/rmg.2017.83.6>

- Kylander-Clark, A.R.C., Hacker, B.R., Cottle, J.M., 2013. Laser-ablation split-stream ICP petrochronology. *Chem. Geol.* 345, 99–112.  
<https://doi.org/10.1016/j.chemgeo.2013.02.019>
- Lallemand, S., Heuret, A., Boutelier, D., 2005. On the relationships between slab dip, back-arc stress, upper plate absolute motion, and crustal nature in subduction zones. *Geochemistry, Geophys. Geosystems* 6, n/a-n/a. <https://doi.org/10.1029/2005GC000917>
- Lawver, L.A., Dalziel, I.W.D., Norton, I.O., Gahagan, L.M., Davis, J., 2014. The PLATES 2013 Atlas of Plate Reconstructions (550 Ma to Present Day). PLATES Prog. Rep. No. 367-0214 University, 212.
- Leat, P.T., Storey, B.C., Pankhurst, R.J., 1993. Geochemistry of Palaeozoic–Mesozoic Pacific rim orogenic magmatism, Thurston Island area, West Antarctica. *Antarct. Sci.* 5, 281–296. <https://doi.org/10.1017/S0954102093000380>
- Lee, C.-T.A., Anderson, D.L., 2015. Continental crust formation at arcs, the arclogite “delamination” cycle, and one origin for fertile melting anomalies in the mantle. *Sci. Bull.* 60, 1141–1156. <https://doi.org/10.1007/s11434-015-0828-6>
- Lee, C.-T.A., Lackey, J.S., 2015. Global Continental Arc Flare-ups and Their Relation to Long-Term Greenhouse Conditions. *Elements* 11, 125–130.  
<https://doi.org/10.2113/gselements.11.2.125>
- LeMasurier, W.E., Landis, C.A., 1996. Mantle-plume activity recorded by low-relief erosion surfaces in West Antarctica and New Zealand. *Geol. Soc. Am. Bull.* 108, 1450–1466.  
[https://doi.org/10.1130/0016-7606\(1996\)108<1450:MPARBL>2.3.CO;2](https://doi.org/10.1130/0016-7606(1996)108<1450:MPARBL>2.3.CO;2)
- Li, P., Rosenbaum, G., Yang, J.-H., Hoy, D., 2015. Australian-derived detrital zircons in the Permian-Triassic Gympie terrane (eastern Australia): Evidence for an autochthonous

- origin. *Tectonics* 34, 858–874. <https://doi.org/10.1002/2015TC003829>
- Limarino, C.O., Césari, S.N., Spalletti, L.A., Taboada, A.C., Isbell, J.L., Geuna, S., Gulbranson, E.L., 2014. A paleoclimatic review of southern South America during the late Paleozoic: A record from icehouse to extreme greenhouse conditions. *Gondwana Res.* 25, 1396–1421. <https://doi.org/10.1016/j.gr.2012.12.022>
- Lister, G., Forster, M., 2009. Tectonic mode switches and the nature of orogenesis. *Lithos* 113, 274–291. <https://doi.org/10.1016/j.lithos.2008.10.024>
- Liu, Y., Hu, Z., Zong, K., Gao, C., Gao, S., Xu, J., Chen, H., 2010. Reappraisal and refinement of zircon U-Pb isotope and trace element analyses by LA-ICP-MS. *Chinese Sci. Bull.* 55, 1535–1546. <https://doi.org/10.1007/s11434-010-3052-4>
- Ludwig, K.R., 2003. User's Manual for Isoplot/EX, version 3.0, a geochronological toolkit for Microsoft Excel. Berkeley Geochronol. Cent. Spec. Publ. 4.
- Luppo, T., López de Luchi, M.G., Rapalini, A.E., Martínez Dopico, C.I., Fanning, C.M., 2018. Geochronologic evidence of a large magmatic province in northern Patagonia encompassing the Permian-Triassic boundary. *J. South Am. Earth Sci.* 82, 346–355. <https://doi.org/10.1016/j.jsames.2018.01.003>
- Luyendyk, B., Cisowski, S., Smith, C., Richard, S., Kimbrough, D., 1996. Paleomagnetic study of the northern Ford Ranges, western Marie Byrd Land, West Antarctica: Motion between West and East Antarctica. *Tectonics* 15, 122–141. <https://doi.org/10.1029/95TC02524>
- Matthews, K.J., Maloney, K.T., Zahirovic, S., Williams, S.E., Seton, M., Müller, R.D., 2016. Global plate boundary evolution and kinematics since the late Paleozoic. *Glob. Planet. Change* 146, 226–250. <https://doi.org/10.1016/j.gloplacha.2016.10.002>

- Matthews, K.J., Seton, M., Müller, R.D., 2012. A global-scale plate reorganization event at 105–100Ma. *Earth Planet. Sci. Lett.* 355–356, 283–298.  
<https://doi.org/10.1016/j.epsl.2012.08.023>
- McKay, M.P., Coble, M.A., Hessler, A.M., Weislogel, A.L., Fildani, A., 2016a. Petrogenesis and provenance of distal volcanic tuffs from the Permian-Triassic Karoo Basin, South Africa: A window into a dissected magmatic province. *Geosphere* 12, 1–14.  
<https://doi.org/10.1130/GES01215.1>
- McKay, M.P., Coble, M.A., Hessler, A.M., Weislogel, A.L., Fildani, A., 2016b. Petrogenesis and provenance of distal volcanic tuffs from the Permian–Triassic Karoo Basin, South Africa: A window into a dissected magmatic province. *Geosphere* 12, 1–14.  
<https://doi.org/10.1130/GES01215.1>
- McKay, M.P., Jackson, W.T., Hessler, A.M., 2018. Tectonic stress regime recorded by zircon Th/U. *Gondwana Res.* 57, 1–9. <https://doi.org/10.1016/j.gr.2018.01.004>
- McKenzie, N.R., Horton, B.K., Loomis, S.E., Stockli, D.F., Planavsky, N.J., Lee, C.-T.A., 2016. Continental arc volcanism as the principal driver of icehouse-greenhouse variability. *Science* (80-. ). 352, 444–447. <https://doi.org/10.1126/science.aad5787>
- Mckibbin, S.J., Landenberger, B., Fanning, C.M., 2017. First magmatism in the New England Batholith, Australia: forearc and arc–back-arc components in the Bakers Creek Suite gabbros. *Solid Earth* 8, 421–434. <https://doi.org/10.5194/se-8-421-2017>
- McKinney, S.T., Cottle, J.M., Lederer, G.W., 2015. Evaluating rare earth element (REE) mineralization mechanisms in Proterozoic gneiss, Music Valley, California. *Geol. Soc. Am. Bull.* 127, B31165.1. <https://doi.org/10.1130/B31165.1>
- Milan, L.A., Daczko, N.R., Clarke, G.L., 2017. Cordillera Zealandia: A Mesozoic arc flare-

up on the palaeo-Pacific Gondwana Margin. *Sci. Rep.* 7, 261.

<https://doi.org/10.1038/s41598-017-00347-w>

Millar, I.L., Pankhurst, R.J., Fanning, C.M., 2002. Basement chronology of the Antarctic Peninsula: recurrent magmatism and anatexis in the Palaeozoic Gondwana Margin. *J. Geol. Soc. London.* 159, 145–157. <https://doi.org/10.1144/0016-764901-020>

Mortimer, N., Gans, P., Calvert, A., Walker, N., 1999. Geology and thermochronometry of the east edge of the Median Batholith (Median Tectonic Zone): A new perspective on Permian to Cretaceous crustal growth of New Zealand. *Isl. Arc* 8, 404–425.

<https://doi.org/10.1046/j.1440-1738.1999.00249.x>

Mortimer, N., Rattenbury, M., King, P., Bland, K., Barrell, D., Bache, F., Begg, J., Campbell, H., Cox, S., Crampton, J., Edbrooke, S., Forsyth, P., Johnston, M., Jongens, R., Lee, J., Leonard, G., Raine, J., Skinner, D., Timm, C., Townsend, D., Tulloch, A.J., Turnbull, I., Turnbull, R., 2014. High-level stratigraphic scheme for New Zealand rocks. *New Zeal. J. Geol. Geophys.* 57, 402–419. <https://doi.org/10.1080/00288306.2014.946062>

Mortimer, N., Turnbull, R.E., Palin, J.M., Tulloch, A.J., Rollet, N., Hashimoto, T., 2015. Triassic–Jurassic granites on the Lord Howe Rise, northern Zealandia. *Aust. J. Earth Sci.* 62, 735–742. <https://doi.org/10.1080/08120099.2015.1081984>

Mukasa, S.B., Dalziel, I.W.D., 2000. Marie Byrd Land, West Antarctica: Evolution of Gondwana's Pacific margin constrained by zircon U-Pb geochronology and feldspar common-Pb isotopic compositions. *Geol. Soc. Am. Bull.* 112, 611–627. [https://doi.org/10.1130/0016-7606\(2000\)112<611:MBLWAE>2.0.CO;2](https://doi.org/10.1130/0016-7606(2000)112<611:MBLWAE>2.0.CO;2)

Mundl, A., Ntaflos, T., Ackerman, L., Bizimis, M., Bjerg, E.A., Hauzenberger, C.A., 2015. Mesoproterozoic and Paleoproterozoic subcontinental lithospheric mantle domains

- beneath southern Patagonia: Isotopic evidence for its connection to Africa and Antarctica. *Geology* 43, 39–42. <https://doi.org/10.1130/G36344.1>
- Nelson, D.A., Cottle, J.M., 2017. Long-Term Geochemical and Geodynamic Segmentation of the Paleo-Pacific Margin of Gondwana: Insight From the Antarctic and Adjacent Sectors. *Tectonics* 36, 3229–3247. <https://doi.org/10.1002/2017TC004611>
- Pankhurst, R.J., Leat, P.T., Sruoga, P., Rapela, C.W., Márquez, M., Storey, B.C., Riley, T.R., 1998a. The Chon Aike province of Patagonia and related rocks in West Antarctica: a silicic large igneous province. *J. Volcanol. Geotherm. Res.* 81, 113–136.
- Pankhurst, R.J., Millar, I.L., Grunow, A.M., Storey, B.C., 1993. The Pre-Cenozoic magmatic history of the Thurston Island Crustal Block, west Antarctica. *J. Geophys. Res. Solid Earth* 98, 11835–11849. <https://doi.org/10.1029/93JB01157>
- Pankhurst, R.J., Rapela, C.W., Fanning, C.M., Márquez, M., 2006. Gondwanide continental collision and the origin of Patagonia. *Earth-Science Rev.* 76, 235–257. <https://doi.org/10.1016/J.EARSCIREV.2006.02.001>
- Pankhurst, R.J., Rapela, C.W., Lopez De Luchi, M.G., Rapalini, a. E., Fanning, C.M., Galindo, C., 2014. The Gondwana connections of northern Patagonia. *J. Geol. Soc. London.* 171, 313–328. <https://doi.org/10.1144/jgs2013-081>
- Pankhurst, R.J., Rapela, C.W., Loske, W.P., Márquez, M., Fanning, C.M., 2003. Chronological study of the pre-Permian basement rocks of southern Patagonia. *J. South Am. Earth Sci.* 16, 27–44. [https://doi.org/10.1016/S0895-9811\(03\)00017-8](https://doi.org/10.1016/S0895-9811(03)00017-8)
- Pankhurst, R.J., Riley, T.R., Fanning, C.M., Kelley, S.P., 2000. Episodic Silicic Volcanism in Patagonia and the Antarctic Peninsula: Chronology of Magmatism Associated with the Break-up of Gondwana. *J. Petrol.* 41, 605–625.

<https://doi.org/10.1093/petrology/41.5.605>

Pankhurst, R.J., Weaver, S.D., Bradshaw, J.D., Storey, B.C., Ireland, T.R., 1998b.

Geochronology and geochemistry of pre-Jurassic superterranes in Marie Byrd Land, Antarctica. *J. Geophys. Res. Solid Earth* 103, 2529–2547.

<https://doi.org/10.1029/97JB02605>

Pankhurst, R.J., Weaver, S.D., Hervé, F., Larrando, P., 1999. Mesozoic-Cenozoic evolution of the North Patagonian Batholith in Aysen, southern Chile. *J. Geol. Soc. London*. 156, 673–694. <https://doi.org/10.1144/gsjgs.156.4.0673>

Patchett, P.J., Tatsumoto, M., 1981. A routine high-precision method for Lu-Hf isotope geochemistry and chronology. *Contrib. to Mineral. Petrol.* 75, 263–267.

<https://doi.org/10.1007/BF01166766>

Patchett, P.J., Tatsumoto, M., 1980. Hafnium isotope variations in oceanic basalts. *Geophys. Res. Lett.* 7, 1077–1080. <https://doi.org/10.1029/GL007i012p01077>

Paterson, S.R., Ducea, M.N., 2015. Arc Magmatic Tempos: Gathering the Evidence.

*Elements* 11, 91–98. <https://doi.org/10.2113/gselements.11.2.91>

Paton, C., Hellstrom, J., Paul, B., Woodhead, J., Hergt, J., 2011. Iolite: Freeware for the visualisation and processing of mass spectrometric data. *J. Anal. At. Spectrom.* 26, 2508. <https://doi.org/10.1039/c1ja10172b>

Paton, C., Woodhead, J.D., Hellstrom, J.C., Hergt, J.M., Greig, A., Maas, R., 2010. Improved laser ablation U-Pb zircon geochronology through robust downhole fractionation correction. *Geochemistry, Geophys. Geosystems* 11, n/a-n/a.

<https://doi.org/10.1029/2009GC002618>

Paul L. Williams, 1969. Petrology of Upper Precambrian and Paleozoic Sandstones in the

Pensacola Mountains, Antarctica. *J. Sediment. Res.* Vol. 39.

<https://doi.org/10.1306/74D71E56-2B21-11D7-8648000102C1865D>

Paulsen, T., Deering, C., Sliwinski, J., Bachmann, O., Guillong, M., 2016. A continental arc tempo discovered in the Pacific-Gondwana margin mudpile? *Geology* 44, 915–918.

<https://doi.org/10.1130/G38189.1>

Paulsen, T.S., Deering, C., Sliwinski, J., Bachmann, O., Guillong, M., 2017a. Evidence for a spike in mantle carbon outgassing during the Ediacaran period. *Nat. Geosci.* 10, 930–934.

<https://doi.org/10.1038/s41561-017-0011-6>

Paulsen, T.S., Deering, C., Sliwinski, J., Valencia, V., Bachmann, O., Guillong, M., 2017b.

Detrital zircon ages and trace element compositions of Permian–Triassic foreland basin strata of the Gondwanide orogen, Antarctica. *Geosphere* 13, 2085–2093.

<https://doi.org/10.1130/GES01482.1>

Paulsen, T.S., Encarnación, J., Grunow, a. M., Valencia, V. a., Pecha, M., Layer, P.W.,

Rasoazanamparany, C., 2013. Age and significance of “outboard” high-grade metamorphics and intrusives of the Ross orogen, Antarctica. *Gondwana Res.* 24, 349–358.

<https://doi.org/10.1016/j.gr.2012.10.004>

Paulsen, T.S., Encarnación, J., Grunow, A.M., Valencia, V.A., Layer, P.W., Pecha, M.,

Stump, E., Roeske, S., Thao, S., Rasoazanamparany, C., 2015. Detrital mineral ages from the Ross Supergroup, Antarctica: Implications for the Queen Maud terrane and outboard sediment provenance on the Gondwana margin. *Gondwana Res.* 27, 377–391.

<https://doi.org/10.1016/j.gr.2013.10.006>

<https://doi.org/10.1016/j.gr.2013.10.006>

Pepper, M., Gehrels, G., Pullen, A., Ibanez-Mejia, M., Ward, K.M., Kapp, P., 2016.

Magmatic history and crustal genesis of western South America: Constraints from U-Pb

ages and Hf isotopes of detrital zircons in modern rivers. *Geosphere* 12, 1532–1555.

<https://doi.org/10.1130/GES01315.1>

Phillips, G., Landenberger, B., Belousova, E.A., 2011. Building the New England Batholith, eastern Australia—Linking granite petrogenesis with geodynamic setting using Hf isotopes in zircon. *Lithos* 122, 1–12. <https://doi.org/10.1016/j.lithos.2010.11.005>

Platt, J.P., Whitehouse, M.J., Kelley, S.P., Carter, A., Hollick, L., 2003. Simultaneous extensional exhumation across the Alboran Basin: Implications for the causes of late orogenic extension. *Geology* 31, 251. [https://doi.org/10.1130/0091-](https://doi.org/10.1130/0091-7613(2003)031<0251:SEEATA>2.0.CO;2)

[7613\(2003\)031<0251:SEEATA>2.0.CO;2](https://doi.org/10.1130/0091-7613(2003)031<0251:SEEATA>2.0.CO;2)

Ramos, V.A., 2009. Anatomy and global context of the Andes: Main geologic features and the Andean orogenic cycle. *Geol. Soc. Am. Mem.* 204, 31–65.

[https://doi.org/10.1130/2009.1204\(02\)](https://doi.org/10.1130/2009.1204(02))

Repository, P.R., 2018. Polar rock and dredge samples available for research and educational use from the PRR. [WWW Document]. <https://doi.org/10.7289/V5RF5S18>

Riel, N., Jaillard, E., Martelat, J.-E., Ephane Guillot, S., Braun, J., 2018. Permian-Triassic Tethyan realm reorganization: Implications for the outward Pangea margin.

<https://doi.org/10.1016/j.jsames.2017.11.007>

Riley, T.R., Burton-Johnson, A., Flowerdew, M.J., Whitehouse, M.J., 2018. Episodicity within a mid-Cretaceous magmatic flare-up in West Antarctica: U-Pb ages of the Lassiter Coast intrusive suite, Antarctic Peninsula, and correlations along the Gondwana margin. *GSA Bull.* <https://doi.org/10.1130/B31800.1>

Riley, T.R., Flowerdew, M.J., Pankhurst, R.J., Leat, P.T., Millar, I.L., Fanning, C.M.,

Whitehouse, M.J., 2017. A revised geochronology of Thurston Island, West Antarctica,

- and correlations along the proto-Pacific margin of Gondwana. *Antarct. Sci.* 29, 47–60.  
<https://doi.org/10.1017/S0954102016000341>
- Riley, T.R., Flowerdew, M.J., Whitehouse, M.J., 2012. U-Pb ion-microprobe zircon geochronology from the basement inliers of eastern Graham Land, Antarctic Peninsula. *J. Geol. Soc. London.* 169, 381–393. <https://doi.org/10.1144/0016-76492011-142>
- Rocchi, S., Di Vincenzo, G., Ghezzi, C., Nardini, I., 2009. Granite-lamprophyre connection in the latest stages of the early Paleozoic Ross Orogeny (Victoria Land, Antarctica). *Geol. Soc. Am. Bull.* 121, 801–819. <https://doi.org/10.1130/B26342.1>
- Rocha-Campos, A.C., Basei, M.A., Nutman, A.P., Kleiman, L.E., Varela, R., Llambias, E., Canile, F.M., da Rosa, O. de C.R., 2011. 30million years of Permian volcanism recorded in the Choiyoi igneous province (W Argentina) and their source for younger ash fall deposits in the Paraná Basin: SHRIMP U-Pb zircon geochronology evidence. *Gondwana Res.* 19, 509–523. <https://doi.org/10.1016/j.gr.2010.07.003>
- Rosenbaum, G., 2018. The Tasmanides: Phanerozoic Tectonic Evolution of Eastern Australia. *Annu. Rev. Earth Planet. Sci.* 46, annurev-earth-082517-010146.  
<https://doi.org/10.1146/annurev-earth-082517-010146>
- Rosenbaum, G., Li, P., Rubatto, D., 2012. The contorted New England Orogen (eastern Australia): New evidence from U-Pb geochronology of early Permian granitoids. *Tectonics* 31, 1–14. <https://doi.org/10.1029/2011TC002960>
- Rubatto, D., 2002. Zircon trace element geochemistry: partitioning with garnet and the link between U–Pb ages and metamorphism. *Chem. Geol.* 184, 123–138.  
[https://doi.org/10.1016/S0009-2541\(01\)00355-2](https://doi.org/10.1016/S0009-2541(01)00355-2)
- Rudnick, R.L., Gao, S., 2003. Composition of the Continental Crust, in: *Treatise on*

- Geochemistry. Elsevier, pp. 1–64. <https://doi.org/10.1016/B0-08-043751-6/03016-4>
- Saito, S., Brown, M., Korhonen, F.J., McFadden, R.R., Siddoway, C.S., 2013. Petrogenesis of Cretaceous mafic intrusive rocks, Fosdick Mountains, West Antarctica: Melting of the sub-continental arc mantle along the Gondwana margin. *Gondwana Res.* 23, 1567–1580. <https://doi.org/10.1016/j.gr.2012.08.002>
- Sato, A.M., Llambías, E.J., Basei, M.A.S., Castro, C.E., 2015. Three stages in the Late Paleozoic to Triassic magmatism of southwestern Gondwana, and the relationships with the volcanogenic events in coeval basins. *J. South Am. Earth Sci.* 63, 48–69. <https://doi.org/10.1016/j.jsames.2015.07.005>
- Schilling, M.E., Carlson, R.W., Tassara, A., Vieira Conceição, R., Bertotto, G.W., Vásquez, M., Muñoz, D., Jalowitzki, T., Gervasoni, F., Morata, D., 2017. The origin of Patagonia revealed by Re–Os systematics of mantle xenoliths. *Precambrian Res.* 294, 15–32. <https://doi.org/10.1016/j.precamres.2017.03.008>
- Schilling, M.E., Carlson, R.W., Vieira Conceição, R., Dantas, C., Bertotto, G.W., Koester, E., 2008. Re–Os isotope constraints on subcontinental lithospheric mantle evolution of southern South America. <https://doi.org/10.1016/j.epsl.2008.01.005>
- Schoener, R., Bomfleur, B., Raymond, C.E., Schneider, J., Viereck-Goette, L., International Symposium on Antarctic Earth, S., 2007. Triassic-Jurassic sediments and multiple volcanic events in north Victoria Land, Antarctica; a revised stratigraphic model. Open-File Rep. - U. S. Geol. Surv. Short Research Paper 102. <https://doi.org/10.3133/of2007-1047.srp102>
- Seton, M., Müller, R.D., Zahirovic, S., Gaina, C., Torsvik, T., Shephard, G., Talsma, A., Gurnis, M., Turner, M., Maus, S., Chandler, M., 2012. Global continental and ocean

basin reconstructions since 200 Ma. *Earth-Science Rev.* 113, 212–270.

<https://doi.org/10.1016/J.EARSCIREV.2012.03.002>

Shaanan, U., Rosenbaum, G., Wormald, R., 2015. Provenance of the Early Permian Nambucca block (eastern Australia) and implications for the role of trench retreat in accretionary orogens. *Geol. Soc. Am. Bull.* 127, B31178.1.

<https://doi.org/10.1130/B31178.1>

Shaw, S.E., Flood, R.H., Pearson, N.J., 2011. The New England Batholith of eastern Australia: Evidence of silicic magma mixing from zircon  $^{176}\text{Hf}/^{177}\text{Hf}$  ratios. *Lithos* 126, 115–126. <https://doi.org/10.1016/j.lithos.2011.06.011>

Shen, W., Wiens, D.A., Stern, T., Anandakrishnan, S., Aster, R.C., Dalziel, I., Hansen, S., Heeszel, D.S., Huerta, A., Nyblade, A., Wilson, T.J., Winberry, J.P., 2018. Seismic evidence for lithospheric foundering beneath the southern Transantarctic Mountains, Antarctica. *Geology* 46, 71–74. <https://doi.org/10.1130/G39555.1>

Siddoway, C.S., Fanning, C.M., 2009. Paleozoic tectonism on the East Gondwana margin: Evidence from SHRIMP U–Pb zircon geochronology of a migmatite–granite complex in West Antarctica. *Tectonophysics* 477, 262–277.

<https://doi.org/10.1016/J.TECTO.2009.04.021>

Siddoway, C.S., Richard, S.M., Fanning, C.M., Luyendyk, B.P., 2004. Origin and emplacement of a middle Cretaceous gneiss dome, Fosdick Mountains, West Antarctica, in: *Special Paper 380: Gneiss Domes in Orogeny*. Geological Society of America, pp. 267–294. <https://doi.org/10.1130/0-8137-2380-9.267>

Sláma, J., Košler, J., Condon, D.J., Crowley, J.L., Gerdes, A., Hanchar, J.M., Horstwood, M.S.A., Morris, G.A., Nasdala, L., Norberg, N., Schaltegger, U., Schoene, B., Tubrett,

- M.N., Whitehouse, M.J., 2008. Plešovice zircon — A new natural reference material for U–Pb and Hf isotopic microanalysis. *Chem. Geol.* 249, 1–35.  
<https://doi.org/10.1016/j.chemgeo.2007.11.005>
- Söderlund, U., Patchett, P.J., Vervoort, J.D., Isachsen, C.E., 2004. The  $^{176}\text{Lu}$  decay constant determined by Lu–Hf and U–Pb isotope systematics of Precambrian mafic intrusions. *Earth Planet. Sci. Lett.* 219, 311–324. [https://doi.org/10.1016/S0012-821X\(04\)00012-3](https://doi.org/10.1016/S0012-821X(04)00012-3)
- Spalletti, L.A., Limarino, C.O., 2017. The Choiyoi magmatism in south western Gondwana: implications for the end-permian mass extinction - a review. *Andean Geol.* 44, 328.  
<https://doi.org/10.5027/andgeoV44n3-a05>
- Stern, T., Houseman, G., Salmon, M., Evans, L., 2013. Instability of a lithospheric step beneath western North Island, New Zealand. *Geology* 41, 423–426.  
<https://doi.org/10.1130/G34028.1>
- Storey, B., Dalziel, I.W., Garrett, S., Grunow, A., Pankhurst, R.J., Vennum, W., 1988. West Antarctica in Gondwanaland: Crustal blocks, reconstruction and breakup processes. *Tectonophysics* 155, 381–390. [https://doi.org/10.1016/0040-1951\(88\)90276-4](https://doi.org/10.1016/0040-1951(88)90276-4)
- Taylor, H.E., Lichte, F.E., 1980. Chemical composition of Mount St. Helens volcanic ash. *Geophys. Res. Lett.* 7, 949–952. <https://doi.org/10.1029/GL007i011p00949>
- Thirlwall, M.F., Anczkiewicz, R., 2004. Multidynamic isotope ratio analysis using MC–ICP–MS and the causes of secular drift in Hf, Nd and Pb isotope ratios. *Int. J. Mass Spectrom.* 235, 59–81. <https://doi.org/10.1016/j.ijms.2004.04.002>
- Tucker, R.T., Roberts, E.M., Henderson, R.A., Kemp, A.I.S., 2016. Large igneous province or long-lived magmatic arc along the eastern margin of Australia during the Cretaceous?

Insights from the sedimentary record. *Geol. Soc. Am. Bull.* 128, 1461–1480.

<https://doi.org/10.1130/B31337.1>

Tulloch, A.J., Ramezani, J., Kimbrough, D.L., Faure, K., Allibone, A.H., 2009. U-Pb geochronology of mid-Paleozoic plutonism in western New Zealand: Implications for S-type granite generation and growth of the east Gondwana margin. *Geol. Soc. Am. Bull.* 121, 1236–1261. <https://doi.org/10.1130/B26272.1>

Vaughan, A.P.M., Eagles, G., Flowerdew, M.J., 2012. Evidence for a two-phase Palmer Land event from crosscutting structural relationships and emplacement timing of the Lassiter Coast Intrusive Suite, Antarctic Peninsula: Implications for mid-Cretaceous Southern Ocean plate configuration. *Tectonics* 31, n/a-n/a.  
<https://doi.org/10.1029/2011TC003006>

Vaughan, A.P.M., Millar, I.L., 1996. Early cretaceous magmatism during extensional deformation within the Antarctic Peninsula Magmatic Arc. *J. South Am. Earth Sci.* 9, 121–129. [https://doi.org/10.1016/0895-9811\(96\)00032-6](https://doi.org/10.1016/0895-9811(96)00032-6)

Veevers, J.J., Belousova, E.A., Saeed, A., Sircombe, K., Cooper, A.F., Read, S.E., 2006. Pan-Gondwanaland detrital zircons from Australia analysed for Hf-isotopes and trace elements reflect an ice-covered Antarctic provenance of 700–500 Ma age, TDM of 2.0–1.0 Ga, and alkaline affinity. *Earth-Science Rev.* 76, 135–174.  
<https://doi.org/10.1016/j.earscirev.2005.11.001>

Veizer, J., Ala, D., Azmy, K., Bruckschen, P., Buhl, D., Bruhn, F., Carden, G.A.F., Diener, A., Ebner, S., Godderis, Y., Jasper, T., Korte, C., Pawellek, F., Podlaha, O.G., Strauss, H., 1999.  $^{87}\text{Sr}/^{86}\text{Sr}$ ,  $\delta^{13}\text{C}$  and  $\delta^{18}\text{O}$  evolution of Phanerozoic seawater. *Chem. Geol.* 161, 59–88. [https://doi.org/10.1016/S0009-2541\(99\)00081-9](https://doi.org/10.1016/S0009-2541(99)00081-9)

- Vermeesch, P., 2012. On the visualisation of detrital age distributions. *Chem. Geol.* 312, 190–194. <https://doi.org/10.1016/j.chemgeo.2012.04.021>
- Vervoort, J.D., Blichert-Toft, J., 1999. Evolution of the depleted mantle: Hf isotope evidence from juvenile rocks through time. *Geochim. Cosmochim. Acta* 63, 533–556. [https://doi.org/10.1016/S0016-7037\(98\)00274-9](https://doi.org/10.1016/S0016-7037(98)00274-9)
- Vervoort, J.D., Patchett, P.J., Blichert-Toft, J., Albarède, F., 1999. Relationships between Lu–Hf and Sm–Nd isotopic systems in the global sedimentary system. *Earth Planet. Sci. Lett.* 168, 79–99. [https://doi.org/10.1016/S0012-821X\(99\)00047-3](https://doi.org/10.1016/S0012-821X(99)00047-3)
- Walker, J.D., Geissman, J.W., Bowring, S.A., Babcock, L.E., 2013. The Geological Society of America Geologic Time Scale. *Geol. Soc. Am. Bull.* 125, 259–272. <https://doi.org/10.1130/B30712.1>
- Wang, H., Currie, C.A., 2015. Magmatic expressions of continental lithosphere removal. *J. Geophys. Res. Solid Earth* 120, 7239–7260. <https://doi.org/10.1002/2015JB012112>
- Wiedenbeck, M., Alle, P., Corfu, F., Griffin, W.L., Meier, M., Oberli, F., Von Quadt, A., Roddick, J.C., Spiegel, W., 1995. Three natural zircon standards for U–Th–Pb, Lu–Hf, trace element and REE analyses. *Geostand. Geoanalytical Res.* 19, 1–23. <https://doi.org/10.1111/j.1751-908X.1995.tb00147.x>
- Wiedenbeck, M., Hanchar, J.M., Peck, W.H., Sylvester, P., Valley, J., Whitehouse, M., Kronz, A., Morishita, Y., Nasdala, L., Fiebig, J., Franchi, I., Girard, J.-P., Greenwood, R.C., Hinton, R., Kita, N., Mason, P.R.D., Norman, M., Ogasawara, M., Piccoli, P.M., Rhede, D., Satoh, H., Schulz-Dobrick, B., Skår, O., Spicuzza, M., Terada, K., Tindle, A., Togashi, S., Vennemann, T., Xie, Q., Zheng, Y.-F., 2004. Further Characterisation of the 91500 Zircon Crystal. *Geostand. Geoanalytical Res.* 28, 9–39.

<https://doi.org/10.1111/j.1751-908X.2004.tb01041.x>

- Woodhead, J.D., Hergt, J.M., 2005. A Preliminary Appraisal of Seven Natural Zircon Reference Materials for In Situ Hf Isotope Determination. *Geostand. Geoanalytical Res.* 29, 183–195. <https://doi.org/10.1111/j.1751-908X.2005.tb00891.x>
- Yakymchuk, C., Brown, C.R., Brown, M., Siddoway, C.S., Fanning, C.M., Korhonen, F.J., 2015. Paleozoic evolution of western Marie Byrd Land, Antarctica. *Geol. Soc. Am. Bull.* 127, 1464–1484. <https://doi.org/10.1130/B31136.1>
- Yakymchuk, C., Kirkland, C.L., Clark, C., 2018. Th/U ratios in metamorphic zircon. *J. Metamorph. Geol.* <https://doi.org/10.1111/jmg.12307>
- Yakymchuk, C., Siddoway, C.S., Fanning, C.M., Mcfadden, R., Korhonen, F.J., Brown, M., 2013. Anatectic reworking and differentiation of continental crust along the active margin of Gondwana: a zircon Hf–O perspective from West Antarctica. *Geol. Soc. London, Spec. Publ.* 383, 169–210. <https://doi.org/10.1144/SP383.7>